國立臺灣大學工學院土木工程學系
碩士論文
Department of Civil Engineering
College of Engineering
National Taiwan University
Master's Thesis

交通號誌配時調整對路口延滯最小化之探討：考量行人優先

Investigation of Traffic Signal Timing Adjustments to Minimize Intersection Delay: Accounting for Pedestrian Priority

鍾淯全
Yu-Cyuan Jhong

指導教授：許聿廷博士
Advisor: Yu-Ting Hsu, Ph.D.

中華民國 114 年 7 月
July, 2025

doi:10.6342/NTU202503442

國立臺灣大學碩士學位論文
口試委員會審定書

NATIONAL TAIWAN UNIVERSITY
MASTER'S THESIS ACCEPTANCE CERTIFICATE

交通號誌配時調整對路口延滯最小化之探討：考量行人優先

Investigation of Traffic Signal Timing Adjustments to Minimize Intersection Delay: Accounting for Pedestrian Priority

本論文係 鍾淯全 (R12521506) 在國立臺灣大學土木工程學系交通工程組完成之碩士學位論文，於民國114年7月15日承下列考試委員審查通過及口試及格，特此證明。

The undersigned, appointed by the Department of Civil Engineering, Transportation Engineering Division on July 15th, 2025 have examined a Master's Thesis entitled above presented by Yu-Cyuan Jhong (R12521506) candidate and hereby certify that it is worthy of acceptance.

口試委員 Oral examination committee:

許聿廷 許聿廷
（指導教授 Advisor）

陳彥向 陳彥向

胡守任 胡守任

系主管 Director： 葛宇甯 葛宇甯

doi:10.6342/NTU202503442

中文誌謝

完成一篇學術論文對我而言是相當大的挑戰，一方面需承接前人的知識，找出可進一步探討的方向；另一方面則需自行建立模型，獲得新的發現，並提出論述以期對社會有所貢獻。首先感謝父母親的栽培與資助，讓我有一個良好的環境成長，並有能力投入研究生涯。再來感謝指導教授許聿廷老師，在研究過程中不斷給予鼓勵與支持，研究成果沒有絕對的對錯，但一定要對自己有自信。

本研究最初是由樓軒宇學長提出號誌調整的概念。人本交通與路口設計是近年來社會關注的重要議題，而在修習陳彥向老師的交通控制等相關課程後，我注意到改善路口交通問題，其實還有另一種方法可切入。感謝彥向老師與軒宇學長提供我延伸發展本研究的契機，也感謝口試委員胡守任老師對本研究提出實務層面的寶貴意見。

感謝同是 YT 家的夥伴，包含文元、哲安、柏森、瑋恬等人，無論是每週的團體會議、或者學期間的 Seminar ，皆能對彼此的發表內容給予回饋；論文口試前也會為彼此加油打氣，平常心面對即能一帆風順。感謝彥向家的成員們，針對我的研究內容提供許多修正與建議。感謝陳建豪同學協助開門，讓我能借用 114 實驗室的電腦操作 Vissim 模擬軟體。感謝 R11 廖柏彥學長的技術支援，讓我更加了解 Vissim 操作的細節。感謝其他老師家的子弟，雖與本研究未必直接相關，但能在這兩年中一起學習、吃飯、聊天，是難得的緣分，也是我的榮幸。

最後感謝自己未被挫折淹沒，即使研究的日子稍嫌枯燥，我依然對交通工程的多個面向抱有好奇心；感謝自己不盲目追隨熱門科系，因為我相信，即便身在交通組，仍能接觸所謂的電腦科學及其相關應用。

doi:10.6342/NTU202503442

doi:10.6342/NTU202503442

Acknowledgements

Completing an academic thesis has been a big challenge for me. It not only involves building upon the knowledge of predecessors and identifying directions for further improvement, but also requires developing models to uncover new insights and formulating arguments that contribute to society. I would like to thank my parents for their support and upbringing, which enabled me to pursue my academic journey in a well-resourced environment. I would also like to thank my advisor, Professor Yu-Ting Hsu, for his encouragement throughout this process. He taught me that while research outcomes may not be absolutely right or wrong, it is essential to have confidence in oneself.

This research was inspired by the idea of signal timing adjustment proposed by Hsuan-Yu Lou. In recent years, the concept of a Humanity-Oriented Traffic Environment and intersection design has become a widely discussed topic in society. However, after taking Professor Yen Chen's courses on traffic control and related subjects, I realized that there are multiple ways to address intersection traffic issues. I sincerely thank Professor Chen and Hsuan-Yu Lou for giving me the motivation to further develop this research. I also appreciate the practical feedback provided by oral defense committee member Professor Shou-Ren Hu.

I am thankful for my labmates in the YT family, including Wen-Yuan Wu, Che-An Lin, Po-Sen Huang, and Wei-Tien Chang. Whether during weekly group meetings or seminars, we consistently provided one another with constructive feedback. In the lead-up to our thesis defenses, we also exchanged words of encouragement, which helped us face challenges with confidence and a positive mindset.

doi:10.6342/NTU202503442

I am also grateful to the members of Professor Chen's lab for offering suggestions to improve my research. In particular, I thank Chien-Hao Chen for helping me access the computers in Lab 114 so I could operate the Vissim simulation software, and senior student Po-Yen Liao from R11 for his technical support, which deepened my understanding of Vissim operations. Thank you also to students from other research groups. Although not directly involved in this study, sharing experiences of learning, dining, and conversation with you over the past two years has been a fortunate and memorable part of my journey.

Finally, I want to thank myself for not being overwhelmed by setbacks. Even when the research process felt tedious at times, I remained curiosities about various aspects of transportation engineering. I am also grateful for not blindly following popular majors, because I believe that, even within the field of transportation, I can still engage with computer science and its related applications.

doi:10.6342/NTU202503442

中文摘要

隨著都市化發展，市區道路在尖峰期間難免發生壅塞，且行人與車輛的互動甚或衝突頻率日益增加。另一方面，隨著人本交通環境意識的提升，近年來臺灣各地方政府積極致力於改善交通環境；法規方面亦將駕駛未禮讓行人的罰鍰提高，期望提升行人安全。然而，在存在右轉車輛與穿越行人同綠的路口設計下，考量行人優先原則，右轉車輛需禮讓行人，導致後方車隊增長，平均延滯時間上升。因此在保障行人安全的同時，如何兼顧交通效率，避免延滯過度增加，亦是甚須探討的問題。

本研究著重在右轉交通車流效率改善，以行人優先為前提，檢視右轉車輛的飽和流率受行人阻擋影響的變化，透過調整行人綠燈長度，以達成兩項最佳化目標：一是最小化行人與右轉車輛的整體平均延滯，二是最小化兩者平均延滯的差異。不同於現行設計手冊僅以單一行人阻擋折減因子處理人車衝突，本研究進一步考量人車同綠情境下的實際紓解行為。行人常於綠燈初期大量通行，而右轉車輛則需待行人紓解率與抵達率趨於平衡後，才逐漸恢復應有的紓解能力。此種人車互動關係可劃分為 12 種型態，本研究並依此建立多流動延滯模型，用以呈現行人與車輛的抵達線與紓解線之交會平衡時間。模型假設行人與車輛抵達率為常數，行人紓解率受行人號誌變化影響，右轉車紓解率則同時受行人紓解變化與車輛號誌控制所影響，整體以分段線性方式表示。

本研究針對臺北市六個主要路口的行穿線與衝突右轉車道進行觀測，以人車衝突區域作為計數區，取得行人與車輛的抵達與不同時段的紓解數據。彙整資料後發現，穿越行人與右轉車輛的紓解率呈對數關係，此結果可作為後續最佳化模型的參數輸入。研究結果顯示，若人車抵達率處於一般狀況，建議給予最長的行人

doi:10.6342/NTU202503442

綠燈時間以獲得整體最小延滯；若考量人車平等，則行人綠燈長度通常會建議調整至可行解範圍的中間區段，以達到人車延滯最小差異之目標。

關鍵字：多流動延滯模型、紓解率、同向穿越行人、右轉車輛、行人優先

doi:10.6342/NTU202503442

Abstract

With ongoing urbanization, traffic congestion in urban areas has become inevitable during peak hours, and interactions or even conflicts between pedestrians and vehicles occur frequently. Meanwhile, as awareness of humanity-oriented traffic environments continues to grow, local governments in Taiwan have been actively working on improving road facilities, and for the regulatory aspect, penalties for drivers who fail to yield to pedestrians have been raised, all to pursue in enhancing pedestrian safety. However, in intersection designs where right-turning vehicles and crossing pedestrians share a concurrent green phase, prioritizing pedestrians generally means right-turning vehicles must yield, which can result in longer queues and increased average delays. While ensuring pedestrian safety, how to maintain traffic efficiency and prevent excessive delay is also worth further investigation.

This study focuses on improving right-turn traffic efficiency under the premise of pedestrian priority. By adjusting the pedestrian green duration, the study proposes two optimization objectives: (1) minimizing the overall average delay of pedestrians and right-turning vehicles, and (2) minimizing the difference between the two delays. Unlike existing design manuals that address pedestrian blockage using a single adjustment factor, this study incorporates real-world discharge behavior under concurrent green conditions. Pedestrians tend to discharge in greater volumes during the early part of the green phase, while right-turning vehicles gradually recover their dischargeability as the pedestrian discharge rate reaches arrival rate. These pedestrian-vehicle interactions are categorized into 12 cases, forming a multi-movement delay model that identifies the timepoint when

doi:10.6342/NTU202503442

arrival and discharge curves intersect. The model assumes constant arrival rates for both pedestrians and vehicles. Pedestrian discharge rates vary with pedestrian signal changes, while right-turn vehicle discharge rates are affected by both pedestrian movement and vehicle signal phases. All discharge trends are represented using piecewise linear functions.

Field data were collected from six major intersections in Taipei City, focusing on pedestrian crosswalks and their conflicting right-turn lanes. The pedestrian-vehicle conflict zone was used as the counting area to capture arrival and discharge volumes during different time intervals. Analysis shows that the discharge rates of pedestrians and right-turning vehicles follow a logarithmic relationship, which is then used as parameter input to the optimization model. Results indicate that under typical arrival conditions, the longest pedestrian green duration yields the lowest total delay. When emphasizing equity between pedestrians and vehicles, the pedestrian green time is generally recommended to be set near the middle of the feasible range to minimize the delay difference between the two user groups.

Key words: Multi-Movement Delay Model, Discharge Rate, Parallel-Crossing Pedestrian, Right-Turning Vehicle, Pedestrian Priority

doi:10.6342/NTU202503442

Contents

doi:10.6342/NTU202503442

doi:10.6342/NTU202503442

doi:10.6342/NTU202503442

doi:10.6342/NTU202503442

List of Figures

doi:10.6342/NTU202503442

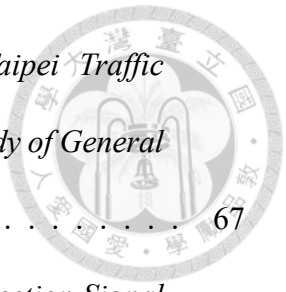

doi:10.6342/NTU202503442

doi:10.6342/NTU202503442

List of Tables

doi:10.6342/NTU202503442

doi:10.6342/NTU202503442

doi:10.6342/NTU202503442

Chapter 1 Introduction

1.1 Research Background

As urbanization continues in most developed countries, it is inevitable that traffic congestion occurs more often in road networks, and interactions (or even conflicts) between pedestrians and vehicles are becoming more frequent, raising concerns about pedestrian crossing safety at intersections. To concretize the concept of the Humanity-Oriented Traffic Environment, local governments in Taiwan have increasingly focused on implementing road traffic improvements in recent years to enhance pedestrian safety, such as installing refuge islands or introducing a pedestrian scramble phase.

From a regulatory aspect, according to the *Road Traffic Management and Penalty Act* (2024), drivers are required to yield to pedestrians when approaching crosswalks. The most recent amendment raised the upper limit of fines from NT$3,600 to NT$6,000, aiming to enhance deterrence and reduce aggressive or unfriendly driving behavior toward pedestrians. This amendment, accompanied by related promotional efforts, has gradually improved driver behavior, with more drivers yielding to pedestrians when turning at intersections, thereby ensuring pedestrian right-of-way.

However, at intersections with concurrent pedestrian and vehicle signal phases, turning vehicles often encounter pedestrians crossing in parallel during their green light. Under moderate to high pedestrian volumes, this can lead to frequent stop-and-go situations for vehicles, resulting in longer queues and potential traffic congestion.

doi:10.6342/NTU202503442

Figure 1.1: Conflict between right-turning vehicles and parallel-crossing pedestrians in the concurrent green phase. *Photograph by the author.*

1.2 Research Motivation

As mentioned in the *Taiwan Highway Capacity Manual* (2022), the capacity and level of service at signalized intersections are typically influenced by signal control strategies, road geometry, and road user behavior.

In most commonly used traffic delay models, both arrival and discharge rates are assumed to be uniform (Webster, 1958). This simplification is reasonable when there are no conflicting movements. However, at intersections with pedestrian interference, the traditional estimation of saturation flow rate for turning vehicles becomes less appropriate due to unpredictable lane blockages.

In Taipei City, it is common to observe concurrent signal phase designs in which Right-Turning Vehicles (RTVs) and Parallel-Crossing Pedestrians (PCPs) are permitted to proceed simultaneously. Under such conditions, the two movements cannot be discharged freely due to mutual conflicts.

doi:10.6342/NTU202503442

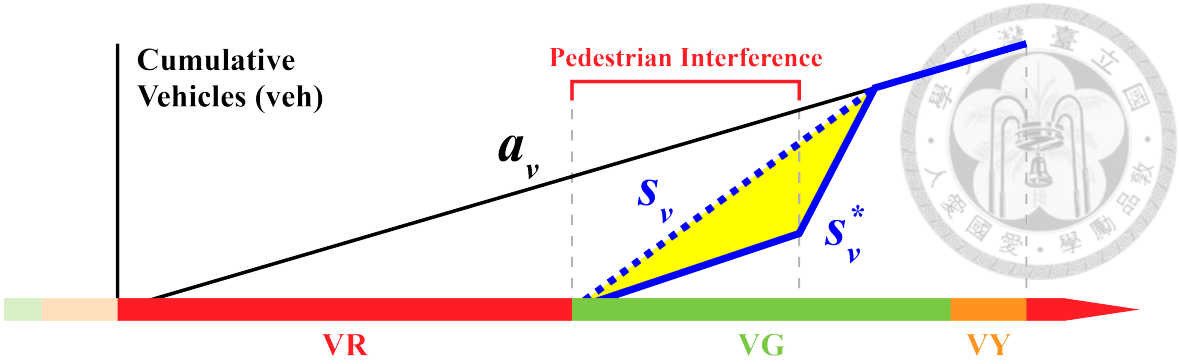

Figure 1.2: The approximate trend of vehicle discharge rate change.

Figure 1.2 illustrates the approximate trend of vehicle discharge rate variation under pedestrian interference, denoted as s_v^* (the entity discharge polyline). Unlike the traditional discharge rate s_v (represented by the dashed line), the piecewise linear form of s_v^* may better capture the reduced discharge performance for vehicles during the early stage of the green phase, which is caused by conflicting pedestrian flows. The discharge capacity gradually recovers as the pedestrian discharge volume approaches a balance with the arrival volume.

It can also be observed in Figure 1.2 that the area enclosed between the lines s_v and s_v^* represents the portion of vehicle delay that would be underestimated if a traditional traffic delay model were applied.

1.3 Research Objectives

With growing emphasis on pedestrian right-of-way and its impact on vehicle flow, this research examines intersection performance from the perspective of traffic efficiency, under the framework of the Humanity-Oriented Traffic Environment.

doi:10.6342/NTU202503442

An optimization model is developed to adjust traffic signal timings with the objective of minimizing delays for both Parallel-Crossing Pedestrians (PCPs) and Right-Turning Vehicles (RTVs) at a given intersection approach. Key features include:

1. incorporating pedestrian priority, and
2. capturing discharge rate variations across different time intervals (e.g., signal phases and dissipation times, as detailed in Chapter 4).

As part of the data collection process, this study also establishes a regression model to describe the relationship between PCP and RTV discharge rates, as well as between discharge rates across different time intervals.

1.4 Thesis Organization

The structure of this research is illustrated in Figure 1.3. Chapter 2 presents a literature review, clarifies the research scope, and establishes preliminary assumptions. Chapter 3 develops an optimization model aimed at minimizing delays for both RTVs and PCPs on a single approach of an isolated intersection within a signal cycle. To simplify the overall model complexity, certain signal timing-related constraints are incorporated directly into the objective function.

Chapter 4 presents the data collection and case study, focusing on selected intersection approaches in Taipei City. The required data include existing signal phase timing designs and traffic flow rates at these intersections. The case study aims to generate improved signal timing adjustments that reduce delays for both PCP and RTV movements. Finally, Chapter 5 summarizes the key research findings and suggestions.

doi:10.6342/NTU202503442

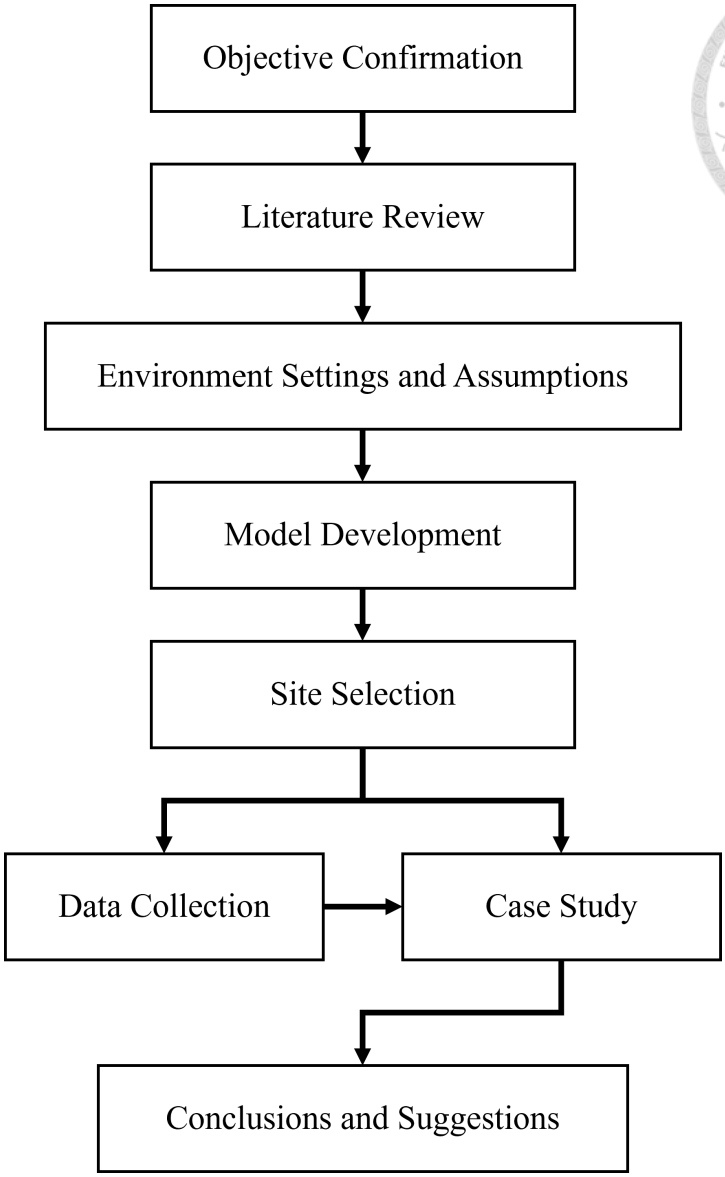

Figure 1.3: Research structure.

doi:10.6342/NTU202503442

doi:10.6342/NTU202503442

Chapter 2 Literature Review

In this chapter, traffic signal regulations and design manuals are reviewed, along with the development of pedestrian and vehicle flow and delay formulas and their applications in optimization models. Various pedestrian-related designs are also discussed, and the chapter concludes with an examination of the research gap and preliminary assumptions.

2.1 Traffic Signal Regulations

2.1.1 Pedestrian Signal Phases

In urban areas, both pedestrians and vehicles play significant roles in traffic operations. In addition to vehicle signal regulations, there are specific traffic signal designs and rules for pedestrian movements. According to Article 207 of the *Regulations on Road Traffic Signs, Markings, and Signals* (2024), pedestrian signal phases are defined as follows:

1. **Green (WALK):** Pedestrians are allowed to cross the road.
2. **Flashing Green (DON'T WALK):** Pedestrians who have already entered the crosswalk should proceed quickly or wait on a traffic island (if available). Those who have not yet entered the roadway are prohibited from crossing.
3. **Red (DON'T WALK):** Pedestrians are prohibited from entering the roadway.

doi:10.6342/NTU202503442

2.1.2 Criteria for Signal Stage Selection

In Article 230 of the *Regulations on Road Traffic Signs, Markings, and Signals* (2024), a two-stage signal design may be implemented at the following locations:

1. T-intersections
2. Four-legged intersections with low left-turn volumes
3. Four-legged intersections without exclusive pedestrian phases
4. Non-intersection locations with exclusive pedestrian signals

By contrast, three- or four-stage signal designs may be adopted under the following conditions:

1. Five-legged intersections
2. Four-legged intersections with high left-turn volumes
3. Intersections with high pedestrian volumes that require exclusive pedestrian phases

2.1.3 Signal Transition Settings

Article 231 of the *Regulations on Road Traffic Signs, Markings, and Signals* (2024) specifies the timing settings for pedestrian flashing signals, vehicle yellow intervals, and clearance times. These parameters are crucial for ensuring intersection safety across all directions of movement.

Pedestrian Flashing Phase Duration

The duration of the pedestrian flashing phase should allow the last pedestrian to fully cross the crosswalk. It is calculated by dividing the effective crossing distance by the pedestrian walking speed:

doi:10.6342/NTU202503442

$$t = \frac{dw}{v} \tag{2.1}$$

where dw is the crosswalk length, or equivalently, the width of the intersection approach. If a refuge island is present, dw is defined as the longer of the two distances from the curb to the island. The pedestrian walking speed v is generally set to 1.0 m/s.

Vehicle Yellow Phase Duration

The yellow phase duration for vehicles should comply with the regulatory values listed in Table 2.1:

Table 2.1: Yellow phase duration settings.

Speed Limit (km/h)	Yellow Phase Length (s)
Below 50	3
51–60	4
Above 60	5

Minimum Clearance (All-Red) Time

A minimum all-red interval of one second should be provided for all traffic movements immediately after the yellow phase ends. The recommended clearance time can be calculated using the reference formula shown in Table 2.2:

Table 2.2: Clearance time (all red) settings.

Traffic Condition	Vehicle	Vehicle & Pedestrian
Clearance Time Length (s)	$\frac{W+L}{2V} \sim \frac{W+L}{2V}$	$\frac{P+L}{2V} \sim \frac{P+L}{2V}$

Note:
W = Distance from the near-end stop line to the far-end road section (m).
P = Distance from the near-end stop line to the far-end pedestrian crossing (m).
L = Average vehicle length (usually 6 m).
V = Average speed or the speed limit (m/s).

doi:10.6342/NTU202503442

2.2 Saturation Flow Rates

2.2.1 Related Definitions

Capacity refers to the maximum number of pedestrians or vehicles that can pass through a specific point or section during a given time period under prevailing conditions. It is commonly used as a design standard and can be derived from the saturation flow rate, adjusted for signal timing. Capacity is typically expressed in units of pedestrians or vehicles per hour.

Saturation flow rate refers to the maximum number of pedestrians or vehicles that can pass through a specific point or section under ideal conditions, such as optimal geometry, signal control, and no interruptions. It is also expressed in units of pedestrians or vehicles per hour. The relationship between capacity and saturation flow rate is shown in Equation 2.2 (*Highway Capacity Manual*, 2010):

$$c = s \cdot \frac{g_{\text{eff}}}{C} \cdot N \tag{2.2}$$

where c is the capacity (vph), s is the saturation flow rate (vphgpl), C is the cycle length (s), g_{eff} is the effective green length (s), and N is the number of lanes in the lane group.

On the other hand, the discharge rate represents the actual number of pedestrians or vehicles passing through a point during a given time interval, as observed in the field. While the discharge rate may approach the maximum value (i.e., the saturation flow rate) under ideal conditions, it often falls short due to delays, behavioral variations, or signal inefficiencies.

doi:10.6342/NTU202503442

The saturation flow rate for vehicles can be estimated by observing the average discharge headway, using the following relationship:

$$s = \frac{3600}{h} \tag{2.3}$$

where s is the saturation flow rate (veh/hr) and h is the average discharge headway (s). In practice, discharge headways vary throughout the green phase in signalized intersections, as the first few vehicles (approximately 4 to 5) experience longer headways while accelerating from a stop. After this initial startup period, the flow stabilizes into a steady state, during which the saturation flow is typically measured. This also explains the difference between actual discharge rates and the theoretical saturation flow rate.

Demand, corresponding to capacity, is the total number of vehicles or pedestrians wishing to access a point or section during a given time period. Arrival rate, corresponding to the discharge rate, is the actual observed number of those road users approaching that point or section. When traffic is uncongested, demand and arrival rate can be considered equivalent. Both are typically expressed in the same units as capacity and discharge rate (e.g., pedestrians or vehicles per hour).

At signalized intersections, different signal phases either permit (green phase) or restrict (red phase) road users from crossing the stop line. Under these interrupted flow conditions, the discharge rate becomes a key factor in performance analysis.

doi:10.6342/NTU202503442

2.2.2 Saturation Flow Rate Adjustments

A base lane saturation flow rate (or base lane capacity, assuming an effective green ratio of $g_{\text{eff}}/C = 1.0$) is commonly provided in most traffic design manuals worldwide, typically ranging from 1750 to 2000 pcuphpl. However, this base rate must be adjusted to reflect the specific conditions at the selected intersection or roadway segment. The adjustment formula shown below is provided in the *Highway Capacity Manual* (2010):

$$s = s_0 f_w f_{HV} f_g f_p f_{bb} f_a f_{LU} f_{LT} f_{RT} f_{Lpb} f_{Rpb} \tag{2.4}$$

where

s = Saturation flow rate for the lane group (pcuphpl)

s_0 = Base saturation flow rate under ideal conditions (pcuphpl)

f_w = Adjustment factor for lane width

f_{HV} = Adjustment factor for heavy vehicles

f_g = Adjustment factor for approach grade

f_p = Adjustment factor for parking activity

f_{bb} = Adjustment factor for bus blockage

f_a = Adjustment factor for area type

f_{LU} = Adjustment factor for lane utilization

f_{LT} = Adjustment factor for left-turn vehicle presence in a lane group

f_{RT} = Adjustment factor for right-turn vehicle presence in a lane group

f_{Lpb} = Pedestrian adjustment factor for left-turn groups

f_{Rpb} = Pedestrian adjustment factor for right-turn groups

doi:10.6342/NTU202503442

The pedestrian adjustment factors in Equation 2.4 are determined based on observed pedestrian volumes and the average occupancy time of the conflict zone (Milazzo et al., 1998). However, this approach, relying on a single aggregated value, oversimplifies the dynamic and time-varying nature of pedestrian flow, which can systematically influence fluctuations in the saturation flow rates of conflicting turning vehicles.

On the other hand, the *Taiwan Highway Capacity Manual* (2022) provides a similar formula for adjusting the base lane capacity, without directly requiring either the effective green time or the saturation flow rate, as shown in Equation 2.5:

$$c = \frac{3600}{C}\left(\sum_{i=1}^{n} N_{gyi}\right) f_V f_g f_b f_S f_Z f_P \tag{2.5}$$

where

c = Lane capacity (vph)

C = Signal cycle length (s)

N_{gyi} = Average number of stopped vehicles that can be discharged during the green and signal change interval of the ith effective phase

i = Index of effective phases

n = Total number of effective phases

f_V = Adjustment factor for vehicle type and movement direction

f_g = Adjustment factor for grade (slope)

f_b = Adjustment factor for bus stops

f_S = Adjustment factor for curbside parking

f_Z = Adjustment factor for urban area characteristics

f_P = Adjustment factor for conflicting pedestrians

doi:10.6342/NTU202503442

For details of the conflicting pedestrian adjustment factor f_P, the manual adopts an empirically simulated relationship curve between the factor and the observed number of conflicting pedestrians during the entire green duration, under various vehicle turning ratios. However, it also states that additional data are needed to improve estimation precision and to better understand how conflicting pedestrians influence lane capacity.

2.2.3 Extended Discussions

Rouphail and Eads (1997) simulated pedestrian impedance to right-turning vehicles by directly assigning random delay times to vehicle discharge headways using the CORSIM software. The simulation yielded a linear relationship between pedestrian volume and the saturation flow rate of turning vehicles, but this differed from field data collected across multiple U.S. intersections, which revealed a logarithmic relationship. Moreover, by pre-assigning delay times, the simulation failed to capture the dynamic interactions between pedestrians and right-turning vehicles, such as yielding behavior and gap negotiation.

Chen et al. (2014) proposed an empirical model describing a four-stage saturation departure process for shared right-turn lanes in Hangzhou, China. The saturation headway analysis (using Equation 2.3) showed that vehicles in the shared right-turn lane can be affected by lane blockage, pedestrian interference, and interactions between right-turning and through vehicles. Sensitivity analyses showed that higher pedestrian crossing demand, a greater proportion of right-turning vehicles, limited storage capacity, and longer crosswalk lengths all contribute to a reduction in the saturation flow rate of shared right-turn lanes. This model more effectively captures the departure characteristics and helps explain the underestimation of delay when Equation 2.4 is applied directly.

doi:10.6342/NTU202503442

Roshani and Bargegol (2017) conducted a case study at six signalized intersections in Rasht, Iran, observing a total of 90 signal cycles and also calculating saturation flow rates using the saturation headway method. A linear regression analysis was performed to examine the relationship between pedestrian volume q'_{ped} and conflicting right-turning vehicle volume q'_{veh} over 10-second intervals, yielding an R^2 value of 0.6261.

$$q'_{veh} = -0.4263 \cdot q'_{ped} + 4.9113 \tag{2.6}$$

Although Roshani and Bargegol reaffirmed the general trend that increasing pedestrian flow tends to reduce the saturation flow rate of right-turning vehicles, the derived relationship is empirical and may vary across countries and regions due to differences in road user behavior and regulatory frameworks.

Lai (2018) developed the Fixed Capacity Regression Method and established an empirical formula to estimate the saturation flow rate of mixed lanes, incorporating passenger car equivalent conversions for various vehicle types. The study identified that that mixed right-turning ratios (including both automobiles and motorcycles) and pedestrian conflict ratios are key factors contributing to reductions in saturation flow rates.

$$SFR = SFR_0 - 9.1 \cdot P_{RT_{all}} - 3.5 \cdot P_{conflict_{all}} \tag{2.7}$$

where

SFR = Saturation flow rate (pcuphgpl)

SFR_0 = Saturation flow rate for through lane = 2327 pcu/hr

$P_{RT_{all}}$ = Mixed right-turning ratio (%)

$P_{conflict_{all}}$ = Pedestrian conflict ratio (%)

doi:10.6342/NTU202503442

Pedestrian saturation flow rate is less frequently addressed in the literature due to the unique characteristics of pedestrian flow, such as freedom of movement and variable density. In practice, observed pedestrian arrival and discharge volumes are typically used to establish empirical relationships and evaluate their effects on other vehicular flow rates.

2.3 Delay Estimations

Delay is the additional travel time experienced by drivers or pedestrians, measured relative to the free-flow travel time required to traverse the same path and distance. Delay can be caused by traffic signal control, congestion, acceleration and deceleration, and blockage from other road users.

2.3.1 Vehicular Delay

The vehicular delay estimation can be found in the *Highway Capacity Manual* (2000), which includes three parts: uniform delay, incremental delay and initial queue delay (optional). The formula is as follows:

$$d = d_1\,(PF) + d_2 + d_3 \tag{2.8}$$

where

d = Control delay per vehicle (s/veh)

d_1 = Uniform control delay assuming uniform arrivals (s/veh)

d_2 = Incremental delay due to random arrivals and oversaturation queues (s/veh)

d_3 = Initial queue delay (s/veh)

PF = Uniform delay progression adjustment factor

doi:10.6342/NTU202503442

In Equation 2.8, PF accounts for the effects of signal coordination and platoon arrival quality. It is not calculated directly but rather obtained from tabulated values based on the degree of saturation and green ratio. However, the subsequent version of the *Highway Capacity Manual* (2010) incorporates the effects of PF within the arrival type analysis, and no longer presents it as an explicit factor in the delay formula.

The uniform control delay d_1, originally derived from Webster's (1958) delay formula, and the incremental delay d_2, are expressed as follows:

$$d_1 = \frac{0.5 \cdot C \cdot \left(1 - \frac{g}{C}\right)^2}{1 - \left[\min\left(1, X\right) \cdot \frac{g}{C}\right]} \tag{2.9}$$

$$d_2 = 900 \cdot T \left[(X - 1) + \sqrt{(X - 1)^2 + \frac{8klX}{cT}} \right] \tag{2.10}$$

where

X = Lane group volume-to-capacity ratio (v/c)

c = Lane group capacity (veh/hr)

g = Lane group effective green time (s)

T = Analysis duration (hr)

k = Incremental delay adjustment factor for controller settings

l = Incremental delay adjustment for filtering or metering by upstream signals

As a supplement, the adjustment factor k is typically set to 0.5 for pretimed signals, while l can be set to 1.0 when analyzing an isolated intersection.

doi:10.6342/NTU202503442

As for the initial queue delay d_3, it occurs when a lane group operates under oversaturated conditions, where vehicles must wait for residual queues carried over from previous signal cycles to discharge. This type of delay is generally considered undesirable in traffic signal optimization, as it indicates persistent congestion. The derivation of this term is relatively complex (no closed-form formula is provided) and is therefore not discussed in detail here.

Since calibration terms vary across countries and regions over time (Akgüngör & Bullen, 1999), but most formulations share a similar basic structure, a well-known generalized form of the delay formula proposed by Akçelik (1988) is presented below:

$$d = 0.5 \cdot \frac{C(1-\lambda)^2}{1-\lambda x} + 900T^n \left[(x-1) + \sqrt{(x-1)^2 + \frac{m\,(x-x_0)}{cT}} \right] \tag{2.11}$$

$$x_0 = a + bsg \tag{2.12}$$

where

λ = Green ratio

x = Degree of saturation

x_0 = Degree of saturation below which the second term delay is zero

m, n, a, b = Calibration parameters

sg = Capacity per cycle

doi:10.6342/NTU202503442

2.3.2 Pedestrian Delay

Pedestrian delay estimation is also provided in the *Highway Capacity Manual* (2000). The formula is as follows:

$$d_p = \frac{(C-G)^2}{2C} \tag{2.13}$$

where

d_p = Average pedestrian delay (s)

G = Effective green time for pedestrians (s)

C = Signal cycle length (s)

Note that Equation 2.13 is derived under the assumptions of a uniform pedestrian arrival rate, complete signal compliance, and a fixed signal cycle length.

A paradox arises in that, although pedestrians are legally expected to wait if they have not entered the crosswalk before the onset of the flashing Don't Walk (FDW) phase, this interval is still treated as part of the effective green time and thus contributes zero delay in the Highway Capacity Manual (HCM) model. Interestingly, this treatment coincides with common pedestrian behavior, as many individuals still initiate crossing during the FDW phase in practice, despite regulatory constraints.

Braun and Roddin (1978) introduced the concept of the fraction of law-abiding pedestrians, denoted as F, and redefined G to refer only to the green Walk phase. The modified formula is as follows:

$$d_p = F \cdot \frac{(C-G)^2}{2C} \tag{2.14}$$

doi:10.6342/NTU202503442

Virkler (1998) conducted a field study at 18 crosswalks in Brisbane, Australia, and observed that a portion of pedestrians entered the crosswalk during the flashing Don't Walk (FDW) phase at higher walking speeds. As a result, approximately 69% of the clearance time should be treated as part of the effective green time. Based on this behavior, a modified pedestrian delay formula was proposed:

$$d_p = \frac{[C - (G + 0.69A)]^2}{2C} \tag{2.15}$$

where

G = Duration of the WALK signal (s)

A = Duration of the clearance interval or FDW signal (s)

Most research has indicated that pedestrian delay at signalized crossings is primarily influenced by signal timing rather than capacity constraints. In other words, pedestrians usually do not experience overflow delay (Virkler, 1998). This assumption is generally reasonable in Taiwan, where pedestrians often exhibit flexible crossing behavior. For example, flow density can vary, and some pedestrians may walk outside the marked crosswalk lines.

2.4 Signal Phase Design Methods

Traffic signal optimization methods have evolved over time, progressing from stage-based to group-based, lane-based, and more recently, time-slot-based models. Each method is suited to different roadway configurations and operational requirements.

doi:10.6342/NTU202503442

Stage-Based (Allsop, 1981; Webster, 1958)

The stage-based method is the most classic and widely used method for traffic signal optimization in practice. It divides the signal cycle into distinct stages, with each stage corresponding to a predefined set of traffic movements. While stages aim to organize movements logically, they may still include permissive or controlled conflicts, depending on the design.

Group-based (Heydecker, 1992; Silcock, 1997)

The group-based method begins by clustering compatible traffic movements into groups and then optimizes signal timing based on those groups. This method can reduce the likelihood of conflicting movements and enhance safety; however, it may result in a more complex traffic signal design.

Lane-Based (Wong & Wong, 2003)

The lane-based method considers each traffic lane individually, allowing signal optimization to account for lane-specific demand. This approach is particularly suitable for intersections where different lanes on the same approach serve distinct movements or experience uneven traffic volumes.

Time-slot-based (Yu et al., 2020)

The time-slot-based method is a novel approach that divides the signal cycle into smaller time slots, allowing flexible allocation of green intervals. Movements with higher demand can receive multiple green phases within a single cycle, while low-demand movements may be skipped.

doi:10.6342/NTU202503442

Many signal optimization models are designed to maximize capacity, minimize cycle length, or minimize delay. Among these objectives, delay minimization is often more challenging due to the nonlinear relationship between delay and factors such as signal timings, queue dynamics, and traffic arrival patterns. In addition, both group-based and lane-based formulations commonly employ a compatibility matrix, which by default treats pedestrian crossing movements as separate from vehicle movements. However, pedestrian movements are still generally less discussed than vehicular traffic in most signal optimization models (Yu et al., 2017).

Among all approaches, the stage-based method is the simplest, as it features lower computational complexity, low installation costs, and predefined signal timing plans that are straightforward for traffic management.

2.5 Other Pedestrian-Related Designs

Exclusive Pedestrian Phases (EPPs)

Exclusive Pedestrian Phases (EPPs), also known as pedestrian scramble phases, are commonly implemented at intersections in Central Business Districts (CBDs). This design separates pedestrian and vehicle movements into distinct phases, thereby enhancing safety by eliminating conflict points. However, EPPs typically increase the signal cycle length due to the insertion of an additional phase (Ma et al., 2014), which can result in longer average waiting times and increased delays for both pedestrians and vehicles (Huang, 2004). EPPs are generally recommended for intersections with high pedestrian and turning vehicle volumes (Hu, 2024).

doi:10.6342/NTU202503442

Leading Pedestrian Intervals (LPIs)

Leading Pedestrian Intervals (LPIs) are commonly implemented in urban areas in Taiwan. This design begins the pedestrian green phase a few seconds earlier than the conflicting vehicle movements, giving drivers a clearer view of crossing pedestrians and allowing safer maneuvers. LPIs can also help reduce the interaction time between pedestrians and vehicles and may serve as a suitable alternative to EPPs at intersections with relatively low pedestrian volumes (Fu, 2011).

Refuge Islands and Two-Stage Crossings

Two-stage crossings are another type of pedestrian facility that offers flexibility in traffic signal design. Both two-stage crossings and the EPP design share the same goal: to separate pedestrian movements from vehicular traffic. Recent optimization models can also incorporate the decision of whether to implement one- or two-stage crosswalks on each approach (Yu et al., 2017).

However, it should be noted that the installation of refuge islands is a fundamental requirement for enabling two-stage crossing strategies (Wu, 2015). In addition, spatial constraints must be carefully considered to ensure that pedestrians can wait safely between traffic streams.

doi:10.6342/NTU202503442

2.6 Research Gap and Discussions

Although vehicle and pedestrian delay formulas are available in traffic design manuals and signal optimization models, they are typically treated independently. As a result, the interaction between the two is often poorly captured, especially in concurrent signal stage designs where right-turning vehicles and crossing pedestrians operate simultaneously, creating potential conflicts. To account for pedestrian priority, the effect of pedestrian blockage on right-turning vehicles is commonly represented by a single adjustment factor applied to the saturation flow rate or capacity. However, this simplified treatment fails to adequately reflect the dynamic and time-varying nature of the discharge process, potentially leading to inconsistent or inaccurate delay estimations.

Therefore, this study aims to develop a multi-delay model that describes the discharge relationship between parallel-crossing pedestrians and right-turning vehicles, explicitly considering their interactions under concurrent signal stage operations. The proposed relationship is also intended to be integrated into an optimization model to evaluate whether adjusting signal timing can lead to improved delay performance.

Since interactions between pedestrian and vehicle movements under concurrent stage designs are not well represented within the basic structures of group-based or lane-based methods, this study begins with a fixed-time control scenario that focuses on these two conflicting movements. A stage-based method is well suited to support this analysis. Moreover, traffic signal planning data are available for Taipei City, where most major intersections adopt stage-based designs with various pre-timed combinations throughout the day. This provides a practical foundation for examining whether peak-hour signal timing plans are appropriately configured.

doi:10.6342/NTU202503442

Another aspect worth noting is that most previous studies use the stop line as the reference point for determining whether a vehicle has discharged (Chen et al., 2014). However, when pedestrian-vehicle interactions are involved, the first few vehicles may pass the stop line but still wait in front of the pedestrian crossing. This creates unaccounted delay. It may be more appropriate to count vehicle discharge based on positions relative to the pedestrian-vehicle conflict area (see Figure 3.2b).

doi:10.6342/NTU202503442

doi:10.6342/NTU202503442

Chapter 3 Methodology

3.1 Modeling Framework

In this study, we focus on the interactions between Parallel-Crossing Pedestrian (PCP) and Right-Turning Vehicle (RTV) movements within a single intersection approach. The proposed modeling framework is illustrated in Figure 3.1. The delay model is designed to accommodate both pedestrian and vehicular flows by deriving an improved signal timing plan, ultimately aiming for two objectives:

- **Obj-1:** Minimize the overall (PCP and RTV) average delay
- **Obj-2:** Minimize the difference in average delay between the two movements

While the first objective aims to improve overall road user efficiency, it does not guarantee equity between different road user types (i.e., crossing pedestrians and turning vehicles), due to varying demand levels. By contrast, the second objective explicitly seeks to balance the efficiency between both user groups.

During the development of traffic delay cases for PCP and RTV movements, the interactions and parameter relationships between the two flows are analyzed. At the same time, signal-related and logical constraints are established. Although these elements can be integrated into a Mixed-Integer Quadratically Constrained Programming (MIQCP) model, we prefer a simplified solution process to more clearly illustrate trends in objective value changes.

doi:10.6342/NTU202503442

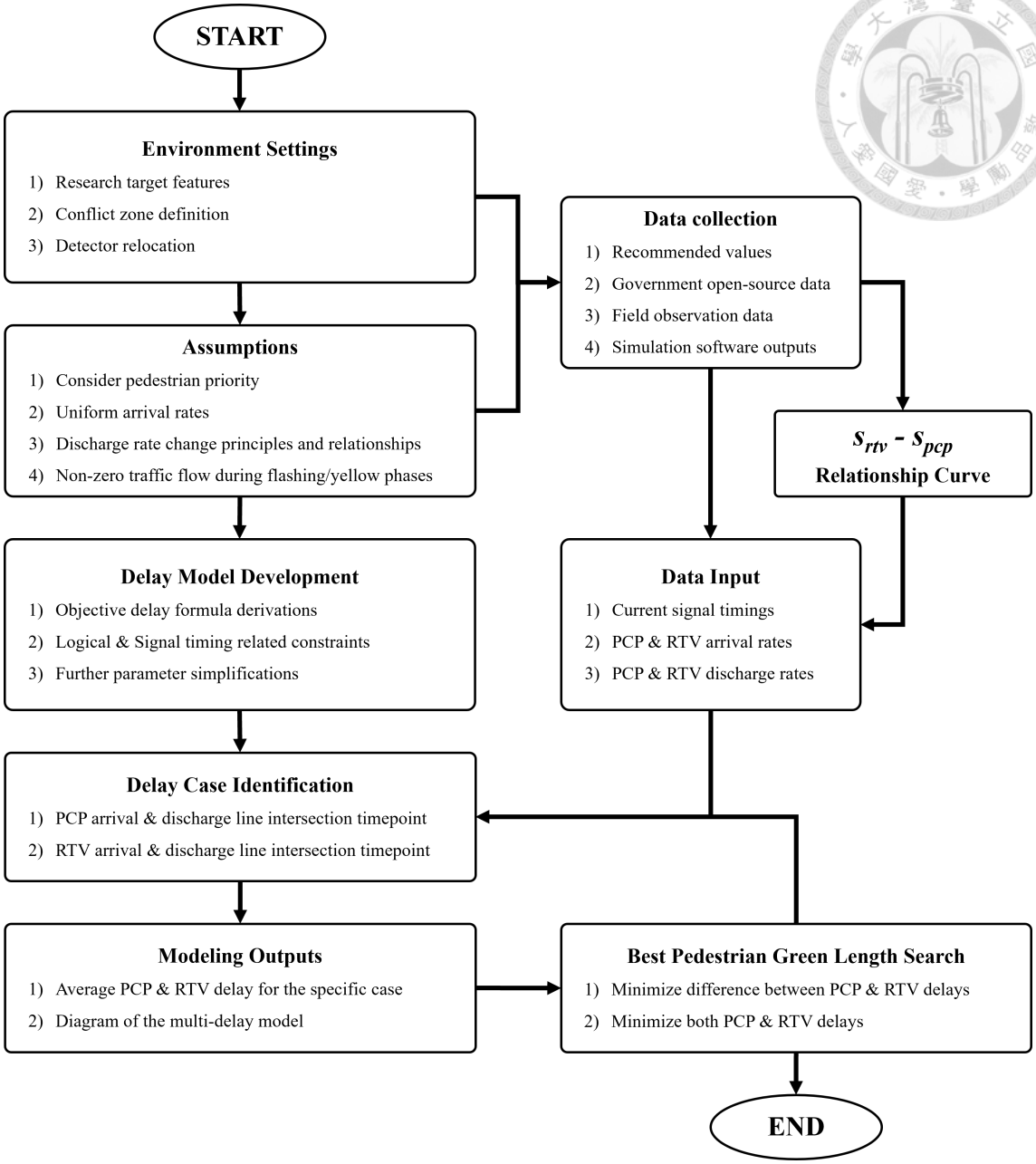

Figure 3.1: The modeling framework.

Regarding data collection, it serves to obtain arrival rates, discharge rates, and the existing signal phase timing plans for each selected intersection. After inputting these parameters, the expected outputs include **multi-movement delay model** diagrams and the recommended signal timing adjustment for the corresponding intersection approach.

doi:10.6342/NTU202503442

3.2 Environment Settings and Assumptions

3.2.1 Intersection Layout and Conflict Area of Focus

The typical layout of an intersection is illustrated in Figure 3.2a. Each approach consists of three dedicated lanes for right-turn, through, and left-turn movements, with no lane-changing behavior permitted. All lanes are assumed to be of infinite length to eliminate short-lane effects. Pedestrians are required to complete their crossings without interruption, as no refuge islands are provided.

Since our aim includes examining the saturation flow characteristics between Parallel-Crossing Pedestrians (PCPs) and Right-Turning Vehicles (RTVs), the primary conflict area is illustrated in Figure 3.2b, where vehicles encounter crossing pedestrians immediately after turning right.

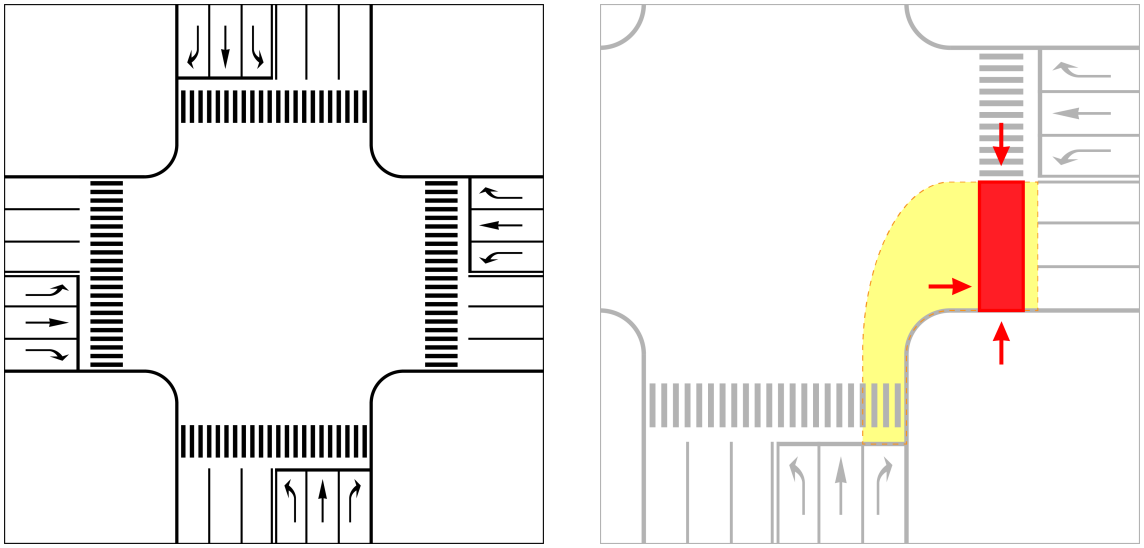

(a) Typical layout of an intersection. (b) The conflict area under focus.

Figure 3.2: Default road intersection environment.

doi:10.6342/NTU202503442

3.2.2 Signal Phase Design of Focus

Regarding the signal design, the aforementioned conflict occurs when both PCP and RTV movements are permitted during a concurrent green phase. This type of concurrent signal phase is typically implemented within a stage-based pattern.

In Taipei City, Leading Pedestrian Interval (LPI) designs are commonly implemented during peak hours at intersections with higher levels of pedestrian-vehicle conflict. Therefore, the LPI design is incorporated into our model, with t_{PE} representing the pedestrian early-start interval, distinct from the standard green time duration t_{PG} (further details are provided in the following sections).

Figure 3.3 presents two examples of traffic signal phase sequence designs. According to the *Taipei Intersection Signal Timing Plan* (2022), the LPI is shown as a separate stage from the standard concurrent green stages, even though both allow pedestrian crossing. Finally, a protected left-turn phase is included, which does not conflict with any other movement.

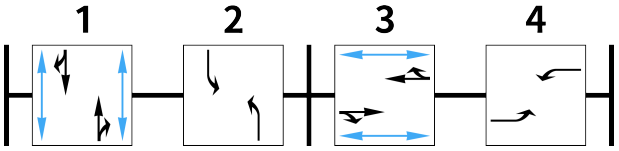

(a) Four-stage design without LPI.

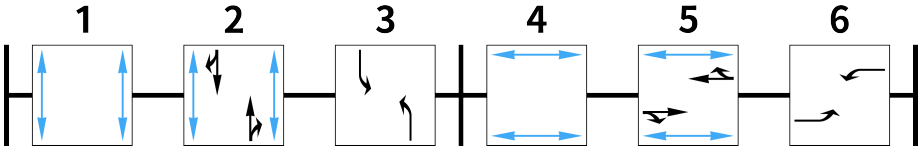

(b) Six-stage design with LPI.

Figure 3.3: Typical signal phase sequence patterns.

doi:10.6342/NTU202503442

3.2.3 Other Assumptions

Uniform Arrival Rates

The PCP and RTV arrival rates are assumed to be uniform, and pedestrian volumes from both sides of the crossing are considered equal. Since we focus on an isolated intersection, upstream influences are not considered.

Changeable Discharge Rates

The slope of the discharge lines in delay models is assumed to vary across different signal timing intervals. We seek to illustrate how PCPs and RTVs interact with each other, and this phenomenon can be displayed by changing their discharge rates in delay models.

Non-Zero Discharge Rates during Flashing/Yellow Phases

Although flashing phases restrict pedestrians from entering the road, and yellow phases restrict vehicles from crossing the stop line, those who have already passed these restricted zones are still allowed to finish crossing. This residual discharge causes conflicts between pedestrians and vehicles, and this phenomenon should also be represented in the multi-movement delay models.

Pedestrian Priority

Vehicles are required to yield to pedestrians to ensure the right-of-way of pedestrians. Under this setting, the pedestrian discharge rate is determined solely by changes in the pedestrian signal phase, whereas the right-turning vehicle discharge rate is influenced by both the pedestrian discharge behavior and changes in the vehicle signal phase.

doi:10.6342/NTU202503442

Early Termination of Pedestrian Phase Design Accommodation

As previously mentioned, leading pedestrian intervals (LPIs) allow right-turning vehicles to better anticipate pedestrian crossings. Conversely, early termination of pedestrian phases provides additional time for vehicles to complete their turns smoothly after pedestrians have cleared the crosswalk. A key design principle is that the pedestrian red signal should start before or at the same time as the vehicle green phase ends.

3.3 Notations

Tables 3.1, 3.2, and 3.3 respectively present the indices, parameters, and variables used in the model. Since the study focuses on a single intersection approach, the cycle length and vehicle signal timing durations are fixed to prevent interference with the performance of other approaches. The analysis centers on how variations in pedestrian green and red phase durations influence the shape of the multi-movement delay model.

The definitions of delay cases Pi for PCP movements and $PiVj$ for RTV movements, as well as the relationships between their discharge rates across different time intervals, will be discussed in the following section. It will also be shown that s_{v2} in Table 3.2 is not utilized, as there are no corresponding conditions under which it applies.

Table 3.1: Indices

Index	Description
i	Delay case index for Parallel-Crossing Pedestrian (PCP) movements $i \in \mathbb{I} = \{0, 1, 2\}$
j	Delay case index for Right-Turning Vehicle (RTV) movements $j \in \mathbb{J} = \{1, 2, 3, 4, 5, 6\}$

doi:10.6342/NTU202503442

Table 3.2: Parameters

Parameter	Unit	Description
C	s	Cycle length
t_{PE}	s	PCP early phase length (LPI design)
t_{PY}	s	PCP flashing phase length
t_{VG}	s	RTV green phase length
t_{VY}	s	RTV yellow phase length
t_{VR}	s	RTV red phase length
$t_{PG_{min}}$	s	Minimum PCP green phase length
$t_{PG_{max}}$	s	Maximum PCP green phase length
$t_{PR_{min}}$	s	Minimum PCP red phase length
$t_{PR_{max}}$	s	Maximum PCP red phase length
a_p	ped/s	PCP arrival rate (from both sides of the crosswalk)
a_v	pcu/s	RTV arrival rate (from the approaching lane)
s_{p1}	ped/s	PCP discharge rate during the PCP early and green phase, before the AL and DL lines intersect
s_{p2}	ped/s	PCP discharge rate during the PCP flashing phase, before the AL and DL lines intersect
s_{v1}	pcu/s	RTV discharge rate during the PCP green phase, before $t = t_{P1}$ or before the AL and DL lines intersect
s_{v2}	pcu/s	RTV discharge rate during the PCP green phase, after $t = t_{P1}$ and before the AL and DL lines intersect
s_{v3}	pcu/s	RTV discharge rate during the PCP flashing phase, before $t = t_{P2}$ or before the AL and DL lines intersect
s_{v4}	pcu/s	RTV discharge rate during the PCP flashing phase, after $t = t_{P2}$ and before the AL and DL lines intersect
s_{v5}	pcu/s	RTV discharge rate during the RTV green phase, after $t = t_{PG} + t_{PY}$ and before the AL and DL lines intersect
s_{v6}	pcu/s	RTV discharge rate during the RTV yellow phase, before the AL and DL lines intersect
ϵ	-	A small positive constant enforcing strict inequality
M	-	A large positive constant used in conditional constraints

Note:
1. PCP is the abbreviation of "Parallel-Crossing Pedestrian."
2. RTV is the abbreviation of "Right-Turning Vehicle."
3. AL is the abbreviation of "Arrival Line" in the delay model.
4. DL is the abbreviation of "Discharge Line" in the delay model.

doi:10.6342/NTU202503442

Table 3.3: Variables

Variable	Unit	Description
D_{avg}	s	Average delay for both PCP and RTV movements within a cycle
D_{total}	s	Total delay for both PCP and RTV movements within a cycle
D_{Pi}	s	Total delay for PCP movement under delay case Pi
D_{PiVj}	s	Total delay for RTV movement under delay case $PiVj$
δ_{Pi}	-	Binary variable indicating whether Delay Case Pi is selected for the PCP movement
δ_{PiVj}	-	Binary variable indicating whether Delay Case $PiVj$ is selected for the RTV movement
t_{PG}	s	Non-negative integer decision variable representing the green phase duration for Parallel-Crossing Pedestrians (PCPs)
t_{PR}	s	Non-negative integer decision variable representing the red phase duration for Parallel-Crossing Pedestrians (PCPs)
t_{Pi}	s	Auxiliary variable representing the timepoint when the PCP AL and DL intersect under Case Pi
t_{PiVj}	s	Auxiliary variable representing the timepoint when the RTV AL and DL intersect under Case $PiVj$

Note:
1. PCP is the abbreviation of "Parallel-Crossing Pedestrian."
2. RTV is the abbreviation of "Right-Turning Vehicle."
3. AL is the abbreviation of "Arrival Line" in the delay model.
4. DL is the abbreviation of "Discharge Line" in the delay model.
5. Both t_{Pi} and t_{PiVj} are measured from the start of the concurrent green phase.

doi:10.6342/NTU202503442

3.4 Delay Model Development

3.4.1 Discharge Rate Variable Relationships

To illustrate how discharge rates are determined across different time intervals, we first define **Case P2V6** as an example. This case exhibits the largest delay areas for both PCP and RTV movements, where $t_{Pi} = t_{P2}$ falls within the PCP flashing phase interval, and $t_{PiVj} = t_{P2V6}$ falls within the RTV yellow phase interval.

PCP							
RTV							
Interval	PE	PG_{front}	PG_{back}	PY_{front}	PY_{back}	VG	VY
$\boldsymbol{s_p} =$	$\overline{s_{p0}}$	$\overline{s_{p1}}$		$\overline{s_{p2}}$		0	
$\boldsymbol{s_v} =$	0	$\overline{s_{v1}}$	$\overline{s_{v2}}$	$\overline{s_{v3}}$	$\overline{s_{v4}}$	$\overline{s_{v5}}$	$\overline{s_{v6}}$

Figure 3.4: Discharge rates for each time interval.

Figure 3.4 presents the default discharge rates assigned to each time interval for both PCP and RTV movements. The barred notations in this figure are temporarily used for explanatory purposes. Recall that the pedestrian discharge rate depends solely on changes in the pedestrian signal phase, whereas the right-turn vehicle discharge rate is influenced both by changes in the pedestrian discharge rate and by changes in the vehicle signal phase.

Under the above condition, the pedestrian discharge rates are determined first. Since $\overline{s_{p0}}$ and $\overline{s_{p1}}$ correspond to the same green interval, they share the same value, s_{p1}. Given that walking speed tends to be slightly higher during the flashing phase compared to the green phase (Virkler, 1998), $\overline{s_{p2}}$ is assumed to be slightly greater than s_{p1}.

doi:10.6342/NTU202503442

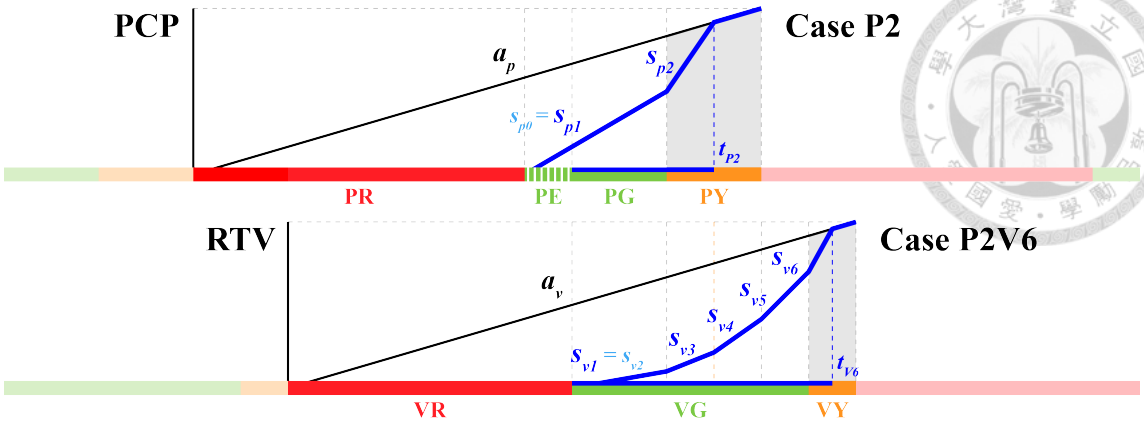

Figure 3.5: Multi-delay model of Case P2V6.

PCP							
RTV							
Interval	PE	PG_{front}	PG_{back}	PY_{front}	PY_{back}	VG	VY
$\boldsymbol{s_p} =$	s_{p1}			s_{p2}	a_p	0	
$\boldsymbol{s_v} =$	0	s_{v1}		s_{v3}	s_{v4}	s_{v5}	s_{v6}

Figure 3.6: Discharge rates for each time interval under Case P2V6.

When $t_{Pi} = t_{P2} = t_{PG} + t_{PY}$, the PCP discharge rate remains at s_{p2} throughout the flashing phase. However, if the PCP Arrival Line (AL) and Discharge Line (DL) intersect earlier, specifically at the end of the PY_{front} interval, as illustrated in Figure 3.4, then the discharge rate is s_{p2} during PY_{front} but changes to a_p during PY_{back}. This indicates that after the intersection point, pedestrian arrival and discharge volumes are balanced. In this situation, the RTV discharge rates are defined such that s_{p2} corresponds to $\overline{s_{v3}} = s_{v3}$ and a_p corresponds to $\overline{s_{v4}} = s_{v4}$.

On the other hand, since $\overline{s_{p1}}$ remains equal to s_{p1} throughout the pedestrian green interval, it corresponds to the RTV discharge rate $\overline{s_{v1}} = \overline{s_{v2}} = s_{v1}$. Figure 3.5 illustrates how the PCP and RTV discharge rates interact under Delay Case P2V6, while Figure 3.6 presents the discharge rate assignments specific to **Case P2V6**.

doi:10.6342/NTU202503442

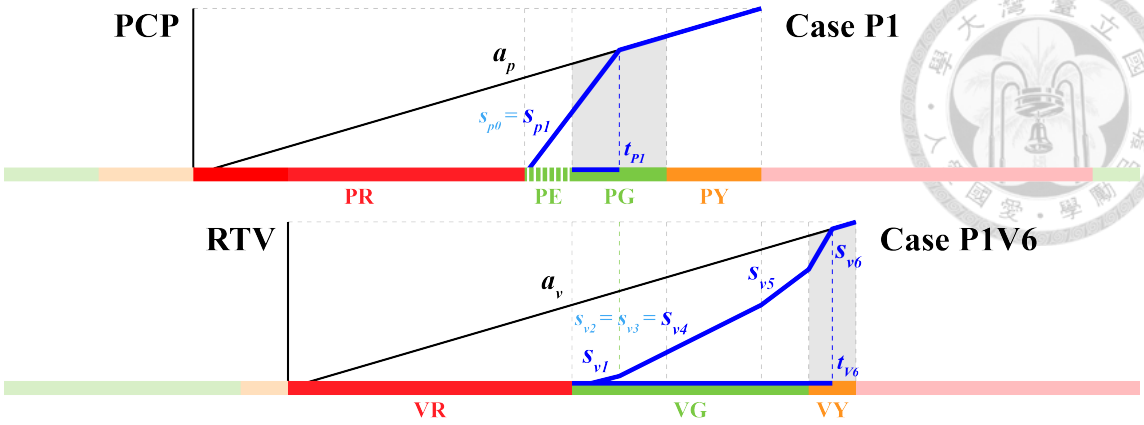

Figure 3.7: Multi-delay model of Case P1V6.

PCP							
RTV							
Interval	PE	PG_{front}	PG_{back}	PY_{front}	PY_{back}	VG	VY
$\boldsymbol{s_p} =$	s_{p1}		a_p			0	
$\boldsymbol{s_v} =$	0	s_{v1}	s_{v4}			s_{v5}	s_{v6}

Figure 3.8: Discharge rates for each time interval under Case P1V6.

Next, we examine Case P1V6 to provide further explanation. In P1 cases, the pedestrian AL and DL intersect at $t_{Pi} = t_{P1}$, which occurs during the pedestrian green phase, but after the leading pedestrian interval (LPI). After this intersection point t_{P1}, pedestrian arrival and discharge volumes are balanced at the same rate a_p, and the corresponding RTV discharge rates are therefore $\overline{s_{v2}} = \overline{s_{v3}} = \overline{s_{v4}} = s_{v4}$. Before t_{P1}, the PCP discharge rate $\overline{s_{p1}} = s_{p1}$ corresponds to the RTV discharge rate $\overline{s_{v1}} = s_{v1}$. Figure 3.7 illustrates how the PCP and RTV discharge rates interact under Delay Case P1V6, and Figure 3.8 presents the discharge rate assignments specific to **Case P1V6**.

doi:10.6342/NTU202503442

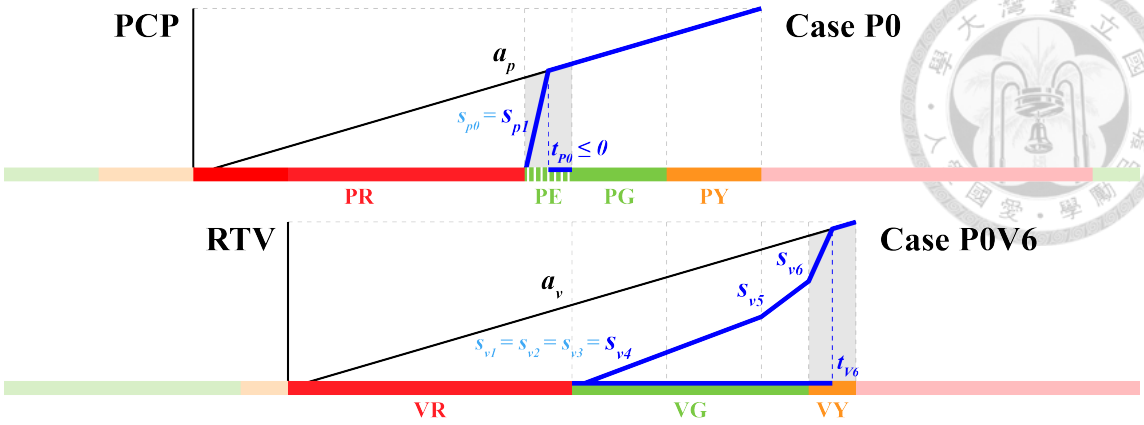

Figure 3.9: Multi-delay model of Case P0V6.

PCP							
RTV							
Interval	PE	PG_{front}	PG_{back}	PY_{front}	PY_{back}	VG	VY
$\boldsymbol{s_p} =$	s_{p1}	a_p				0	
$\boldsymbol{s_v} =$	0	s_{v4}				s_{v5}	s_{v6}

Figure 3.10: Discharge rates for each time interval under Case P0V6.

Last but not least, we discuss delay Case P0V6. In P0 cases, the pedestrian AL and DL intersect at $t_{Pi} = t_{P0}$, which occurs during the Leading Pedestrian Interval (LPI). After this intersection point t_{P0}, pedestrian arrival and discharge volumes are balanced at the same rate a_p. As previously noted, when the PCP discharge rate is a_p, the corresponding RTV discharge rates become $\overline{s_{v1}} = \overline{s_{v2}} = \overline{s_{v3}} = \overline{s_{v4}} = s_{v4}$. Since the LPI prohibits vehicle movements, RTV discharge rate is zero during this period. Figure 3.10 presents the discharge rate assignments specific to **Case P0V6**.

As for the RTV discharge rates s_{v5} and s_{v6}, RTV movements are no longer impeded by crossing pedestrians once the PCP red phase begins. In other words, s_{v5} can be regarded as the free-flow discharge rate for RTV movements. Additionally, s_{v6} is assumed to be slightly higher due to drivers' tendency to accelerate during the transition period.

doi:10.6342/NTU202503442

Using this framework, PCP delay can be categorized into three distinct cases: P0, P1 and P2. And under each of these, six corresponding delay cases are defined for RTV movements. For each case, there are 6 delay cases for RTV movements. A similar principle applies to right-turning vehicles: whenever the RTV Arrival Line (AL) and Discharge Line (DL) intersect earlier during a specific time interval, the discharge rate after the intersection time point t_{PiVj} becomes equal to the arrival rate a_v. Additionally, once the signal enters the red phase, the discharge rate drops to zero.

Under the three PCP delay cases, it is found that $\overline{s_{v2}} = s_{v4}$ in Cases P0V6 and P1V6, and $\overline{s_{v2}} = s_{v1}$ in Case P2V6. This indicates that s_{v2} is case-dependent and does not correspond to a unique PCP discharge rate symbol of its own.

3.4.2 PCP Delay Formulas

Figure 3.11 illustrates the three PCP delay shapes. The total delay experienced by parallel-crossing pedestrians within a signal cycle on a single intersection approach is represented by the area enclosed by the Arrival Line (AL), the Discharge Line (DL), and the time axis. This enclosed area can be computed using integration.

Recall that the intersection time point t_{Pi} is defined relative to the start of the concurrent green phase for both movements. Therefore, when this time point falls within the LPI (i.e., the pedestrian "early" phase), it takes on a negative value, ranging from $-t_{PE}$ to zero.

Note that the area integration process is similar for all delay cases. To conserve space, only the complete derivation for Case P0 is presented as an example.

doi:10.6342/NTU202503442

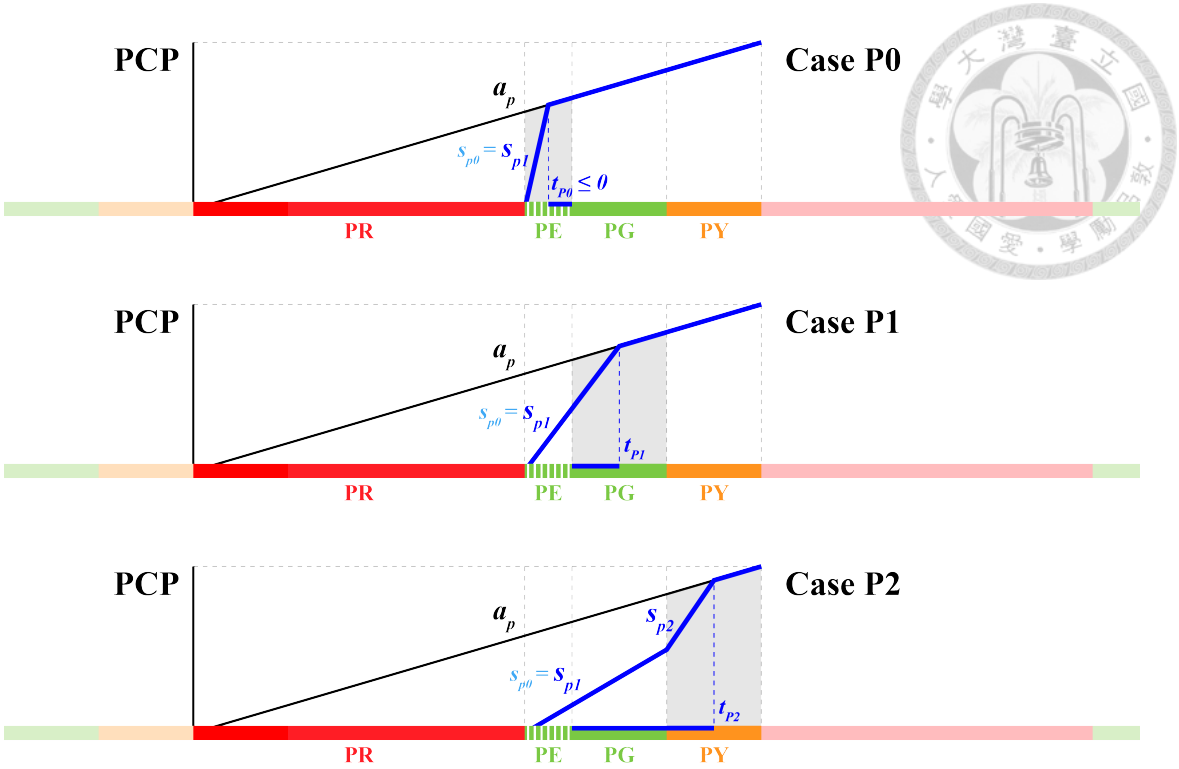

Figure 3.11: Paraller-crossing pedestrian (PCP) delay models.

Case P0 Delay Formula

The following formulation is valid when $t_{Pi} = t_{P0}$ falls within the pedestrian early phase $(-t_{PE} < t_{P0} \le 0)$.

$$
\begin{aligned}
D_{P0} &= \int_0^{t_{PR}} a_p t \, dt + \int_{t_{PR}}^{t_{PR}+t_{PE}+t_{P0}} a_p t - s_{p1}\left(t - t_{PR}\right) \, dt \\
&= \left(\frac{1}{2} a_p t^2\right)_0^{t_{PR}} + \left(\frac{1}{2}\left(a_p - s_{p1}\right) t^2 + s_{p1} t_{PR} t\right)_{t_{PR}}^{t_{PR}+t_{PE}+t_{P0}} \\
&= \frac{1}{2} a_p t_{PR}^2 + \frac{1}{2}\left(a_p - s_{p1}\right)\left(t_{PR}^2 + t_{PE}^2 + t_{P0}^2 + 2 t_{PR} t_{PE} + 2 t_{PR} t_{P0} + 2 t_{PE} t_{P0}\right) + \\
&\quad s_{p1} t_{PR}\left(t_{PR} + t_{PE} + t_{P0}\right) - \frac{1}{2}\left(a_p - s_{p1}\right) t_{PR}^2 - s_{p1} t_{PR}^2
\end{aligned}
$$

doi:10.6342/NTU202503442

Finally, the delay expression can be simplified and presented as Equation 3.1:

$$D_{P0} = \left(\frac{a_p}{2}\right) t_{PR}^2 + \left(\frac{a_p - s_{p1}}{2}\right) t_{PE}^2 + \left(\frac{a_p - s_{p1}}{2}\right) t_{P0}^2 + \\ (a_p)\, t_{PR} t_{PE} + (a_p)\, t_{PR} t_{P0} + (a_p - s_{p1})\, t_{PE} t_{P0} \tag{3.1}$$

Case P1 Delay Formula

The delay expression is simplified and presented as Equation 3.2, which is valid when $t_{Pi} = t_{P1}$ falls within the pedestrian green phase ($0 < t_{P1} \leq t_{PG}$).

$$D_{P1} = \left(\frac{a_p}{2}\right) t_{PR}^2 + \left(\frac{a_p - s_{p1}}{2}\right) t_{PE}^2 + \left(\frac{a_p - s_{p1}}{2}\right) t_{P1}^2 + \\ (a_p)\, t_{PR} t_{PE} + (a_p)\, t_{PR} t_{P1} + (a_p - s_{p1})\, t_{PE} t_{P1} \tag{3.2}$$

Case P2 Delay Formula

The delay expression is simplified and presented as Equation 3.3, which is valid when $t_{Pi} = t_{P2}$ falls within the pedestrian flashing phase ($-t_{PG} < t_{Pi} = t_{P2} \leq t_{PG} + t_{PY}$).

$$D_{P2} = \left(\frac{a_p}{2}\right) t_{PR}^2 + \left(\frac{a_p - s_{p1}}{2}\right) t_{PE}^2 + \left(\frac{s_{p1} - s_{p2}}{2}\right) t_{PG}^2 + \left(\frac{a_p - s_{p2}}{2}\right) t_{P2}^2 + \\ (a_p)\, t_{PR} t_{PE} + (a_p)\, t_{PR} t_{P2} + (a_p - s_{p1})\, t_{PE} t_{P2} + (-s_{p1} + s_{p2})\, t_{PG} t_{P2} \tag{3.3}$$

It is observed that all time-related terms in the three delay formulas are quadratic. As the case index i increases, the delay shapes become more complex; however, the formulas maintain a consistent structural pattern. The corresponding coefficients for each case can be systematically organized, as shown in Table 3.4.

doi:10.6342/NTU202503442

Table 3.4: Coefficients for PCP delay formulas.

Case Pi	$i=0$	$i=1$	$i=2$
$\boldsymbol{t^2_{PR}}$	$\frac{a_p}{2}$	$\frac{a_p}{2}$	$\frac{a_p}{2}$
$\boldsymbol{t^2_{PE}}$	$\frac{a_p-s_{p0}}{2}$	$\frac{a_p-s_{p0}}{2}$	$\frac{a_p-s_{p0}}{2}$
$\boldsymbol{t^2_{PG}}$			$\frac{s_{p1}-s_{p2}}{2}$
$\boldsymbol{t^2_{Pi}}$	$\frac{a_p-s_{p0}}{2}$	$\frac{a_p-s_{p1}}{2}$	$\frac{a_p-s_{p2}}{2}$
$\boldsymbol{t_{PR}t_{PE}}$	a_p	a_p	a_p
$\boldsymbol{t_{PR}t_{Pi}}$	a_p	a_p	a_p
$\boldsymbol{t_{PE}t_{Pi}}$	$a_p - s_{p0}$	$a_p - s_{p0}$	$a_p - s_{p0}$
$\boldsymbol{t_{PG}t_{Pi}}$			$-s_{p1} + s_{p2}$

3.4.3 RTV Delay Formulas

Under each PCP delay case, there are originally six distinct delay cases for RTV movements. However, as illustrated in Figures 3.12, 3.13, and 3.14, it can be observed that during certain time intervals, when the PCP discharge rate remains unchanged, the corresponding RTV delay cases can be simplified. Specifically, some RTV discharge rates can be treated as equal, resulting in delay formulas that share similar expressions and structures.

In Case P0, the RTV delay cases range from P0V1 to P0V6. Among them, **Cases P0V1, P0V2, P0V3, and P0V4 can be grouped together** because their discharge lines share the same constant slope (s_{v4}) after the start of the RTV green phase until they intersect the arrival line (before the PCP red phase begins). These cases also share identical expressions for the intersection time point between the AL and DL. Therefore, when $0 < t_{P0V1} = t_{P0V2} = t_{P0V3} = t_{P0V4} \leq t_{PG} + t_{PY}$, the RTV delay can be represented by Case P0V4 (i.e., $\delta_{P0V4} = 1$).

doi:10.6342/NTU202503442

In Case P1, the RTV delay cases range from P1V1 to P1V6. Among them, **Cases P1V2, P1V3, and P1V4 can be grouped together** because their discharge lines share the same constant slope (s_{v4}) after the time point t_{P1} until they intersect the arrival line (before the PCP red phase begins). These cases also share identical expressions for the intersection time point between the AL and DL. Therefore, when $t_{P1} < t_{P0V2} = t_{P0V3} = t_{P0V4} \leq t_{PG} + t_{PY}$, the RTV delay can be represented by Case P1V4 (i.e., $\delta_{P1V4} = 1$).

In Case P2, the RTV delay cases range from P2V1 to P2V6. Among them, **Cases P2V1 and P2V2 can be grouped together** because their discharge lines share the same constant slope (s_{v1}) after the start of the RTV green phase until they intersect the arrival line (before the time point t_{P2}). These cases also share identical expressions for the intersection time point between the AL and DL. Therefore, when $0 < t_{P2V1} = t_{P2V2} \leq t_{P2}$, the RTV delay can be represented by Case P2V1 (i.e., $\delta_{P2V1} = 1$).

To sum up, **the RTV delay cases can be simplified and reduced from 18 to 12 cases,** which include three under P0, four under P1, and five under P2. Similarly, all time-related terms in these twelve RTV delay formulas are quadratic. As the case index j increases, the delay shapes become more complex; however, the formulas maintain a consistent structural pattern. The corresponding coefficients for each case can be systematically organized, as shown in Tables 3.5, 3.6 and 3.7.

doi:10.6342/NTU202503442

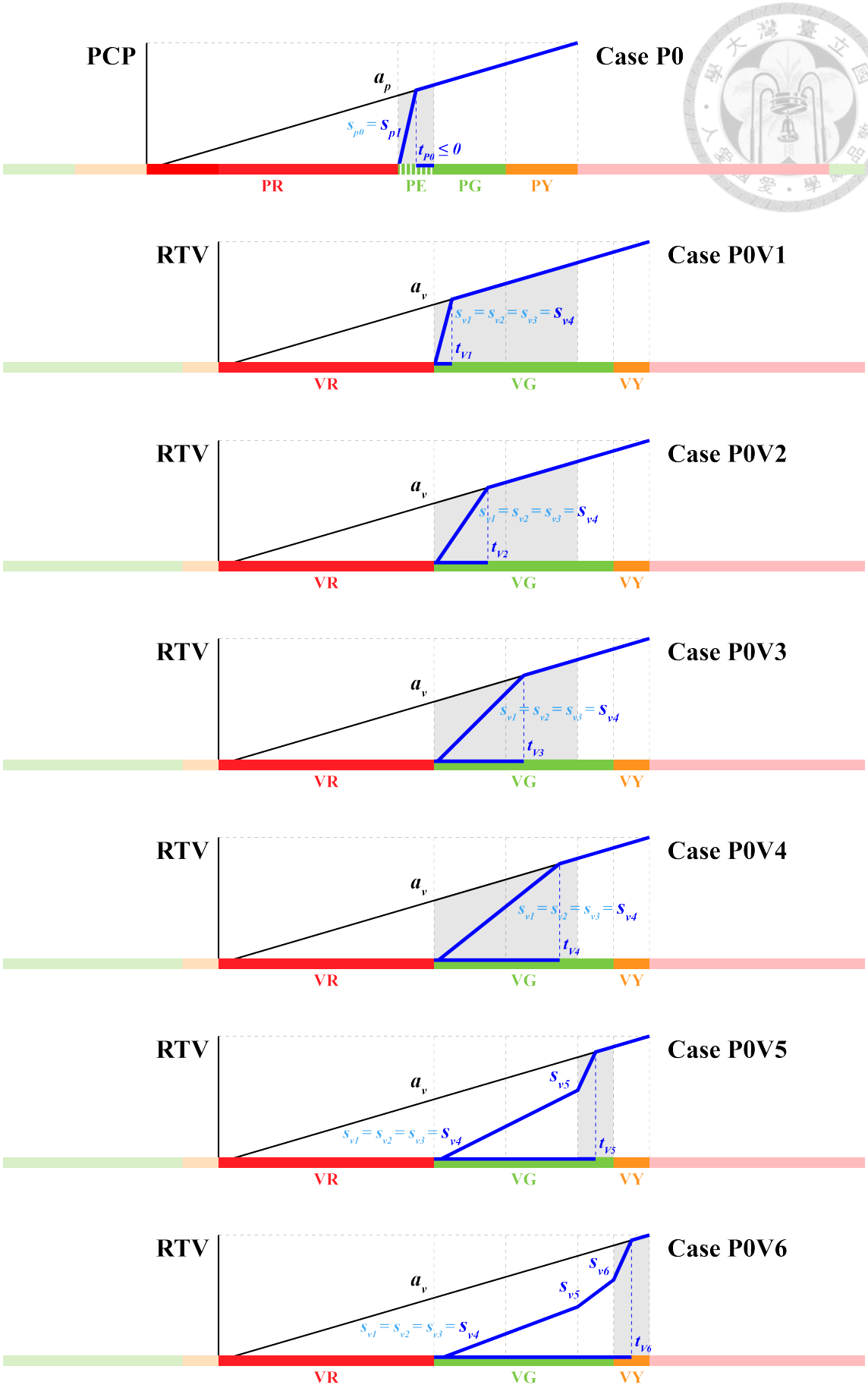

Figure 3.12: Right-turning vehicle (RTV) delay models under the P0 case.

doi:10.6342/NTU202503442

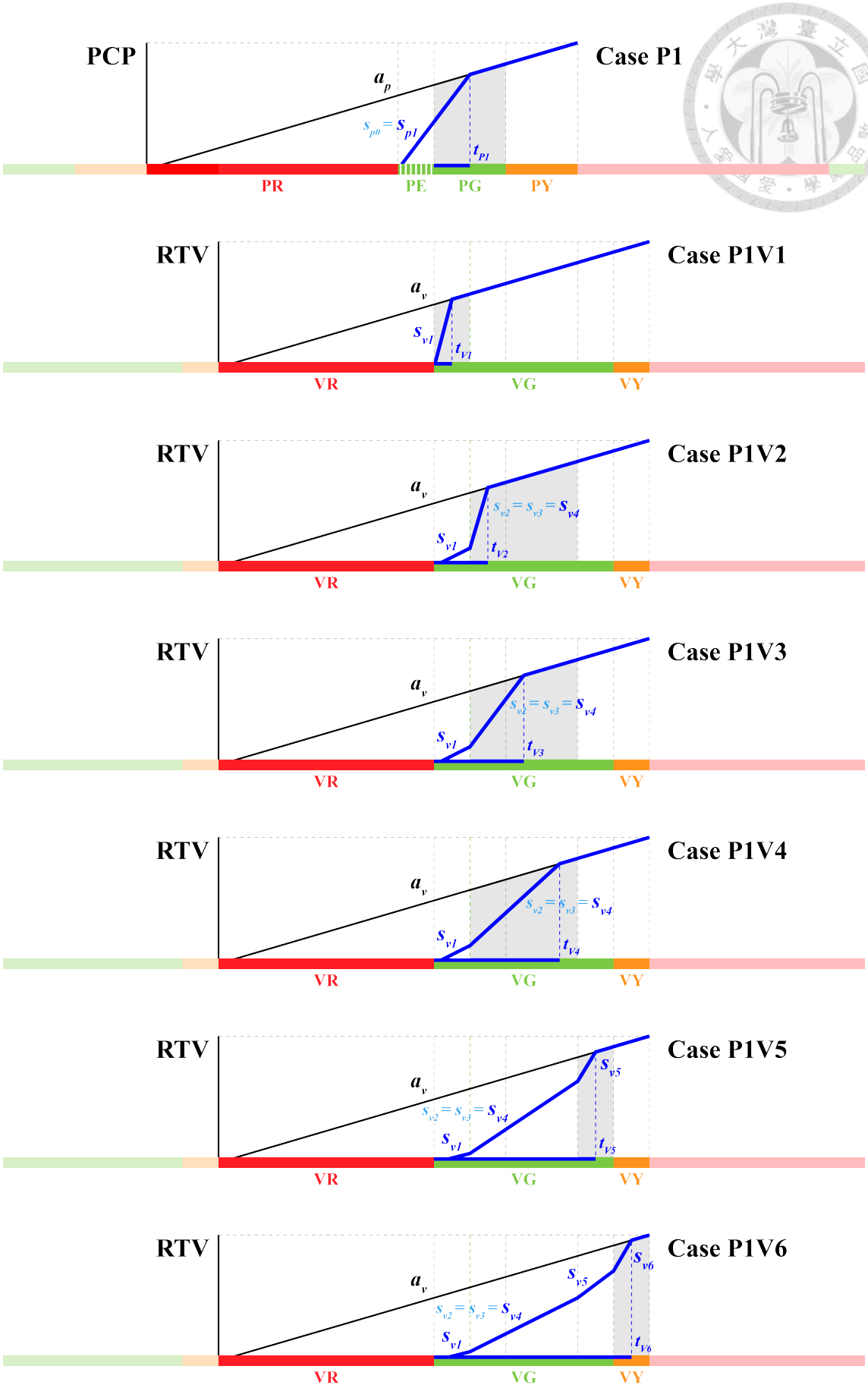

Figure 3.13: Right-turning vehicle (RTV) delay models under the P1 case.

doi:10.6342/NTU202503442

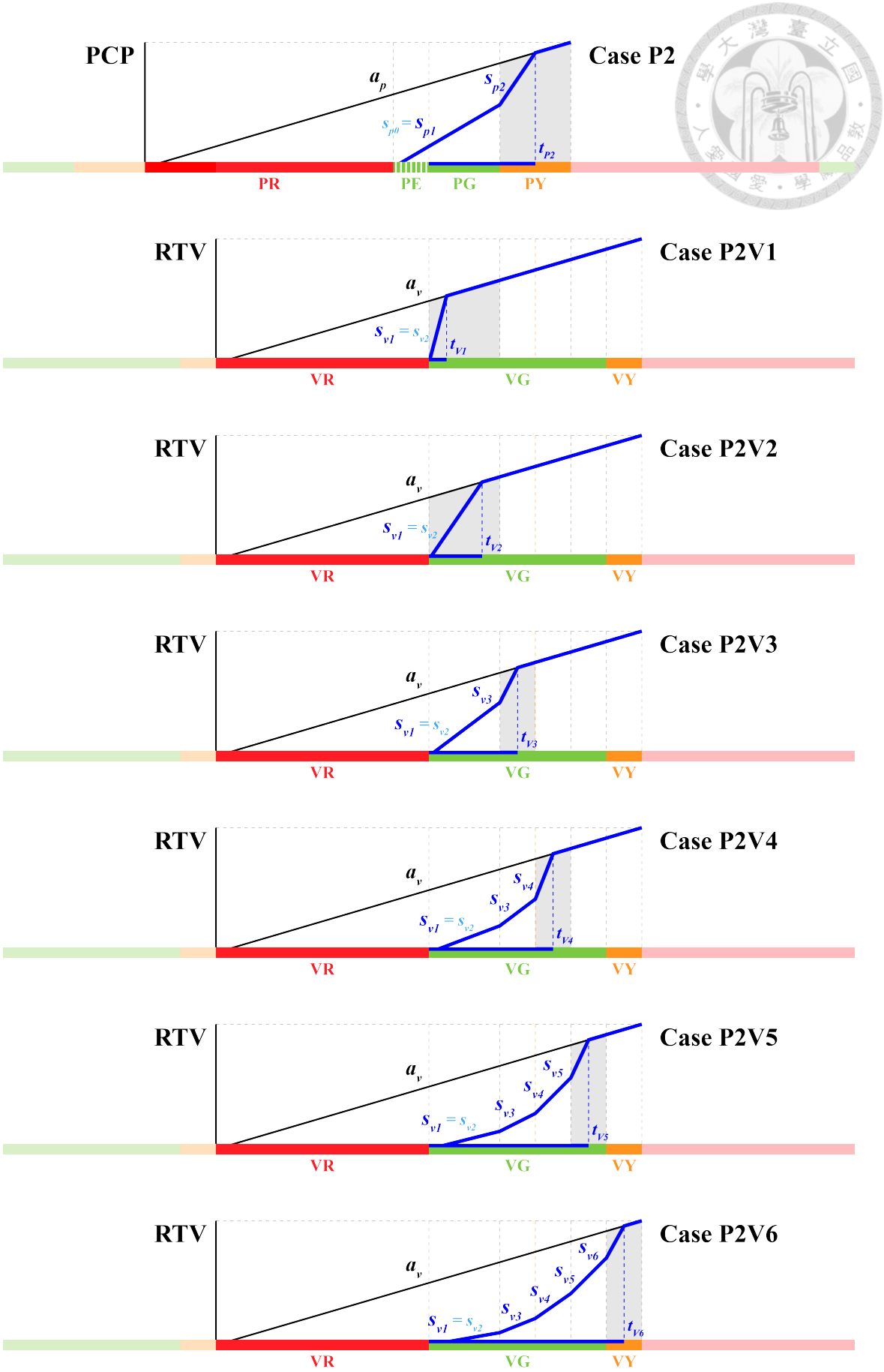

Figure 3.14: Right-turning vehicle (RTV) delay models under the P2 case.

doi:10.6342/NTU202503442

Case P0V4 Delay Formula

The delay expression is simplified and presented as Equation 3.4, which is valid when $0 < t_{PiVj} = t_{P0V4} <= t_{PG} + t_{PY}$.

$$D_{P0V4} = \left(\frac{a_v}{2}\right) t_{VR}^2 + \left(\frac{a_v - s_{v4}}{2}\right) t_{P0V4}^2 + (a_v)\, t_{VR} t_{V4} \tag{3.4}$$

Case P0V5 Delay Formula

The delay expression is simplified and presented as Equation 3.5, which is valid when $t_{PG} + t_{PY} < t_{PiVj} = t_{P0V5} <= t_{VG}$.

$$\begin{aligned} D_{P0V5} = {} & \left(\frac{a_v}{2}\right) t_{VR}^2 + \left(\frac{a_v - s_{v5}}{2}\right) t_{P0V5}^2 + \left(\frac{s_{v4} - s_{v5}}{2}\right) t_{PG}^2 + \\ & \left(\frac{s_{v4} - s_{v5}}{2}\right) t_{PY}^2 + (s_{v4} - s_{v5})\, t_{PG} t_{PY} + \\ & (a_v)\, t_{VR} t_{P0V5} + (-s_{v4} + s_{v5})\, t_{PG} t_{P0V5} + (-s_{v4} + s_{v5})\, t_{PY} t_{P0V5} \end{aligned} \tag{3.5}$$

Case P0V6 Delay Formula

The delay expression is simplified and presented as Equation 3.6, which is valid when $t_{VG} < t_{PiVj} = t_{P0V6} <= t_{VG} + t_{VY}$.

$$\begin{aligned} D_{P0V6} = {} & \left(\frac{a_v}{2}\right) t_{VR}^2 + \left(\frac{a_v - s_{v6}}{2}\right) t_{P0V6}^2 + \left(\frac{s_{v4} - s_{v5}}{2}\right) t_{PG}^2 + \\ & \left(\frac{s_{v4} - s_{v5}}{2}\right) t_{PY}^2 + (s_{v4} - s_{v5})\, t_{PG} t_{PY} + \left(\frac{s_{v5} - s_{v6}}{2}\right) t_{VG}^2 + \\ & (a_v)\, t_{VR} t_{P0V6} + (-s_{v4} + s_{v5})\, t_{PG} t_{P0V6} + (-s_{v4} + s_{v5})\, t_{PY} t_{P0V6} + \\ & (-s_{v5} + s_{v6})\, t_{VG} t_{P0V6} \end{aligned} \tag{3.6}$$

doi:10.6342/NTU202503442

Case P1V1 Delay Formula

The delay expression is simplified and presented as Equation 3.7, which is valid when $0 < t_{PiVj} = t_{P1V1} <= t_{P1}$.

$$D_{P1V1} = \left(\frac{a_v}{2}\right) t_{VR}^2 + \left(\frac{a_v - s_{v1}}{2}\right) t_{P1V1}^2 + (a_v)\, t_{VR} t_{P1V1} \tag{3.7}$$

Case P1V4 Delay Formula

The delay expression is simplified and presented as Equation 3.8, which is valid when $t_{P1} < t_{PiVj} = t_{P1V4} <= t_{PG} + t_{PY}$.

$$D_{P1V4} = \left(\frac{a_v}{2}\right) t_{VR}^2 + \left(\frac{a_v - s_{v4}}{2}\right) t_{P1V4}^2 + \left(\frac{s_{v1} - s_{v4}}{2}\right) t_{P1}^2 + (a_v)\, t_{VR} t_{P1V4} + (-s_{v1} + s_{v4})\, t_{P1} t_{P1V4} \tag{3.8}$$

Case P1V5 Delay Formula

The delay expression is simplified and presented as Equation 3.9, which is valid when $t_{PG} + t_{PY} < t_{PiVj} = t_{P1V5} <= t_{VG}$.

$$\begin{aligned} D_{P1V5} = {} & \left(\frac{a_v}{2}\right) t_{VR}^2 + \left(\frac{a_v - s_{v5}}{2}\right) t_{P1V5}^2 + \left(\frac{s_{v1} - s_{v4}}{2}\right) t_{P1}^2 + \left(\frac{s_{v4} - s_{v5}}{2}\right) t_{PG}^2 + \\ & \left(\frac{s_{v4} - s_{v5}}{2}\right) t_{PY}^2 + (s_{v4} - s_{v5})\, t_{PG} t_{PY} + \\ & (a_v)\, t_{VR} t_{P1V5} + (-s_{v1} + s_{v4})\, t_{P1} t_{P1V5} + (-s_{v4} + s_{v5})\, t_{PG} t_{P1V5} + \\ & (-s_{v4} + s_{v5})\, t_{PY} t_{P1V5} \end{aligned} \tag{3.9}$$

doi:10.6342/NTU202503442

Case P1V6 Delay Formula

The delay expression is simplified and presented as Equation 3.10, which is valid when $t_{VG} < t_{PiVj} = t_{P1V6} <= t_{VG} + t_{VY}$.

$$\begin{aligned} D_{P1V6} = & \left(\frac{a_v}{2}\right) t_{VR}^2 + \left(\frac{a_v - s_{v6}}{2}\right) t_{P1V6}^2 + \left(\frac{s_{v1} - s_{v4}}{2}\right) t_{P1}^2 + \left(\frac{s_{v4} - s_{v5}}{2}\right) t_{PG}^2 + \\ & \left(\frac{s_{v4} - s_{v5}}{2}\right) t_{PY}^2 + (s_{v4} - s_{v5})\, t_{PG} t_{PY} + \left(\frac{s_{v5} - s_{v6}}{2}\right) t_{VG}^2 + \\ & (a_v)\, t_{VR} t_{P1V6} + (-s_{v1} + s_{v4})\, t_{P1} t_{P1V6} + (-s_{v4} + s_{v5})\, t_{PG} t_{P1V6} + \\ & (-s_{v4} + s_{v5})\, t_{PY} t_{P1V6} + (-s_{v5} + s_{v6})\, t_{VG} t_{P1V6} \end{aligned} \tag{3.10}$$

Case P2V1 Delay Formula

The delay expression is simplified and presented as Equation 3.11, which is valid when $0 < t_{PiVj} = t_{P2V1} <= t_{PG}$.

$$\begin{aligned} D_{P2V1} = & \left(\frac{a_v}{2}\right) t_{VR}^2 + \left(\frac{a_v - s_{v1}}{2}\right) t_{P2V1}^2 + \\ & (a_v)\, t_{VR} t_{P2V1} \end{aligned} \tag{3.11}$$

Case P2V3 Delay Formula

The delay expression is simplified and presented as Equation 3.12, which is valid when $t_{PG} < t_{PiVj} = t_{P2V3} <= t_{P2}$.

$$\begin{aligned} D_{P2V3} = & \left(\frac{a_v}{2}\right) t_{VR}^2 + \left(\frac{a_v - s_{v3}}{2}\right) t_{P2V3}^2 + \left(\frac{s_{v1} - s_{v3}}{2}\right) t_{PG}^2 + \\ & (a_v)\, t_{VR} t_{P2V3} + (-s_{v1} + s_{v3})\, t_{PG} t_{P2V3} \end{aligned} \tag{3.12}$$

doi:10.6342/NTU202503442

Case P2V4 Delay Formula

The delay expression is simplified and presented as Equation 3.13, which is valid when $t_{P2} < t_{PiVj} = t_{P2V4} <= t_{PG} + t_{PY}$.

$$\begin{aligned} D_{P2V4} = & \left(\frac{a_v}{2}\right) t_{VR}^2 + \left(\frac{a_v - s_{v4}}{2}\right) t_{P2V4}^2 + \left(\frac{s_{v1} - s_{v3}}{2}\right) t_{PG}^2 + \left(\frac{s_{v3} - s_{v4}}{2}\right) t_{P2}^2 + \\ & (a_v)\, t_{VR} t_{P2V4} + (-s_{v1} + s_{v3})\, t_{PG} t_{P2V4} + (-s_{v3} + s_{v4})\, t_{P2} t_{P2V4} \end{aligned} \tag{3.13}$$

Case P2V5 Delay Formula

The delay expression is simplified and presented as Equation 3.14, which is valid when $t_{PG} + t_{PY} < t_{PiVj} = t_{P2V5} <= t_{VG}$.

$$\begin{aligned} D_{P2V5} = & \left(\frac{a_v}{2}\right) t_{VR}^2 + \left(\frac{a_v - s_{v5}}{2}\right) t_{P2V5}^2 + \left(\frac{s_{v1} - s_{v3}}{2} + \frac{s_{v4} - s_{v5}}{2}\right) t_{PG}^2 + \\ & \left(\frac{s_{v3} - s_{v4}}{2}\right) t_{P2}^2 + \left(\frac{s_{v4} - s_{v5}}{2}\right) t_{PY}^2 + (s_{v4} - s_{v5})\, t_{PG} t_{PY} + \\ & (a_v)\, t_{VR} t_{P2V5} + (-s_{v1} + s_{v3} - s_{v4} + s_{v5})\, t_{PG} t_{P2V5} + \\ & (-s_{v3} + s_{v4})\, t_{P2} t_{P2V5} + (-s_{v4} + s_{v5})\, t_{PY} t_{P2V5} \end{aligned} \tag{3.14}$$

Case P2V6 Delay Formula

The delay expression is simplified and presented as Equation 3.15, which is valid when $t_{VG} < t_{PiVj} = t_{P2V6} <= t_{VG} + t_{VY}$.

$$\begin{aligned} D_{P2V6} = & \left(\frac{a_v}{2}\right) t_{VR}^2 + \left(\frac{a_v - s_{v6}}{2}\right) t_{P2V6}^2 + \left(\frac{s_{v1} - s_{v3}}{2} + \frac{s_{v4} - s_{v5}}{2}\right) t_{PG}^2 + \\ & \left(\frac{s_{v3} - s_{v4}}{2}\right) t_{P2}^2 + \left(\frac{s_{v4} - s_{v5}}{2}\right) t_{PY}^2 + (s_{v4} - s_{v5})\, t_{PG} t_{PY} + \\ & \left(\frac{s_{v5} - s_{v6}}{2}\right) t_{VG}^2 + (a_v)\, t_{VR} t_{P2V6} + \\ & (-s_{v1} + s_{v3} - s_{v4} + s_{v5})\, t_{PG} t_{P2V6} + (-s_{v3} + s_{v4})\, t_{P2} t_{P2V6} + \\ & (-s_{v4} + s_{v5})\, t_{PY} t_{P2V6} + (-s_{v5} + s_{v6})\, t_{VG} t_{P2V6} \end{aligned} \tag{3.15}$$

doi:10.6342/NTU202503442

Table 3.5: Coefficients for RTV delay formulas under the P0 case.

Case $P0Vj$	$j = 1, 2, 3, 4$	$j = 5$	$j = 6$
$\boldsymbol{t^2_{VR}}$	$\frac{a_v}{2}$	$\frac{a_v}{2}$	$\frac{a_v}{2}$
$\boldsymbol{t^2_{PG}}$		$\frac{s_{v4}-s_{v5}}{2}$	$\frac{s_{v4}-s_{v5}}{2}$
$\boldsymbol{t^2_{PY}}$		$\frac{s_{v4}-s_{v5}}{2}$	$\frac{s_{v4}-s_{v5}}{2}$
$\boldsymbol{t_{PG}t_{PY}}$		$s_{v4} - s_{v5}$	$s_{v4} - s_{v5}$
$\boldsymbol{t^2_{VG}}$			$\frac{s_{v5}-s_{v6}}{2}$
$\boldsymbol{t^2_{Vj}}$	$\frac{a_v-s_{v4}}{2}$	$\frac{a_v-s_{v5}}{2}$	$\frac{a_v-s_{v6}}{2}$
$\boldsymbol{t_{VR}t_{Vj}}$	a_v	a_v	a_v
$\boldsymbol{t_{PG}t_{Vj}}$		$-s_{v4} + s_{v5}$	$-s_{v4} + s_{v5}$
$\boldsymbol{t_{PY}t_{Vj}}$		$-s_{v4} + s_{v5}$	$-s_{v4} + s_{v5}$
$\boldsymbol{t_{VG}t_{Vj}}$			$-s_{v5} + s_{v6}$

Table 3.6: Coefficients for RTV delay formulas under the P1 case.

Case $P1Vj$	$j = 1$	$j = 2, 3, 4$	$j = 5$	$j = 6$
$\boldsymbol{t^2_{VR}}$	$\frac{a_v}{2}$	$\frac{a_v}{2}$	$\frac{a_v}{2}$	$\frac{a_v}{2}$
$\boldsymbol{t^2_{P1}}$		$\frac{s_{v1}-s_{v4}}{2}$	$\frac{s_{v1}-s_{v4}}{2}$	$\frac{s_{v1}-s_{v4}}{2}$
$\boldsymbol{t^2_{PG}}$			$\frac{s_{v4}-s_{v5}}{2}$	$\frac{s_{v4}-s_{v5}}{2}$
$\boldsymbol{t^2_{PY}}$			$\frac{s_{v4}-s_{v5}}{2}$	$\frac{s_{v4}-s_{v5}}{2}$
$\boldsymbol{t_{PG}t_{PY}}$			$s_{v4} - s_{v5}$	$s_{v4} - s_{v5}$
$\boldsymbol{t^2_{VG}}$				$\frac{s_{v5}-s_{v6}}{2}$
$\boldsymbol{t^2_{Vj}}$	$\frac{a_v-s_{v1}}{2}$	$\frac{a_v-s_{v4}}{2}$	$\frac{a_v-s_{v5}}{2}$	$\frac{a_v-s_{v6}}{2}$
$\boldsymbol{t_{VR}t_{Vj}}$	a_v	a_v	a_v	a_v
$\boldsymbol{t_{P1}t_{Vj}}$		$-s_{v1} + s_{v4}$	$-s_{v1} + s_{v4}$	$-s_{v1} + s_{v4}$
$\boldsymbol{t_{PG}t_{Vj}}$			$-s_{v4} + s_{v5}$	$-s_{v4} + s_{v5}$
$\boldsymbol{t_{PY}t_{Vj}}$			$-s_{v4} + s_{v5}$	$-s_{v4} + s_{v5}$
$\boldsymbol{t_{VG}t_{Vj}}$				$-s_{v5} + s_{v6}$

doi:10.6342/NTU202503442

Table 3.7: Coefficients for RTV delay formulas under the P2 case.

Case $P2Vj$	$j=1,2$	$j=3$	$j=4$	$j=5$	$j=6$
$\boldsymbol{t_{VR}^2}$	$\frac{a_v}{2}$	$\frac{a_v}{2}$	$\frac{a_v}{2}$	$\frac{a_v}{2}$	$\frac{a_v}{2}$
$\boldsymbol{t_{PG}^2}$		$\frac{s_{v1}-s_{v3}}{2}$	$\frac{s_{v1}-s_{v3}}{2}$	$\frac{s_{v1}-s_{v3}}{2}+$	$\frac{s_{v1}-s_{v3}}{2}+$
				$\frac{s_{v4}-s_{v5}}{2}$	$\frac{s_{v4}-s_{v5}}{2}$
$\boldsymbol{t_{P2}^2}$			$\frac{s_{v3}-s_{v4}}{2}$	$\frac{s_{v3}-s_{v4}}{2}$	$\frac{s_{v3}-s_{v4}}{2}$
$\boldsymbol{t_{PY}^2}$				$\frac{s_{v4}-s_{v5}}{2}$	$\frac{s_{v4}-s_{v5}}{2}$
$\boldsymbol{t_{PG}t_{PY}}$				$s_{v4}-s_{v5}$	$s_{v4}-s_{v5}$
$\boldsymbol{t_{VG}^2}$					$\frac{s_{v5}-s_{v6}}{2}$
$\boldsymbol{t_{Vj}^2}$	$\frac{a_v-s_{v1}}{2}$	$\frac{a_v-s_{v3}}{2}$	$\frac{a_v-s_{v4}}{2}$	$\frac{a_v-s_{v5}}{2}$	$\frac{a_v-s_{v6}}{2}$
$\boldsymbol{t_{VR}t_{Vj}}$	a_v	a_v	a_v	a_v	a_v
$\boldsymbol{t_{PG}t_{Vj}}$		$-s_{v1}+s_{v3}$	$-s_{v1}+s_{v3}$	$-s_{v1}+s_{v3}$	$-s_{v1}+s_{v3}$
			$-s_{v4}+s_{v5}$	$-s_{v4}+s_{v5}$	
$\boldsymbol{t_{P2}t_{Vj}}$			$-s_{v3}+s_{v4}$	$-s_{v3}+s_{v4}$	$-s_{v3}+s_{v4}$
$\boldsymbol{t_{PY}t_{Vj}}$				$-s_{v4}+s_{v5}$	$-s_{v4}+s_{v5}$
$\boldsymbol{t_{VG}t_{Vj}}$					$-s_{v5}+s_{v6}$

doi:10.6342/NTU202503442

3.5 Objective Functions and Constraints

3.5.1 Objective Functions

Recall that the objectives are, in respective:

- **Obj-1:** Minimize the overall (PCP and RTV) average delay within a signal cycle
- **Obj-2:** Minimize the difference in average delay between the two movements

$$\min D_{avg} = \min \frac{\sum_{i\in\mathbb{I}} \delta_{Pi} D_{Pi} + \sum_{i\in\mathbb{I}} \sum_{j\in\mathbb{J}} \delta_{PiVj} D_{PiVj}}{a_p C + a_v C} \tag{3.16}$$

$$\min \left| \frac{\sum_{i\in\mathbb{I}} \delta_{Pi} D_{Pi}}{a_p C} - \frac{\sum_{i\in\mathbb{I}} \sum_{j\in\mathbb{J}} \delta_{PiVj} D_{PiVj}}{a_v C} \right| \tag{3.17}$$

3.5.2 Signal Timing-Related Constraints

A signal cycle consists of green, yellow, and red phases for both PCP and RTV movements. Since this study focuses on pedestrian signal adjustments, the durations of the red and green phases are required to remain within predefined upper and lower bounds to ensure effective discharge and to avoid introducing additional conflicts (see Equations 3.18 to 3.21).

$$C = t_{PE} + t_{PG} + t_{PY} + t_{PR} \tag{3.18}$$

$$C = t_{VG} + t_{VY} + t_{VR} \tag{3.19}$$

$$t_{PG_{min}} \leq t_{PG} \leq t_{PG_{max}} \tag{3.20}$$

$$t_{PR_{min}} \leq t_{PR} \leq t_{PR_{max}} \tag{3.21}$$

doi:10.6342/NTU202503442

3.5.3 Delay Area Enclosure Constraints

To ensure that the delay areas in the multi-delay models are properly enclosed, it is essential that the Discharge Line (DL) intersects the Arrival Line (AL) within a single signal cycle. This condition guarantees that all arriving entities are eventually discharged, thereby preventing oversaturation.

Since the DLs are modeled as piecewise linear functions, we impose a logical constraint: the slope of the final segment of each DL must be greater than that of the corresponding AL. If a given parameter set fails to satisfy this intersection condition, the associated binary variable (δ_{Pi} or δ_{Vj}) is set to zero, indicating that the corresponding delay case is infeasible and thus not selected (see Equations 3.22 and 3.23).

$$s_{pi} \geq a_p + \epsilon - M(1 - \delta_{Pi}), \quad \forall i \in \mathbb{I} \tag{3.22}$$

$$s_{vj} \geq a_v + \epsilon - M(1 - \delta_{PiVj}), \quad \forall i \in \mathbb{I}, \forall j \in \mathbb{J} \tag{3.23}$$

3.5.4 Intersection Timepoint Constraints

To correctly activate each delay case, the intersection timepoints (t_{Pi} or t_{PiVj}) must lie within a predefined time interval. If this condition is satisfied, the corresponding binary variable (δ_{Pi} or δ_{PiVj}) is set to 1; otherwise, it remains 0.

$$t_{P0} \geq -t_{PE} + \epsilon - M(1 - \delta_{P0}) \tag{3.24}$$

$$t_{P0} \leq 0 + M(1 - \delta_{P0}) \tag{3.25}$$

doi:10.6342/NTU202503442

$$t_{P1} \geq 0 + \epsilon - M(1 - \delta_{P1}) \tag{3.26}$$

$$t_{P1} \leq t_{PG} + M(1 - \delta_{P1}) \tag{3.27}$$

$$t_{P2} \geq -t_{PG} + \epsilon - M(1 - \delta_{P2}) \tag{3.28}$$

$$t_{P2} \leq t_{PG} + t_{PY} + M(1 - \delta_{P2}) \tag{3.29}$$

$$t_{P0V4} \geq \epsilon - M(1 - \delta_{P0V4}) \tag{3.30}$$

$$t_{P0V4} \leq t_{PG} + t_{PY} + M(1 - \delta_{P0V4}) \tag{3.31}$$

$$t_{P0V5} \geq t_{PG} + t_{PY} + \epsilon - M(1 - \delta_{P0V5}) \tag{3.32}$$

$$t_{P0V5} \leq t_{VG} + M(1 - \delta_{P0V5}) \tag{3.33}$$

$$t_{P0V6} \geq t_{VG} + \epsilon - M(1 - \delta_{P0V6}) \tag{3.34}$$

$$t_{P0V6} \leq t_{VG} + t_{VY} + M(1 - \delta_{P0V6}) \tag{3.35}$$

$$t_{P1V1} \geq \epsilon - M(1 - \delta_{P1V1}) \tag{3.36}$$

$$t_{P1V1} \leq t_{P1} + M(1 - \delta_{P1V1}) \tag{3.37}$$

$$t_{PiVj} \geq t_{P1} + \epsilon - M(1 - \delta_{P1V4}) \tag{3.38}$$

$$t_{PiVj} \leq t_{PG} + t_{PY} + M(1 - \delta_{P1V4}) \tag{3.39}$$

$$t_{PiVj} \geq t_{PG} + t_{PY} + \epsilon - M(1 - \delta_{P1V5}) \tag{3.40}$$

$$t_{PiVj} \leq t_{VG} + M(1 - \delta_{P1V5}) \tag{3.41}$$

$$t_{PiVj} \geq t_{VG} + \epsilon - M(1 - \delta_{P1V6}) \tag{3.42}$$

$$t_{PiVj} \leq t_{VG} + t_{VY} + M(1 - \delta_{P1V6}) \tag{3.43}$$

doi:10.6342/NTU202503442

$$t_{P2V1} \geq \epsilon - M(1 - \delta_{P2V1}) \tag{3.44}$$

$$t_{P2V1} \leq t_{PG} + M(1 - \delta_{P2V1}) \tag{3.45}$$

$$t_{P2V3} \geq t_{PG} + \epsilon - M(1 - \delta_{P2V3}) \tag{3.46}$$

$$t_{P2V3} \leq t_{P2} + M(1 - \delta_{P2V3}) \tag{3.47}$$

$$t_{P2V4} \geq t_{P2} + \epsilon - M(1 - \delta_{P2V4}) \tag{3.48}$$

$$t_{P2V4} \leq t_{PG} + t_{PY} + M(1 - \delta_{P2V4}) \tag{3.49}$$

$$t_{P2V5} \geq t_{PG} + t_{PY} + \epsilon - M(1 - \delta_{P2V5}) \tag{3.50}$$

$$t_{P2V5} \leq t_{VG} + M(1 - \delta_{P2V5}) \tag{3.51}$$

$$t_{P2V6} \geq t_{VG} + \epsilon - M(1 - \delta_{P2V6}) \tag{3.52}$$

$$t_{P2V6} \leq t_{VG} + t_{VY} + M(1 - \delta_{P2V6}) \tag{3.53}$$

According to the discussion in Section 3.4.3, Case P0V1, P0V2, and P0V3 share the same delay pattern as P0V4; P1V2 and P1V3 share the same delay pattern as P1V4; and P2V2 shares the same delay pattern as P2V1. Therefore, these six cases are simplified and excluded from the delay case selection.

$$\delta_{P0V1} = \delta_{P0V2} = \delta_{P0V3} = 0 \tag{3.54}$$

$$\delta_{P1V2} = \delta_{P1V3} = 0 \tag{3.55}$$

$$\delta_{P2V2} = 0 \tag{3.56}$$

doi:10.6342/NTU202503442

3.5.5 Volume Conservation Constraints

To ensure a proper balance between arrivals and discharges before the end of a signal cycle, it is essential to maintain volume conservation. Specifically, the total arrival volume must equal the total discharge volume at the intersection timepoints, which are denoted as t_{Pi} for the PCP delay model and t_{PiVj} for the RTV delay model. Refer to Figures 3.11, 3.12, 3.13, and 3.14 for graphical illustrations, and we begin by examining Case P0 as an example:

Case P0 Volume Conservation

$$(t_{PR} + t_{PE} + t_{P0})\, a_p = (t_{PE} + t_{P0})\, s_{p1}$$

Since the parameters (arrival rates, discharge rates, and certain fixed signal timings) are predefined, the above equation can be rearranged into a closed-form expression for the intersection timepoint t_{P0}. This formulation can then be incorporated into the intersection timepoint constraints (Section 3.5.4) to determine which delay case is feasible. (All other cases can be derived using a similar rearrangement process and are omitted here for brevity.)

$$t_{P0} = \left(\frac{a_p}{s_{p1} - a_p}\right) t_{PR} - t_{PE} \tag{3.57}$$

Case P1 Volume Conservation

$$t_{P1} = \left(\frac{a_p}{s_{p1} - a_p}\right) t_{PR} - t_{PE} \tag{3.58}$$

doi:10.6342/NTU202503442

Case P2 Volume Conservation

$$t_{P2} = \left(\frac{a_p}{s_{p2} - a_p}\right) t_{PR} - \left(\frac{s_{p1} - a_p}{s_{p2} - a_p}\right) t_{PE} + \left(\frac{s_{p2} - s_{p1}}{s_{p2} - a_p}\right) t_{PG} \tag{3.59}$$

Equations 3.57 to 3.59 define the intersection timepoint formulas for PCP movements. When deriving the corresponding formulas for RTV movements, these expressions can be substituted into the RTV formulations as needed to simplify the resulting equations.

Case P0V4 Volume Conservation

$$t_{P0V4} = \left(\frac{a_v}{s_{v4} - a_v}\right) t_{VR} \tag{3.60}$$

Case P0V5 Volume Conservation

$$t_{P0V5} = \left(\frac{a_v}{s_{v5} - a_v}\right) t_{VR} - \left(\frac{s_{v5} - s_{v4}}{s_{v5} - a_v}\right) t_{PG} + \left(\frac{s_{v5} - s_{v4}}{s_{v5} - a_v}\right) t_{PY} \tag{3.61}$$

Case P0V6 Volume Conservation

$$\begin{aligned} t_{P0V6} = &\left(\frac{a_v}{s_{v5} - a_v}\right) t_{VR} - \left(\frac{s_{v5} - s_{v4}}{s_{v5} - a_v}\right) t_{PG} + \\ &\left(\frac{s_{v5} - s_{v4}}{s_{v5} - a_v}\right) t_{PY} + \left(\frac{s_{v6} - s_{v5}}{s_{v5} - a_v}\right) t_{VG} \end{aligned} \tag{3.62}$$

Case P1V1 Volume Conservation

$$t_{P1V1} = \left(\frac{a_v}{s_{v1} - a_v}\right) t_{VR} \tag{3.63}$$

doi:10.6342/NTU202503442

Case P1V4 Volume Conservation

$$t_{P1V4} = \left(\frac{a_v}{s_{v4} - a_v}\right) t_{VR} + \left(\frac{a_p \left(s_{v4} - s_{v1}\right)}{\left(s_{p1} - a_p\right)\left(s_{v4} - a_v\right)}\right) t_{PR} - \left(\frac{s_{v4} - s_{v1}}{s_{v4} - a_v}\right) t_{PE} \tag{3.64}$$

Case P1V5 Volume Conservation

$$\begin{aligned} t_{P1V5} = &\left(\frac{a_v}{s_{v5} - a_v}\right) t_{VR} + \left(\frac{a_p \left(s_{v4} - s_{v1}\right)}{\left(s_{p1} - a_p\right)\left(s_{v5} - a_v\right)}\right) t_{PR} - \left(\frac{s_{v4} - s_{v1}}{s_{v5} - a_v}\right) t_{PE} + \\ &\left(\frac{s_{v5} - s_{v4}}{s_{v5} - a_v}\right) t_{PG} + \left(\frac{s_{v5} - s_{v4}}{s_{v5} - a_v}\right) t_{PY} \end{aligned} \tag{3.65}$$

Case P1V6 Volume Conservation

$$\begin{aligned} t_{P1V6} = &\left(\frac{a_v}{s_{v6} - a_v}\right) t_{VR} + \left(\frac{a_p \left(s_{v4} - s_{v1}\right)}{\left(s_{p1} - a_p\right)\left(s_{v6} - a_v\right)}\right) t_{PR} - \left(\frac{s_{v4} - s_{v1}}{s_{v6} - a_v}\right) t_{PE} + \\ &\left(\frac{s_{v5} - s_{v4}}{s_{v6} - a_v}\right) t_{PG} + \left(\frac{s_{v5} - s_{v4}}{s_{v6} - a_v}\right) t_{PY} + \left(\frac{s_{v6} - s_{v5}}{s_{v6} - a_v}\right) t_{VG} \end{aligned} \tag{3.66}$$

Case P2V1 Volume Conservation

$$t_{P2V1} = \left(\frac{a_v}{s_{v1} - a_v}\right) t_{VR} \tag{3.67}$$

Case P2V3 Volume Conservation

$$t_{P2V3} = \left(\frac{a_v}{s_{v3} - a_v}\right) t_{VR} + \left(\frac{s_{v3} - s_{v1}}{s_{v3} - a_v}\right) t_{PG} \tag{3.68}$$

Case P2V4 Volume Conservation

$$\begin{aligned} t_{P2V4} = &\left(\frac{a_v}{s_{v4} - a_v}\right) t_{VR} + \left(\frac{s_{v3} - s_{v1}}{s_{v4} - a_v} + \frac{\left(s_{p2} - s_{p1}\right)\left(s_{v4} - s_{v3}\right)}{\left(s_{p2} - a_p\right)\left(s_{v4} - a_v\right)}\right) t_{PG} + \\ &\left(\frac{a_p \left(s_{v4} - s_{v3}\right)}{\left(s_{p2} - a_p\right)\left(s_{v4} - a_v\right)}\right) t_{PR} - \left(\frac{\left(s_{p1} - a_p\right)\left(s_{v4} - s_{v3}\right)}{\left(s_{p2} - a_p\right)\left(s_{v4} - a_v\right)}\right) t_{PE} \end{aligned} \tag{3.69}$$

doi:10.6342/NTU202503442

Case P2V5 Volume Conservation

$$
\begin{aligned}
t_{P2V5} = & \left(\frac{a_v}{s_{v5}-a_v}\right) t_{VR} + \\
& \left(\frac{s_{v3}-s_{v1}}{s_{v5}-a_v} + \frac{s_{v5}-s_{v4}}{s_{v5}-a_v} + \frac{(s_{p2}-s_{p1})(s_{v4}-s_{v3})}{(s_{p2}-a_p)(s_{v5}-a_v)}\right) t_{PG} + \\
& \left(\frac{a_p(s_{v4}-s_{v3})}{(s_{p2}-a_p)(s_{v5}-a_v)}\right) t_{PR} - \left(\frac{(s_{p1}-a_p)(s_{v4}-s_{v3})}{(s_{p2}-a_p)(s_{v5}-a_v)}\right) t_{PE} + \\
& \left(\frac{s_{v5}-s_{v4}}{s_{v5}-a_v}\right) t_{PY}
\end{aligned}
\tag{3.70}
$$

Case P2V6 Volume Conservation

$$
\begin{aligned}
t_{P2V6} = & \left(\frac{a_v}{s_{v6}-a_v}\right) t_{VR} + \\
& \left(\frac{s_{v3}-s_{v1}}{s_{v6}-a_v} + \frac{s_{v5}-s_{v4}}{s_{v6}-a_v} + \frac{(s_{p2}-s_{p1})(s_{v4}-s_{v3})}{(s_{p2}-a_p)(s_{v6}-a_v)}\right) t_{PG} + \\
& \left(\frac{a_p(s_{v4}-s_{v3})}{(s_{p2}-a_p)(s_{v6}-a_v)}\right) t_{PR} - \left(\frac{(s_{p1}-a_p)(s_{v4}-s_{v3})}{(s_{p2}-a_p)(s_{v6}-a_v)}\right) t_{PE} + \\
& \left(\frac{s_{v5}-s_{v4}}{s_{v6}-a_v}\right) t_{PY} + \left(\frac{s_{v6}-s_{v5}}{s_{v6}-a_v}\right) t_{VG}
\end{aligned}
\tag{3.71}
$$

As the case indices i and j increase, the intersection timepoint formulas become more complex while preserving a consistent structural pattern. Equations 3.57 to 3.71 can be systematically organized into coefficient tables (see Tables 3.8, 3.9, 3.10, and 3.11).

Table 3.8: Coefficients for PCP intersection timepoint formulas.

$\boldsymbol{t_{Pi}}$	$i=0$	$i=1$	$i=2$
$\boldsymbol{t_{PR}}$	$\frac{a_p}{s_{p0}-a_p}$	$\frac{a_p}{s_{p1}-a_p}$	$\frac{a_p}{s_{p2}-a_p}$
$\boldsymbol{t_{PE}}$	-1	-1	$-\frac{s_{p1}-a_p}{s_{p2}-a_p}$
$\boldsymbol{t_{PG}}$			$\frac{s_{p2}-s_{p1}}{s_{p2}-a_p}$

doi:10.6342/NTU202503442

Table 3.9: Coefficients for RTV intersection timepoint formulas under Case P0.

t_{P0Vj}	$j=1,2,3,4$	$j=5$	$j=6$
t_{VR}	$\frac{a_v}{s_{v4}-a_v}$	$\frac{a_v}{s_{v5}-a_v}$	$\frac{a_v}{s_{v6}-a_v}$
t_{PG}		$\frac{s_{v5}-s_{v4}}{s_{v5}-a_v}$	$\frac{s_{v5}-s_{v4}}{s_{v6}-a_v}$
t_{PY}		$\frac{s_{v5}-s_{v4}}{s_{v5}-a_v}$	$\frac{s_{v5}-s_{v4}}{s_{v6}-a_v}$
t_{VG}			$\frac{s_{v6}-s_{v5}}{s_{v6}-a_v}$

Table 3.10: Coefficients for RTV intersection timepoint formulas under Case P1.

t_{P1Vj}	$j=1$	$j=2,3,4$	$j=5$	$j=6$
t_{VR}	$\frac{a_v}{s_{v1}-a_v}$	$\frac{a_v}{s_{v4}-a_v}$	$\frac{a_v}{s_{v5}-a_v}$	$\frac{a_v}{s_{v6}-a_v}$
t_{PG}			$\frac{s_{v5}-s_{v4}}{s_{v5}-a_v}$	$\frac{s_{v5}-s_{v4}}{s_{v6}-a_v}$
t_{PR}		$\frac{a_p(s_{v4}-s_{v1})}{(s_{p1}-a_p)(s_{v4}-a_v)}$	$\frac{a_p(s_{v4}-s_{v1})}{(s_{p1}-a_p)(s_{v5}-a_v)}$	$\frac{a_p(s_{v4}-s_{v1})}{(s_{p1}-a_p)(s_{v6}-a_v)}$
t_{PE}		$-\frac{s_{v4}-s_{v1}}{s_{v4}-a_v}$	$-\frac{s_{v4}-s_{v1}}{s_{v5}-a_v}$	$-\frac{s_{v4}-s_{v1}}{s_{v6}-a_v}$
t_{PY}			$\frac{s_{v5}-s_{v4}}{s_{v5}-a_v}$	$\frac{s_{v5}-s_{v4}}{s_{v6}-a_v}$
t_{VG}				$\frac{s_{v6}-s_{v5}}{s_{v6}-a_v}$

Table 3.11: Coefficients for RTV intersection timepoint formulas under Case P2.

t_{P2Vj}	$j=1,2$	$j=3$	$j=4$	$j=5$	$j=6$
t_{VR}	$\frac{a_v}{s_{v1}-a_v}$	$\frac{a_v}{s_{v3}-a_v}$	$\frac{a_v}{s_{v4}-a_v}$	$\frac{a_v}{s_{v5}-a_v}$	$\frac{a_v}{s_{v6}-a_v}$
t_{PG}		$\frac{s_{v3}-s_{v1}}{s_{v3}-a_v}$	$\frac{s_{v3}-s_{v1}}{s_{v4}-a_v}$ $+\frac{(s_{p2}-s_{p1})(s_{v4}-s_{v3})}{(s_{p2}-a_p)(s_{v4}-a_v)}$	$\frac{s_{v3}-s_{v1}}{s_{v5}-a_v}+\frac{s_{v5}-s_{v4}}{s_{v5}-a_v}$ $+\frac{(s_{p2}-s_{p1})(s_{v4}-s_{v3})}{(s_{p2}-a_p)(s_{v5}-a_v)}$	$\frac{s_{v3}-s_{v1}}{s_{v6}-a_v}+\frac{s_{v5}-s_{v4}}{s_{v6}-a_v}$ $+\frac{(s_{p2}-s_{p1})(s_{v4}-s_{v3})}{(s_{p2}-a_p)(s_{v6}-a_v)}$
t_{PR}			$\frac{a_p(s_{v4}-s_{v3})}{(s_{p2}-a_p)(s_{v4}-a_v)}$	$\frac{a_p(s_{v4}-s_{v3})}{(s_{p2}-a_p)(s_{v5}-a_v)}$	$\frac{a_p(s_{v4}-s_{v3})}{(s_{p2}-a_p)(s_{v6}-a_v)}$
t_{PE}			$-\frac{(s_{p1}-a_p)(s_{v4}-s_{v3})}{(s_{p2}-a_p)(s_{v4}-a_v)}$	$-\frac{(s_{p1}-a_p)(s_{v4}-s_{v3})}{(s_{p2}-a_p)(s_{v5}-a_v)}$	$-\frac{(s_{p1}-a_p)(s_{v4}-s_{v3})}{(s_{p2}-a_p)(s_{v6}-a_v)}$
t_{PY}				$\frac{s_{v5}-s_{v4}}{s_{v5}-a_v}$	$\frac{s_{v5}-s_{v4}}{s_{v6}-a_v}$
t_{VG}					$\frac{s_{v6}-s_{v5}}{s_{v6}-a_v}$

doi:10.6342/NTU202503442

3.5.6 Other Constraints

For both PCP and RTV movements, exactly one delay case must be selected to represent the traffic condition at the signalized intersection.

$$\sum_{i \in \mathbb{I}} \delta_{Pi} = 1 \tag{3.72}$$

$$\sum_{i \in \mathbb{I}} \sum_{j \in \mathbb{J}} \delta_{PiVj} = 1 \tag{3.73}$$

Additionally, only the selected delay cases contribute to the total delay area calculation, and all delay values are required to be non-negative.

$$D_{Pi} \geq 0, \quad \forall i \in \mathbb{I} \tag{3.74}$$

$$D_{PiVj} \geq 0, \quad \forall i \in \mathbb{I}, j \in \mathbb{J} \tag{3.75}$$

$$D_{total_{PCP}} = \sum_{i \in \mathbb{I}} (\delta_{Pi} \cdot D_{Pi}) \tag{3.76}$$

$$D_{total_{RTV}} = \sum_{i \in \mathbb{I}} \sum_{j \in \mathbb{J}} (\delta_{PiVj} \cdot D_{PiVj}) \tag{3.77}$$

doi:10.6342/NTU202503442

3.6 Model Implementation

In summary, the proposed model is formulated as a Mixed-Integer Quadratically Constrained Programming (MIQCP) problem. While such models can be directly solved using commercial optimization solvers, we opt for a rule-based, step-by-step solution process, as it provides better clarity into the underlying decision logic and throughput relationships.

As illustrated in Figure 3.1, the implementation process begins with data input, followed by delay case identification through the calculation of intersection timepoints (using Equations 3.57 to 3.71). These identifications are then used to activate the corresponding delay formulas (see Equations 3.1 to 3.15). Throughout this process, the pedestrian green duration t_{PG} serves as the decision variable and is iteratively adjusted to minimize the defined objective (Equation 3.16 or 3.17). If no delay case satisfies the required conditions under the imposed constraints, it indicates that either the PCP or RTV movement becomes oversaturated at the given t_{PG} setting.

The resulting delay performance can be compared with outputs from the Vissim simulation software by measuring the average travel time difference between the signal-controlled condition and the free-flow condition, as detailed in Section 4.4.3. PTV Vissim is a microscopic, time-step-based, behavior-oriented simulation tool designed for the detailed modeling of both vehicular and pedestrian traffic in urban and interurban settings (PTV Group, 2025).

doi:10.6342/NTU202503442

doi:10.6342/NTU202503442

Chapter 4 Case Study

4.1 Site Selections

Since this research focuses on the interaction between Parallel-Crossing Pedestrians (PCPs) and Right-Turning Vehicles (RTVs), the selected intersections are expected to meet the following criteria:

1. Located within an urban area;
2. Medium to high PCP and RTV traffic volumes during peak hours;
3. A concurrent green phase for PCP and RTV movements on the target approach; and
4. Sufficient sidewalk space and visibility for camera observation.

Accordingly, the following intersections in Taipei City were selected for analysis. Signal timing data and traffic flow rates at these sites will be collected and examined:

- Bade Rd. and Guangfu N. Rd. intersection (八德光復路口)
- Heping E Rd. and Xinsheng S. Rd. intersection (和平新生路口)
- Songgao Rd. and Songren Rd. intersection (松高松仁路口)
- Zhongxiao E. Rd. and Guangfu S. Rd. intersection (忠孝光復路口)

4.2 Data Collection

The analysis of each isolated intersection requires information on the existing signal timing plans, as well as the discharge and arrival rates for each movement. These data are mainly obtained from government open-source datasets and field observations.

doi:10.6342/NTU202503442

4.2.1 Government Open-Source Datasets

The government's open-source datasets provide both traffic flow data and existing signal timing plans. The traffic flow information is available in the *2021 Taipei Traffic Volume and Characteristics Survey and 2022 Expansion Study of General Intersections, Roundabouts, and Road Sections* (2022), while the signal timing plans can be found in the *Taipei Intersection Signal Timing Plan* (2022).

Figure 4.1 presents a sample page from the *Traffic Volume and Characteristics Survey*, while Figure 4.2 displays a sample page from the *Signal Timing Plan*. Each investigation primarily focuses on a single pedestrian crosswalk and the corresponding approach of the conflicting right-turning vehicle movement.

However, the *Traffic Volume and Characteristics Survey* provides only peak-hour vehicular traffic flow data, without corresponding pedestrian flow information. Moreover, discharge rates for each time interval cannot be determined from the available data. As a result, on-site observations are necessary to obtain comprehensive traffic data. At the same time, peak-hour vehicular flow (used as arrival rates) should also be re-obtained to ensure volume conservation. **In summary, the survey serves only to identify candidate intersections; its data are not used.**

As for the *Taipei Signal Timing Plan*, it provides current information on stage sequences and the duration of each signal phase. A certain number of intersections adopt different timing combinations across various time intervals throughout the day. This study focuses on the peak-hour signal design, during which field observations were conducted as well. Minor adjustments were made to the phase durations to reflect slight discrepancies observed between the field data and the official timing plan.

doi:10.6342/NTU202503442

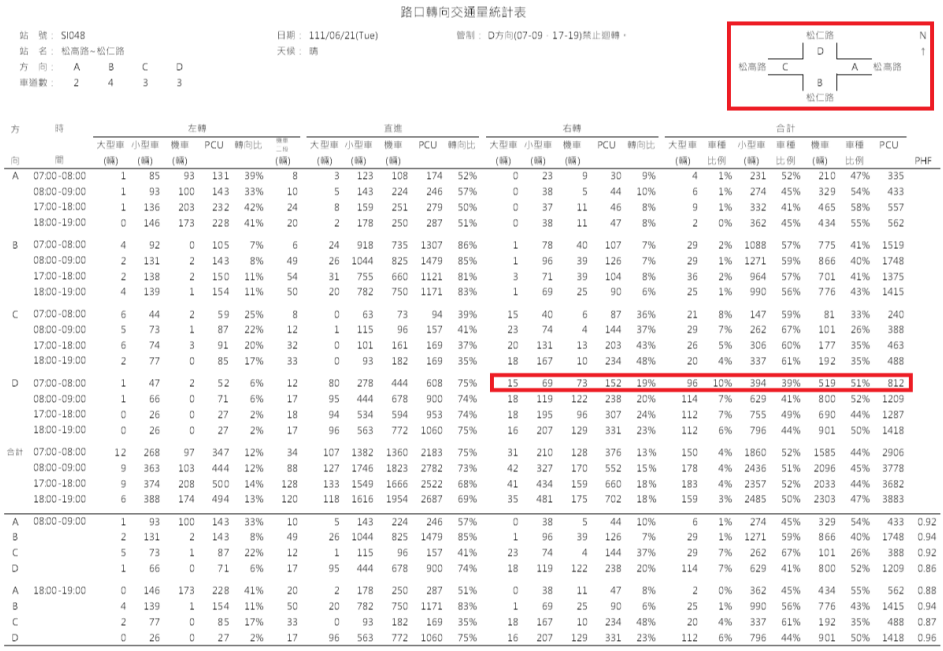

路口轉向交通量統計表

站　號：SI048　　日期：111/06/21(Tue)　　管制：D方向(07-09、17-19)禁止迴轉。
站　名：松高路~松仁路　　天候：晴
方　向：A　B　C　D
車道數：2　4　3　3

方向	時間	左轉 大型車(輛)	左轉 小型車(輛)	左轉 機車(輛)	左轉 PCU	左轉 轉向比	左轉 機車二向(輛)	直進 大型車(輛)	直進 小型車(輛)	直進 機車(輛)	直進 PCU	直進 轉向比	右轉 大型車(輛)	右轉 小型車(輛)	右轉 機車(輛)	右轉 PCU	右轉 轉向比	合計 大型車(輛)	合計 車種比例	合計 小型車(輛)	合計 車種比例	合計 機車(輛)	合計 車種比例	合計 PCU	PHF
A	07:00-08:00	1	85	93	131	39%	8	3	123	108	174	52%	0	23	9	30	9%	4	1%	231	52%	210	47%	335	
	08:00-09:00	1	93	100	143	33%	10	5	143	224	246	57%	0	38	5	44	10%	6	1%	274	45%	329	54%	433	
	17:00-18:00	1	136	203	232	42%	24	8	159	251	279	50%	0	37	11	46	8%	9	1%	332	41%	465	58%	557	
	18:00-19:00	0	146	173	228	41%	20	2	178	250	287	51%	0	38	11	47	8%	2	0%	362	45%	434	55%	562	
B	07:00-08:00	4	92	0	105	7%	6	24	918	735	1307	86%	1	78	40	107	7%	29	2%	1088	57%	775	41%	1519	
	08:00-09:00	2	131	2	143	8%	49	26	1044	825	1479	85%	1	96	39	126	7%	29	1%	1271	59%	866	40%	1748	
	17:00-18:00	2	138	2	150	11%	54	31	755	660	1121	81%	3	71	39	104	8%	36	2%	964	57%	701	41%	1375	
	18:00-19:00	4	139	1	154	11%	50	20	782	750	1171	83%	1	69	25	90	6%	25	1%	990	56%	776	43%	1415	
C	07:00-08:00	6	44	2	59	25%	8	0	63	73	94	39%	15	40	6	87	36%	21	8%	147	59%	81	33%	240	
	08:00-09:00	5	73	1	87	22%	12	1	115	96	157	41%	23	74	4	144	37%	29	7%	262	67%	101	26%	388	
	17:00-18:00	6	74	3	91	20%	32	0	101	161	169	37%	20	131	13	203	43%	26	5%	306	60%	177	35%	463	
	18:00-19:00	2	77	0	85	17%	33	0	93	182	169	35%	18	167	10	234	48%	20	4%	337	61%	192	35%	488	
D	07:00-08:00	1	47	2	52	6%	12	80	278	444	608	75%	15	69	73	152	19%	96	10%	394	39%	519	51%	812	
	08:00-09:00	1	66	0	71	6%	17	95	444	678	900	74%	18	119	122	238	20%	114	7%	629	41%	800	52%	1209	
	17:00-18:00	0	26	0	27	2%	18	94	534	594	953	74%	18	195	96	307	24%	112	7%	755	49%	690	44%	1287	
	18:00-19:00	0	26	0	27	2%	17	96	563	772	1060	75%	16	207	129	331	23%	112	6%	796	44%	901	50%	1418	
合計	07:00-08:00	12	268	97	347	12%	34	107	1382	1360	2183	75%	31	210	128	376	13%	150	4%	1860	52%	1585	44%	2906	
	08:00-09:00	9	363	103	444	12%	88	127	1746	1823	2782	73%	42	327	170	552	15%	178	4%	2436	51%	2096	45%	3778	
	17:00-18:00	9	374	208	500	14%	128	133	1549	1666	2522	68%	41	434	159	660	18%	183	4%	2357	52%	2033	44%	3682	
	18:00-19:00	6	388	174	494	13%	120	118	1616	1954	2687	69%	35	481	175	702	18%	159	3%	2485	50%	2303	47%	3883	
A	08:00-09:00	1	93	100	143	33%	10	5	143	224	246	57%	0	38	5	44	10%	6	1%	274	45%	329	54%	433	0.92
B		2	131	2	143	8%	49	26	1044	825	1479	85%	1	96	39	126	7%	29	1%	1271	59%	866	40%	1748	0.94
C		5	73	1	87	22%	12	1	115	96	157	41%	23	74	4	144	37%	29	7%	262	67%	101	26%	388	0.92
D		1	66	0	71	6%	17	95	444	678	900	74%	18	119	122	238	20%	114	7%	629	41%	800	52%	1209	0.86
A	18:00-19:00	0	146	173	228	41%	20	2	178	250	287	51%	0	38	11	47	8%	2	0%	362	45%	434	55%	562	0.88
B		4	139	1	154	11%	50	20	782	750	1171	83%	1	69	25	90	6%	25	1%	990	56%	776	43%	1415	0.94
C		2	77	0	85	17%	33	0	93	182	169	35%	18	167	10	234	48%	20	4%	337	61%	192	35%	488	0.87
D		0	26	0	27	2%	17	96	563	772	1060	75%	16	207	129	331	23%	112	6%	796	44%	901	50%	1418	0.96

Figure 4.1: Sample traffic flow data. *Modified from the 2021 Taipei Traffic Volume and Characteristics Survey and 2022 Expansion Study of General Intersections, Roundabouts, and Road Sections.*

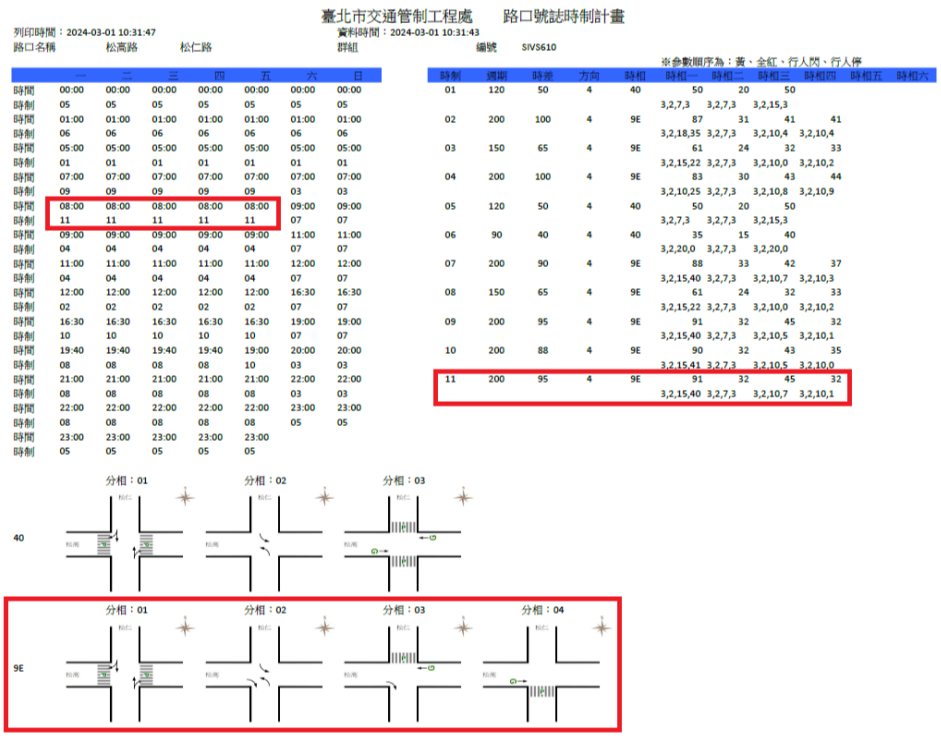

臺北市交通管制工程處　路口號誌時制計畫

列印時間：2024-03-01 10:31:47
資料時間：2024-03-01 10:31:43
路口名稱　松高路　松仁路　群組　編號　SIVS610

※參數順序為：黃、全紅、行人閃、行人停

時制	一	二	三	四	五	六	日
時間	00:00	00:00	00:00	00:00	00:00	00:00	00:00
時制	05	05	05	05	05	05	05
時間	01:00	01:00	01:00	01:00	01:00	01:00	01:00
時制	06	06	06	06	06	06	06
時間	05:00	05:00	05:00	05:00	05:00	05:00	05:00
時制	01	01	01	01	01	01	01
時間	07:00	07:00	07:00	07:00	07:00	07:00	07:00
時制	09	09	09	09	09	03	03
時間	08:00	08:00	08:00	08:00	08:00	09:00	09:00
時制	11	11	11	11	11	07	07
時間	09:00	09:00	09:00	09:00	09:00	11:00	11:00
時制	04	04	04	04	04	07	07
時間	11:00	11:00	11:00	11:00	11:00	12:00	12:00
時制	04	04	04	04	04	07	07
時間	12:00	12:00	12:00	12:00	12:00	16:30	16:30
時制	02	02	02	02	02	07	07
時間	16:30	16:30	16:30	16:30	16:30	19:00	19:00
時制	10	10	10	10	10	07	07
時間	19:40	19:40	19:40	19:40	19:00	20:00	20:00
時制	08	08	08	08	10	03	03
時間	21:00	21:00	21:00	21:00	21:00	22:00	22:00
時制	08	08	08	08	08	03	03
時間	22:00	22:00	22:00	22:00	22:00	23:00	23:00
時制	08	08	08	08	08	05	05
時間	23:00	23:00	23:00	23:00	23:00		
時制	05	05	05	05	05		

時制	週期	時差	方向	時相	時相一	時相二	時相三	時相四	時相五	時相六
01	120	50	4	40	50	20	50			
					3,2,7,3	3,2,7,3	3,2,15,3			
02	200	100	4	9E	87	31	41	41		
					3,2,18,35	3,2,7,3	3,2,10,4	3,2,10,4		
03	150	65	4	9E	61	24	32	33		
					3,2,15,22	3,2,7,3	3,2,10,0	3,2,10,2		
04	200	100	4	9E	83	30	43	44		
					3,2,10,25	3,2,7,3	3,2,10,8	3,2,10,9		
05	120	50	4	40	50	20	50			
					3,2,7,3	3,2,7,3	3,2,15,3			
06	90	40	4	40	35	15	40			
					3,2,20,0	3,2,7,3	3,2,20,0			
07	200	90	4	9E	88	33	42	37		
					3,2,15,40	3,2,7,3	3,2,10,7	3,2,10,3		
08	150	65	4	9E	61	24	32	33		
					3,2,15,22	3,2,7,3	3,2,10,0	3,2,10,2		
09	200	95	4	9E	91	32	45	32		
					3,2,15,40	3,2,7,3	3,2,10,5	3,2,10,1		
10	200	88	4	9E	90	32	43	35		
					3,2,15,41	3,2,7,3	3,2,10,5	3,2,10,0		
11	200	95	4	9E	91	32	45	32		
					3,2,15,40	3,2,7,3	3,2,10,7	3,2,10,1		

Figure 4.2: Sample signal timing plan. *Modified from the Taipei Intersection Signal Timing Plan.*

doi:10.6342/NTU202503442

4.2.2 Field Observations

Table 4.1 presents six selected pedestrian crossings along with their corresponding conflicting right-turning vehicle movements at intersections in Taipei City, and the definitions of approach labels A, B, C, and D for each intersection are provided in Appendix A. Observations were conducted during weekday peak hours. Certain signal cycle data were excluded due to external interferences such as emergency vehicle passage or manual traffic control.

Table 4.1: Basic info of the selected intersection approaches.

Intersection	Bade Guangfu		Heping Xinsheng		Songgao Songren	Zhongxiao Guangfu
PCP crosswalk	B	A	A	B	C	A
RTV movement	C →B	B →A	B →A	C →B	D →C	B →A
Observe date	2025/4/1	2025/4/1	2025/4/7	2025/4/7	2025/4/8	2025/4/11
Start time	18:00	18:20	07:30	08:00	08:00	18:00
End time	18:20	18:40	08:00	08:30	08:30	18:50
Valid cycles	6	5	9	8	10	12

Note:
A, B, C, and D represent the four approaches of the road intersection: westbound, northbound, eastbound, and southbound, respectively.

Signal Timing Data

The actual signal timing plans for the six crossings during their respective observation periods are summarized in Table 4.2. A Leading Pedestrian Interval (LPI) design was implemented during peak hours at the intersections of Heping and Xinsheng Roads, Songgao and Songren Roads, and Zhongxiao and Guangfu Roads. By contrast, the RTV movements of interest span two signal stages at the intersections of Bade and Guangfu Roads, and Heping and Xinsheng Roads. Table 4.3 reorganizes these data into a structured parameter input format.

doi:10.6342/NTU202503442

Table 4.2: Current traffic signal data of selected intersections. *Modified from the Taipei Intersection Signal Timing Plan*.

Intersection	Crosswalk location	Observation time
Bade & Guangfu	Approach B	18:00 - 18:20
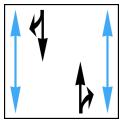  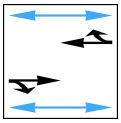 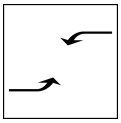		
68 3,2,15,38	27 3,3,0,0	70 3,3,25,35	35 3,3,0,0	
Bade & Guangfu	Approach A	18:00 - 18:20
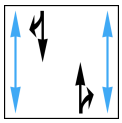 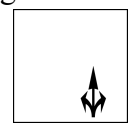 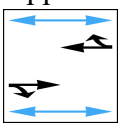 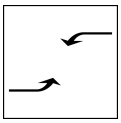		
68 3,2,15,38	27 3,3,0,0	70 3,3,25,35	35 3,3,0,0	
Heping & Xinsheng	Approach A	07:30 - 08:00
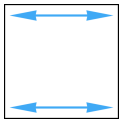 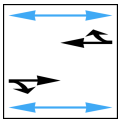 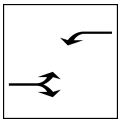 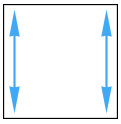 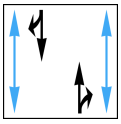 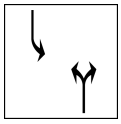		
5 0,0,0,0	59 4,3,20,14	27 3,3,0,0	10 0,0,0,0	68 4,3,20,29	31 3,3,0,0
Heping & Xinsheng	Approach B	08:00 - 08:30
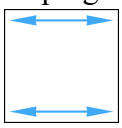 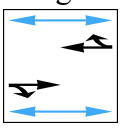 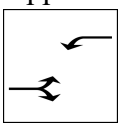 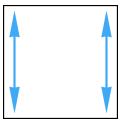 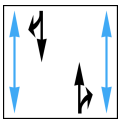 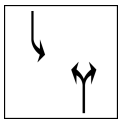		
5 0,0,0,0	59 4,3,20,14	32 3,3,0,0	5 0,0,0,0	68 4,3,20,29	31 3,3,0,0
Songgao & Songren	Approach C	08:00 - 08:30
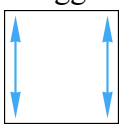 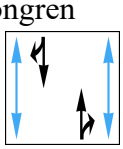 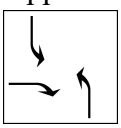 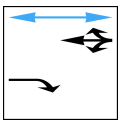 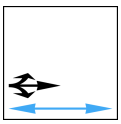		
3 0,0,0,0	88 3,2,15,40	32 3,2,0,0	45 3,2,10,7	32 3,2,10,1
Zhongxiao & Guangfu	Approach A	18:00 - 18:50
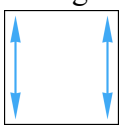 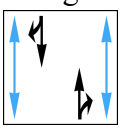 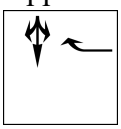 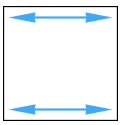 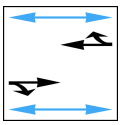		
5 0,0,0,0	57 3,3,30,20	54 3,4,0,0	5 0,0,0,0	79 3,3,30,42

Note:
1. The values in the first row under each phase stage represent the duration of that stage.
2. The values in the second row indicate, respectively: Yellow, Red, Ped-Flash, and Ped-Stop.

doi:10.6342/NTU202503442

Table 4.3: Current signal timing settings of the selected crosswalks.

Intersection	Bade Guangfu		Heping Xinsheng		Songgao Songren	Zhongxiao Guangfu
PCP crosswalk	B	A	A	B	C	A
RTV movement	C →B	B →A	B →A	C →B	D →C	B →A
Concurrent (s)	70	68	68	59	88	57
Clearance (s)	3	3	3	3	2	3
C (s)	200	200	200	200	200	200
t_{PE} (s)	0	0	10	5	3	5
t_{PG} (s)	4	10	15	21	28	1
t_{PY} (s)	25	15	20	20	15	30
t_{PR} (s)	171	175	155	154	154	164
t_{VG} (s)	64	89	93	85	83	51
t_{VY} (s)	3	3	4	4	3	3
t_{VR} (s)	133	108	103	111	114	146
$t_{PG_{min}}$ (s)	1	1	0	0	0	0
$t_{PG_{max}}$ (s)	39	47	41	32	68	21
$t_{PR_{min}}$ (s)	136	138	129	143	114	144
$t_{PR_{max}}$ (s)	174	184	170	175	182	165

Note:
1. "Concurrent" refers to the concurrent stage length for both PCP and RTV movements.
2. "Clearance" refers to the clearance time at the end of the stage.
3. Both t_{PG} and t_{PR} have default values but are treated as variables during the optimization process.

The principles and logic behind setting the minimum and maximum pedestrian green and red phase lengths are as follows:

1. If a Leading Pedestrian Interval (LPI) is implemented ($t_{PE} > 0$), the minimum pedestrian green time can be 0. Otherwise, it should be at least 1 second to ensure that pedestrian flow is valid.
2. The combined duration of the PCP flashing phase, RTV yellow phase, clearance time, and the maximum pedestrian green time must not exceed the stage length. This prevents the PCP movement from creating new conflicts with other movements.
3. These values must also satisfy Equation 3.18.

doi:10.6342/NTU202503442

Passenger Car Equivalents (PCE)

When counting right-turning vehicles, it is necessary to convert all vehicle types into a common unit using Passenger Car Equivalents (PCE), as different vehicle types exhibit varying physical and operational characteristics that influence their effect on traffic flow. In this study, the PCE conversion table from the *Taiwan Highway Capacity Manual* (2022) is adopted (see Table 4.4).

Specifically, all right-turning vehicles are converted into the standard unit of a "right-turning automobile" using a PCE ratio of **0.42 : 1.00 : 2.50**. For adjusting the motorcycle equivalent, the proportion of motorcycles for each right-turning movement at a given intersection approach is determined by dividing the average motorcycle volume per cycle by the average total vehicle volume per cycle.

Table 4.4: Passenger Car Equivalents (PCEs). *Translated from THCM*.

Vehicle type and movement		Convert to standard type				
		Through auto	Right-turn auto	Left-turn auto	Through motor	Right-turn motor
Through	Motor	0.42	0.39	0.40	1.00	0.93
	Auto	1.00	0.93	0.95	2.38	2.22
	Heavy	1.80	1.67	1.71	4.33	4.00
Left-turn	Motor	0.43	0.40	0.41	1.02	0.96
	Auto	1.05	0.97	1.00	2.50	2.33
	Heavy	2.00	1.85	1.90	4.76	4.44
Right-turn	Motor	0.45	**0.42**	0.43	1.07	1.00
	Auto	1.08	**1.00**	1.03	2.57	2.40
	Heavy	2.70	**2.50**	2.57	6.43	6.00

Note:
1. If the motorcycle proportion is 90% ~, reduce the motorcycle equivalent by 0.05.
2. If the motorcycle proportion is 30% ~50%, increase the motorcycle equivalent by 0.05.
3. If the motorcycle proportion is ~30%, increase the motorcycle equivalent by 0.10.

doi:10.6342/NTU202503442

Observed Arrival Rates

Pedestrians and vehicles were counted once they entered the conflict area, as illustrated in Figures 4.3a to 4.3f, with the counts reset at the beginning of each signal cycle. The arrival rates for both PCP and RTV movements were calculated by averaging the observed arrival volumes across all valid cycles (see Table 4.5).

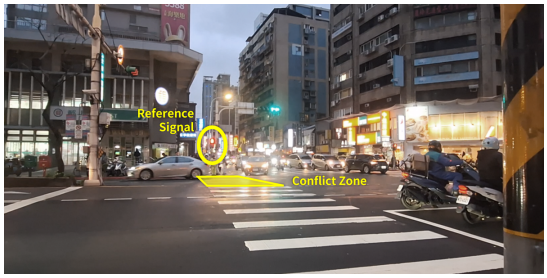

(a) Bade-Guangfu, Approach B

(b) Bade-Guangfu, Approach A

(c) Heping-Xinsheng, Approach A

(d) Heping-Xinsheng, Approach B

(e) Songgao-Songren, Approach C

(f) Zhongxiao-Guangfu, Approach A

Figure 4.3: Conflict areas at six selected crosswalks. *Photographs by the author.*

doi:10.6342/NTU202503442

Table 4.5: Observed arrival rates for selected intersection approaches.

Intersection	Bade Guangfu		Heping Xinsheng		Songgao Songren	Zhongxiao Guangfu
PCP crosswalk	B	A	A	B	C	A
RTV movement	C →B	B →A	B →A	C →B	D →C	B →A
pcp_arr_near	10.50	9.80	10.89	13.25	15.50	24.08
pcp_arr_far	14.67	9.40	12.33	10.50	2.90	10.92
rtv_arr_motor	3.50	4.80	22.33	4.13	4.40	4.67
rtv_arr_auto	10.00	3.60	13.44	2.50	4.80	5.50
rtv_arr_heavy	0.17	0.00	0.89	0.13	1.60	0.17
motor_ratio	26%	57%	61%	61%	41%	45%
motor_add_pce	0.10	0.00	0.00	0.00	0.05	0.05
a_p (ped/s)	0.126	0.096	0.116	0.119	0.092	0.175
a_v (pcu/s)	0.061	0.028	0.125	0.023	0.054	0.041
a_p (ped/hr)	453	346	418	428	331	630
a_v (ped/hr)	220	101	451	82	196	146

Note:
pcp_arr_near = PCP arrival rate from the near end of the crosswalk.
pcp_arr_far = PCP arrival rate from the far end of the crosswalk.
rtv_arr_motor = RTV arrival rate of motorcycle-type vehicles.
rtv_arr_auto = RTV arrival rate of automobile-type vehicles.
rtv_arr_heavy = RTV arrival rate of heavy vehicles (buses or trucks).
motor_ratio = Proportion of motorcycles in the RTV flow.
motor_add_pce = Additional PCE factor for motorcycles.

Observed Discharge Rates

Pedestrian and vehicle counts were recorded during each signal phase interval. However, since they completed discharging at different times within each cycle, the average dissipation times for PCP and RTV movements were first estimated as their respective intersection timepoints (initial t_{Pi} and t_{PiVj}). These timepoints also served as the boundaries of the count intervals, as discharge rates before and after them differed significantly.

The discharge volumes across different signal phases and timepoint intervals, as well as the predetermined intersection timepoints, are detailed in Appendix A. Here, only the final discharge rate results for each selected crosswalk are presented.

doi:10.6342/NTU202503442

Duration	130	0	4	24	1	23	12	3	3	Total 200
PCP	PR	PE + PG		PY		PR				
RTV	VR		VG					VY	VR	
s_p =	0.000	-	1.125	0.778	1.333	0.007	0.014	0.000	0.111	0.126
s_v =	0.000	-	0.000	0.004	0.253	0.307	0.285	0.473	0.000	0.061

(a) Bade-Guangfu, Approach B

Duration	105	0	10	12	3	10	54	3	3	Total 200
PCP	PR	PE + PG		PY		PR				
RTV	VR		VG					VY	VR	
s_p =	0.000	-	1.140	0.567	0.133	0.020	0.007	0.000	0.000	0.096
s_v =	0.000	-	0.000	0.014	0.112	0.214	0.042	0.228	0.000	0.028

(b) Bade-Guangfu, Approach A

Duration	91	10	15	5	15	24	34	3	3	Total 200
PCP	PR	PE + PG		PY		PR				
RTV	VR		VG					VY	VR	
s_p =	0.000	0.782		0.244	0.156	0.005	0.000	0.000	0.000	0.116
s_v =	0.000	0.000	0.006	0.145	0.193	0.393	0.284	0.750	0.000	0.125

(c) Heping-Xinsheng, Approach A

Duration	104	5	21	8	12	44	3	3	Total 200
PCP	PR	PE + PG		PY		PR			
RTV	VR		VG				VY	VR	
s_p =	0.000	0.774		0.188	0.146	0.009	0.000	0.000	0.119
s_v =	0.000	0.000	0.000	0.085	0.138	0.050	0.000	0.000	0.023

(d) Heping-Xinsheng, Approach B

Duration	109	3	21	7	15	4	36	3	2	Total 200
PCP	PR	PE + PG			PY	PR				
RTV	VR		VG					VY	VR	
s_p =	0.000	0.675		0.091		0.050	0.000	0.000	0.000	0.092
s_v =	0.000	0.000	0.028	0.205		0.299	0.126	0.016	0.000	0.054

(e) Songgao-Songren, Approach C

Duration	138	5	1	23	7	6	14	3	3	Total 200
PCP	PR	PE + PG		PY		PR				
RTV	VR		VG					VY	VR	
s_p =	0.000	1.153		1.145	0.238	0.014	0.000	0.000	0.000	0.175
s_v =	0.000	0.000	0.000	0.007	0.093	0.387	0.265	0.422	0.000	0.041

(f) Zhongxiao-Guangfu, Approach A

Figure 4.4: Discharge rates recorded over different time intervals.

doi:10.6342/NTU202503442

Table 4.6: Observed discharge rates for selected intersection approaches.

Intersection	Bade Guangfu		Heping Xinsheng		Songgao Songren	Zhongxiao Guangfu
PCP crosswalk	B	A	A	B	C	A
RTV movement	C →B	B →A	B →A	C →B	D →C	B →A
Observed Delay Case	P2V5	P2V5	P2V5	P1V4	P1V5	P2V5
s_{p1} (ped/s)	1.125	1.140	0.782	0.774	0.675	1.153
s_{p2} (ped/s)	0.778	0.567	0.244	-	-	1.145
s_{v1} (pcu/s)	0.000	0.000	0.006	0.000	0.028	0.000
s_{v2} (pcu/s)	-	-	-	-	-	-
s_{v3} (pcu/s)	0.004	0.014	0.145	-	-	0.007
s_{v4} (pcu/s)	0.253	0.112	0.193	0.085	0.205	0.093
s_{v5} (pcu/s)	0.307	0.214	0.393	-	0.299	0.387
s_{v6} (pcu/s)	-	-	-	-	-	-

Note:
Some discharge rates are not reported because the vehicle queues or pedestrian crowds had already dissipated before the corresponding time intervals began.

Table 4.6 categorizes the observed discharge rates across different time intervals, based on the data presented in Figure 4.4. These discharge rates serve as preliminary values for constructing the upcoming relationship function.

4.3 Discharge Rate Relationship Curve

As mentioned in Section 3.4.1, without the influence of RTV signal phase changes, the maximum RTV dischargeability is affected by the PCP discharge rate across different time intervals. Specifically, s_{p1} corresponds to s_{v1}; s_{p2} to s_{v3}; a_p to s_{v4}; and 0 to s_{v5}. The discharge rate pairs mentioned above are reorganized from Table 4.6 and summarized in Table 4.7, which is used to establish the relationship function. The corresponding scatter plot is shown in Figure 4.5.

doi:10.6342/NTU202503442

Table 4.7: Discharge rate pairs for the curve fitting.

Intersection approach	Observed delay case	s_p	s_v	Corresponding relationship	
Bade-Guangfu Approach B	P2V5	1.12500	0.00000	s_{p1} - s_{v1}	
		0.77778	0.00361	s_{p2} - s_{v3}	
		1.33333	0.25333	a_p - s_{v4}	*
		0.00725	0.30667	0 - s_{v5}	
Bade-Guangfu Approach A	P2V5	1.14000	0.00000	s_{p1} - s_{v1}	
		0.56667	0.01400	s_{p2} - s_{v3}	
		0.13333	0.11200	a_p - s_{v4}	
		0.02000	0.21360	0 - s_{v5}	
Heping-Xinsheng Approach A	P2V5	0.78222	0.00622	s_{p1} - s_{v1}	
		0.24444	0.14489	s_{p2} - s_{v3}	
		0.15556	0.19304	a_p - s_{v4}	
		0.00463	0.39250	0 - s_{v5}	
Heping-Xinsheng Approach B	P1V4	0.77404	0.00000	s_{p1} - s_{v1}	
		0.18750	0.08531	a_p - s_{v4}	
Songgao-Songren Approach C	P1V5	0.67500	0.02814	s_{p1} - s_{v1}	
		0.09091	0.20507	a_p - s_{v4}	
		0.05000	0.29850	0 - s_{v5}	
Zhongxiao-Guangfu Approach A	P2V5	1.15278	0.00000	s_{p1} - s_{v1}	
		1.14493	0.00681	s_{p2} - s_{v3}	
		0.23810	0.09310	a_p - s_{v4}	
		0.01389	0.38667	0 - s_{v5}	

Note:
The discharge pair (1.33333, 0.25333) was identified as an outlier and was therefore excluded from the curve fitting.

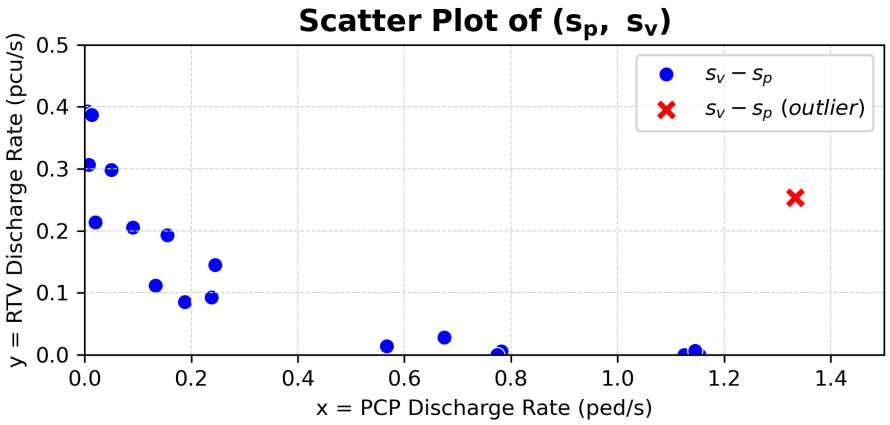

Figure 4.5: Scatter plot of (s_p, s_v) pairs.

doi:10.6342/NTU202503442

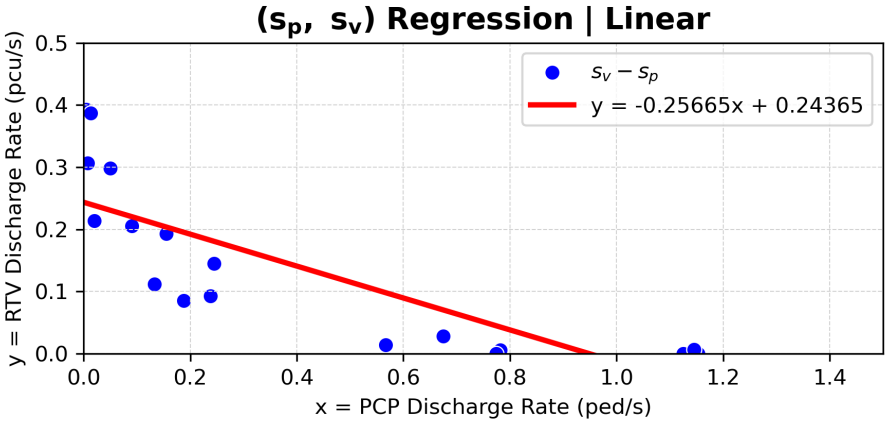

(a) s_v - s_p linear regression

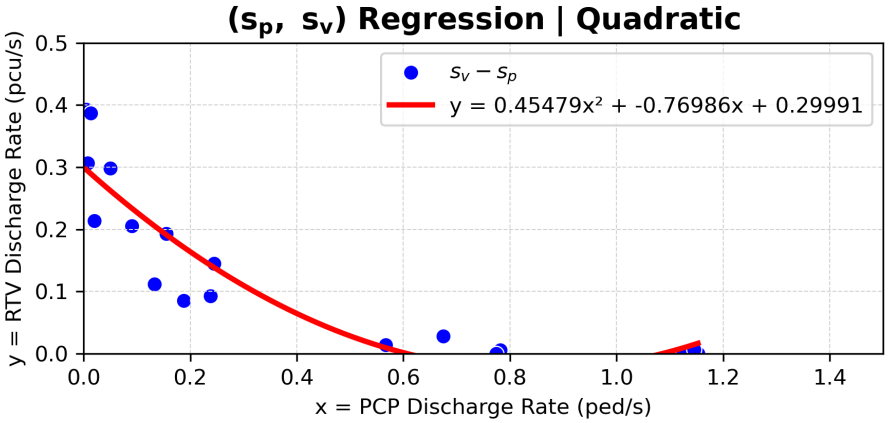

(b) s_v - s_p quadratic regression

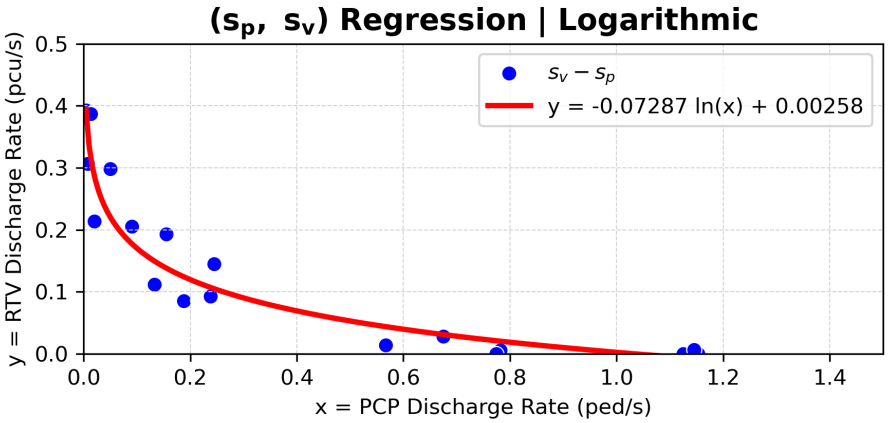

(c) s_v - s_p logarithmic regression

Figure 4.6: Linear, quadratic, and logarithmic regression curve fittings.

doi:10.6342/NTU202503442

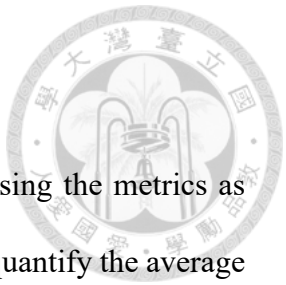

Curve Fitting Metrics

The goodness of fit between regression models was evaluated using the metrics as follows. First, the Root Mean Squared Error (RMSE) was applied to quantify the average magnitude of the prediction errors, with lower RMSE values indicating a better fit.

$$RMSE = \sqrt{\frac{1}{n}\sum_{i=1}^{n}(\hat{y}_i - y_i)^2} = \sqrt{\frac{RSS}{n}} \tag{4.1}$$

where $\hat{y}_i$ are the predicted values, y_i are the observed values, and RSS is the residual sum of squares.

To compare models of differing complexity, the Akaike Information Criterion (AIC) and Bayesian Information Criterion (BIC) were used. These criteria balance model fit and parsimony, with lower values indicating a more favorable tradeoff. The log-likelihood is estimated from the Residual Sum of Squares (RSS) as follows:

$$AIC = n\ln\left(\frac{RSS}{n}\right) + 2k \tag{4.2}$$

$$BIC = n\ln\left(\frac{RSS}{n}\right) + k\ln(n) \tag{4.3}$$

where k is the number of model parameters and n is the number of observations.

Although the coefficient of determination (R^2) is widely used to quickly assess fit quality, it is less appropriate for nonlinear regression models, such as logarithmic ones, and was therefore excluded from this analysis. Additionally, the Mean Absolute Percentage Error (MAPE) was not adopted due to the presence of values close to zero, which can result in disproportionately large percentage errors.

doi:10.6342/NTU202503442

Formulated Discharge Rates

Table 4.8 shows the metric results for the linear, quadratic, and logarithmic regression models (see Figures 4.6a to 4.6c). Among them, the logarithmic relationship function yields the lowest RMSE, AIC, and BIC values, and is therefore adopted as a reference for the time-varying maximum discharge rate input in the optimization model.

Table 4.8: Fitted relationship functions and comparison of curve types.

Regression type	Relationship function	RMSE	AIC	BIC
Linear	$y = -0.25665x + 0.24365$	0.0738	-100.25	-98.26
Quadratic	$y = 0.45479x^2 - 0.76986x + 0.29991$	0.0496	-111.19	-110.16
Logarithmic	$y = -0.07287\ln(x) + 0.00258$	**0.0390**	**-125.73**	**-123.73**

$$s_v = -0.07287\ln(s_p) + 0.00258 \tag{4.4}$$

Given that Equation 4.4 was selected to express the interaction between PCP and RTV discharge rates, the values of s_{v1}, s_{v3}, and s_{v4} were recalculated accordingly. Since discharge rates cannot be negative by definition, **any negative value predicted by the regression function is replaced with zero.** This adjustment reflects the condition where a high PCP discharge rate fully blocks RTV movement during that time interval.

Value Determinations for s_{p1} and s_{v5}

As discussed in Section 3.4.1, s_{v5} can be interpreted as the free-flow discharge rate for RTV movements. However, its observed values may vary due to random pedestrian non-compliance occurring after the onset of the pedestrian red phase.

doi:10.6342/NTU202503442

In this study, we adopt a basic lane capacity of 2000 pcuphpl for urban arterial road sections, as recommended in the *Research on the Planning and Design Guidelines for Urban Road Engineering* (2001). This value represents the base saturation flow rate under ideal conditions, including the assumption of uninterrupted flow, where the g_{eff}/C ratio equals 100%.

This rate also reflects the theoretical maximum discharge under ideal conditions. However, further adjustments are necessary to account for right-turning movements. These are applied using Equation 2.4. **Note that the pedestrian blockage reduction factor is not applied here**, as the influence of PCP discharge rates on RTV discharge rates has already been incorporated into the primary modeling assumptions.

Assuming the area type adjustment factor $f_a = 0.9$, the right-turn adjustment factor $f_{RT} = 0.85$, and all other adjustment factors equal to 1, the revised expression becomes:

$$s_{v5} = s_{\text{base}} \cdot f_a \cdot f_{RT} \tag{4.5}$$

Equation 4.5 also converts the unit of s_{v5} from pcu/hr to pcu/s.

As for the free-flow pedestrian discharge rate s_{p1}, since there are no universally accepted maximum or standard values for base pedestrian saturation flow rates, we directly use the observed values.

Value Determinations for s_{p2} and s_{v6}

Although s_{p2} is considered related to s_{p1}, it was difficult to obtain accurate values for s_{p2} through direct observation. To simplify, we preliminarily assume s_{p2} to be 1.1 times s_{p1} across different crosswalks within the intersection, based on the assumption that pedestrians tend to speed up when the flashing phase begins (Virkler, 1998).

doi:10.6342/NTU202503442

A similar assumption is made for s_{v6} relative to s_{v5}, as vehicles may accelerate slightly when the yellow phase begins. These assumptions are summarized as follows:

$$s_{p2} = 1.1\, s_{p1} \tag{4.6}$$

$$s_{v6} = 1.1\, s_{v5} \tag{4.7}$$

Reorganized Arrival and Discharge Rate Parameter Input

The observed values are replaced with formula-based and derived discharge rates to facilitate a more systematic discussion during model input preparation. The rate determination principles are summarized in Table 4.9, and the corresponding values are presented in Table 4.10.

Table 4.9: Summary of principles used to determine arrival and discharge rates.

Notation	Unit	Determination
a_p	ped/s	Directly use the observed values
a_v	pcu/s	Directly use the observed values
s_{p1}	ped/s	Directly use the observed values
s_{p2}	ped/s	$1.1 \cdot s_{p1}$
s_{v1}	pcu/s	$\max(0, -0.07287 \ln(s_{p1}) + 0.00258)$
s_{v2}	pcu/s	Undefined
s_{v3}	pcu/s	$\max(0, -0.07287 \ln(s_{p2}) + 0.00258)$
s_{v4}	pcu/s	$\max(0, -0.07287 \ln(a_p) + 0.00258)$
s_{v5}	pcu/s	$s_{\text{base}} \cdot f_a \cdot f_{RT} = (2000/3600) \cdot 0.9 \cdot 0.85 = 0.425$
s_{v6}	pcu/s	$1.1 \cdot s_{v5}$

doi:10.6342/NTU202503442

Table 4.10: Reorganized rate values used as model inputs.

Intersection	Bade Guangfu		Heping Xinsheng		Songgao Songren	Zhongxiao Guangfu
PCP crosswalk	B	A	A	B	C	A
RTV movement	C →B	B →A	B →A	C →B	D →C	B →A
a_p (ped/s)	0.126	0.096	0.116	0.119	0.092	0.175
a_v (pcu/s)	0.061	0.028	0.125	0.023	0.054	0.041
s_{p1} (ped/s)	1.125	1.140	0.782	0.774	0.675	1.153
s_{p2} (ped/s)	1.238	1.254	0.860	0.851	0.743	1.268
s_{v1} (pcu/s)	0.000	0.000	0.021	0.022	0.032	0.000
s_{v2} (pcu/s)	-	-	-	-	-	-
s_{v3} (pcu/s)	0.000	0.000	0.014	0.014	0.024	0.000
s_{v4} (pcu/s)	0.154	0.173	0.159	0.158	0.176	0.130
s_{v5} (pcu/s)	0.425	0.425	0.425	0.425	0.425	0.425
s_{v6} (pcu/s)	0.468	0.468	0.468	0.468	0.468	0.468

4.4 Results

4.4.1 Multi-Delay Models

Based on the current signal timing plan and the input arrival and discharge rates, the delay models for both PCP and RTV movements at each intersection approach are illustrated. Figures 4.7 to 4.12 present the multi-delay models for the six examined approaches, with intersection timepoints t_{Pi} and t_{PiVj} indicated.

Most intersection approaches are modeled as exhibiting delay Case P2V5. This means that pedestrians dissipate during the flashing phase, and right-turning vehicles dissipate afterward, still within the green interval. The piecewise linear discharge curves also show that pedestrian discharge at the beginning of the concurrent green phase typically blocks right-turning vehicles from proceeding.

doi:10.6342/NTU202503442

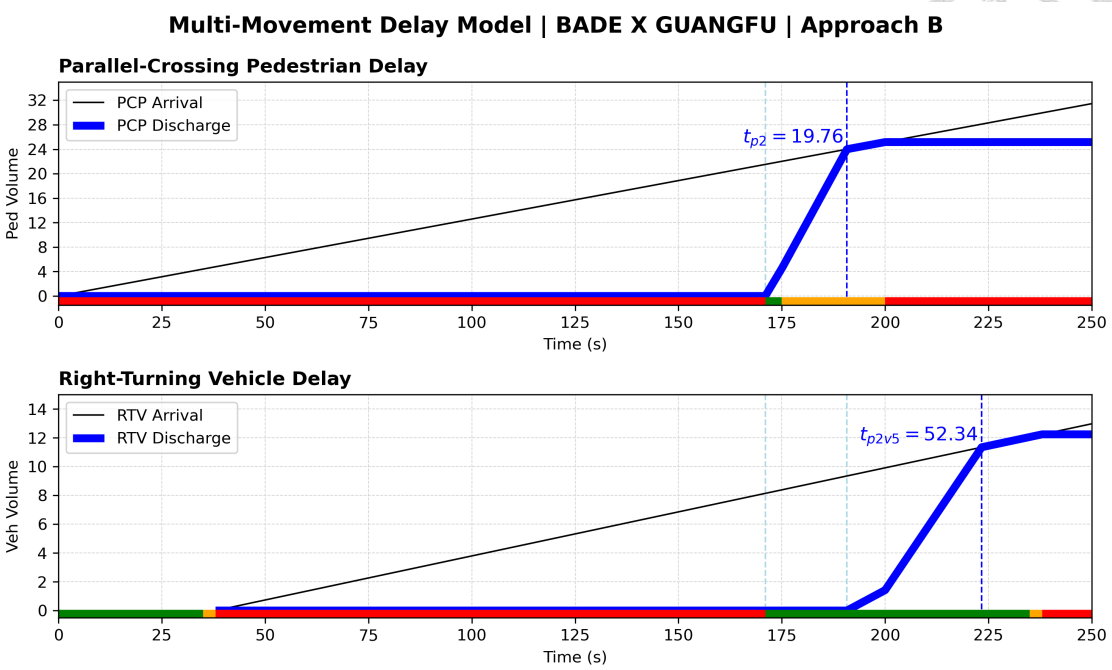

Figure 4.7: Multi-movement delay model for Bade-Guangfu, Approach B under current signal settings.

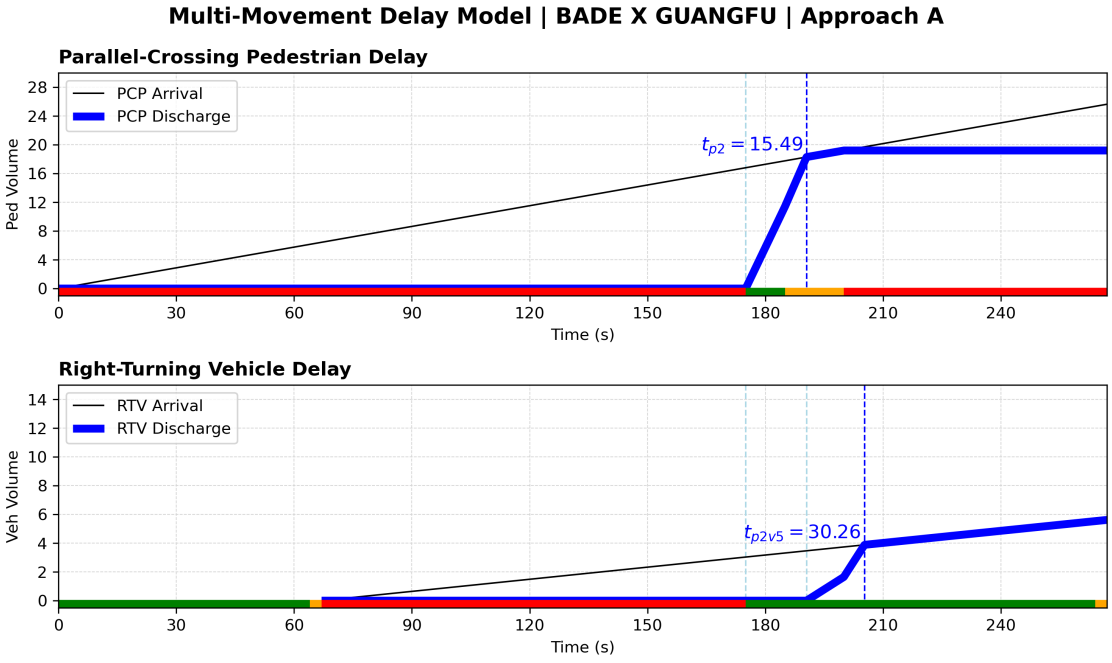

Figure 4.8: Multi-movement delay model for Bade-Guangfu, Approach A under current signal settings.

doi:10.6342/NTU202503442

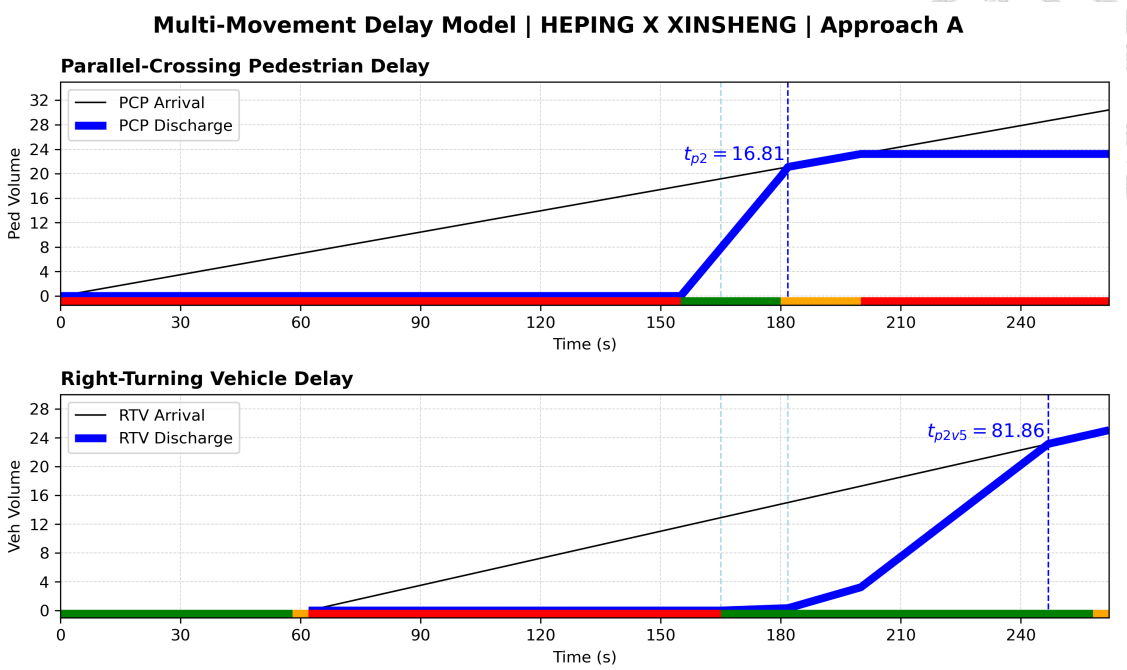

Figure 4.9: Multi-movement delay model for Heping-Xinsheng, Approach A under current signal settings.

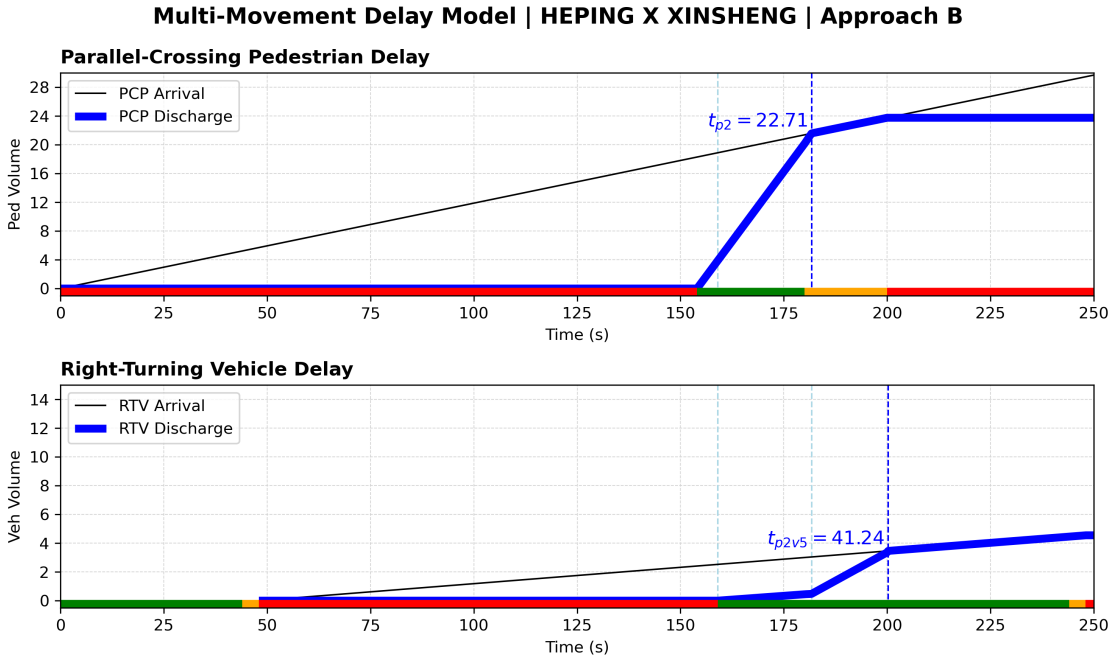

Figure 4.10: Multi-movement delay model for Heping-Xinsheng, Approach B under current signal settings.

doi:10.6342/NTU202503442

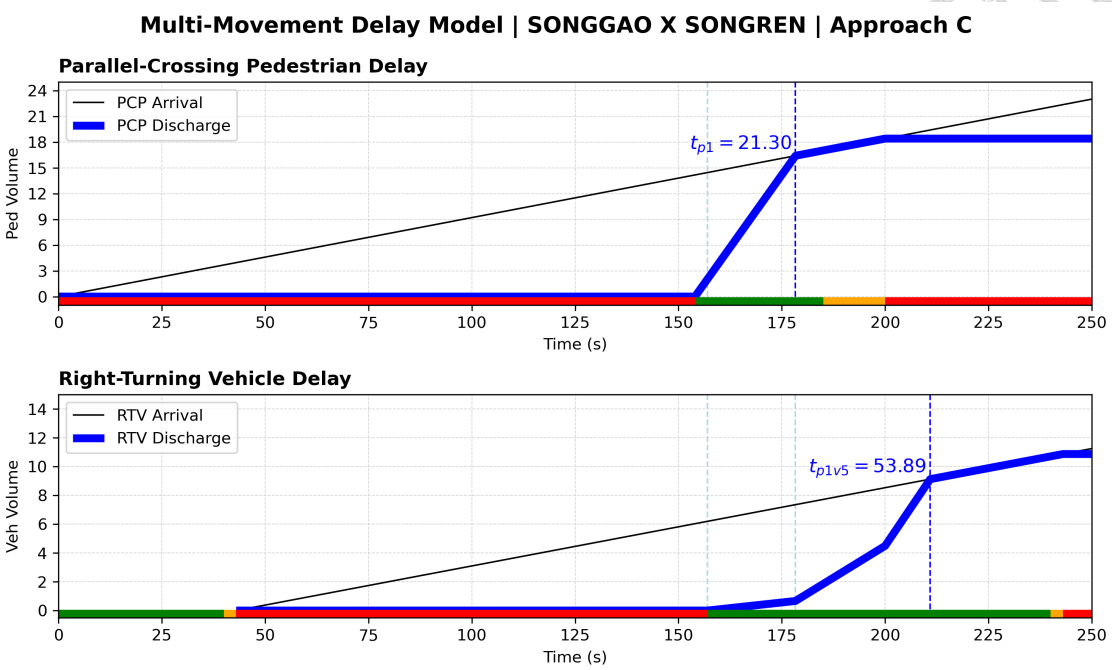

Figure 4.11: Multi-movement delay model for Songgao-Songren, Approach C under current signal settings.

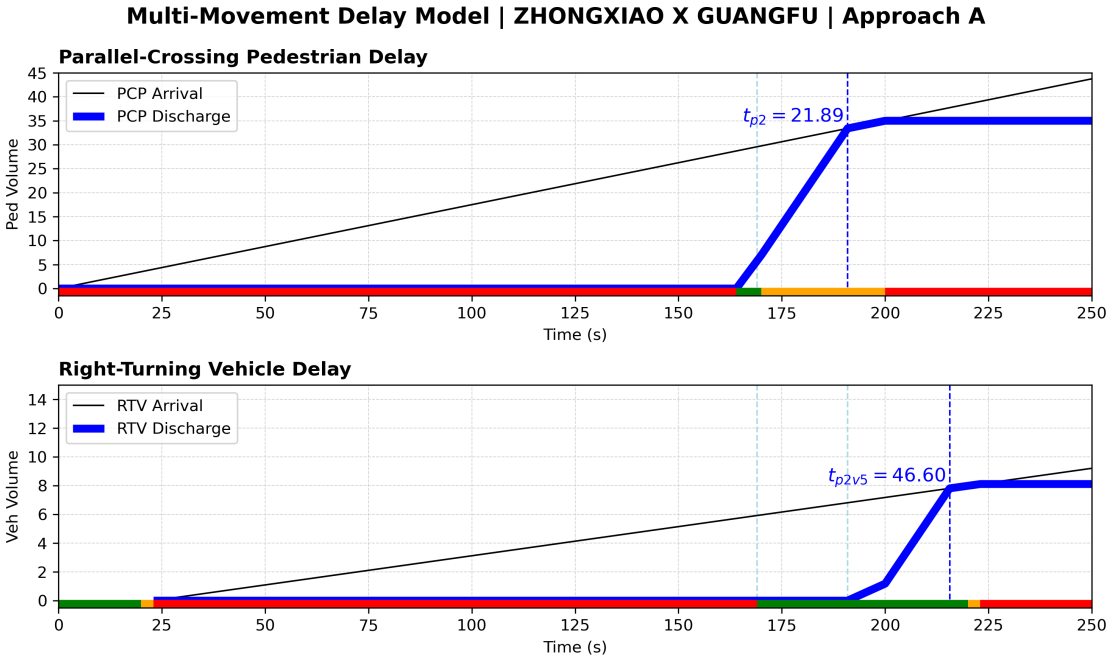

Figure 4.12: Multi-movement delay model for Zhongxiao-Guangfu, Approach A under current signal settings.

doi:10.6342/NTU202503442

Table 4.11: Details from the multi-delay models of six intersection approaches based on current signal settings.

Intersection	Bade Guangfu		Heping Xinsheng		Songgao Songren	Zhongxiao Guangfu
PCP crosswalk	B	A	A	B	C	A
RTV movement	C →B	B →A	B →A	C →B	D →C	B →A
Observed case	P2V5	P2V5	P2V5	P1V4	P1V5	P2V5
Modeled case	P2V5	P2V5	P2V5	P2V5	P1V5	P2V5
(Current) t_{PG}	4	10	15	21	28	1
t_{Pi}	19.760	15.492	16.806	22.706	21.302	21.889
t_{PiVj}	52.340	30.257	81.864	41.241	53.893	46.598
PCP average delay	81.691	83.503	70.526	70.029	68.646	78.471
RTV average delay	73.173	43.804	59.343	48.856	57.845	83.426
Overall average delay	78.904	74.519	64.723	66.628	64.635	79.403
Average delay difference	8.518	39.699	11.183	21.173	10.802	4.955

Table 4.11 reorganizes the information based on the above multi-delay models. Although Heping-Xinsheng-B is the only exception where the estimated delay case (P2V5) differs from the observed case (P1V4), the intersection time points fall near the edge of the interval, suggesting that the difference may be marginal (see Figure 4.10).

4.4.2 Best Pedestrian Green Duration

For each intersection approach, the optimization was conducted step by step. As the variable t_{PG} (pedestrian green duration) is adjusted, the average delay for both PCP and RTV flows changes accordingly. Figures 4.13 to 4.18 illustrate the trends of increasing and decreasing average delays for PCP and RTV movements. The overall average delay trend line is also provided. Details including delay case identifications, intersection timepoints, and average delay values are organized in Tables 4.12 to 4.17.

doi:10.6342/NTU202503442

Table 4.12: Optimization results for Bade-Guangfu, Approach B.

a_p = 453 ped/hr a_v = 220 pcu/hr	Current	min Obj-1	min Obj-2
t_{PG}	4	24	10
Delay case	P2V5	P1V6	P2V5
PCP intersection timepoint	19.760	19.016	19.688
RTV intersection timepoint	52.340	66.636	56.785
PCP average delay	81.691	64.181	76.400
RTV average delay	73.173	81.940	76.144
Overall average delay	78.904	69.991	76.317
Average delay difference	8.518	17.759	0.256
Reduce PCP delay		-17.510	-5.291
(%)		-21.434%	-6.477%
Reduce RTV delay		+8.317	+2.971
(%)		+11.366%	+4.060%
Reduce overall delay		-8.913	-2.587
(%)		-11.296%	-3.278%

Note:
Obj-1: Minimize the overall (PCP and RTV) average delay.
Obj-2: Minimize the difference in average delay between the two movements.
Negative signs indicate a decrease in delay; positive signs indicate an increase.

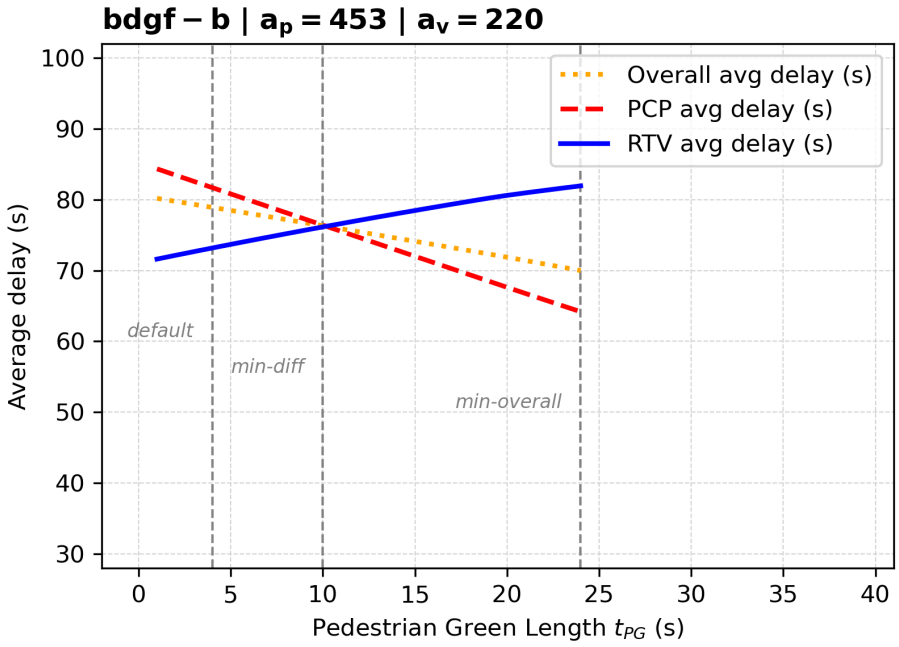

Figure 4.13: Trend of delay values for Bade-Guangfu, Approach B.

doi:10.6342/NTU202503442

Table 4.13: Optimization results for Bade-Guangfu, Approach A.

a_p = 346 ped/hr a_v = 101 pcu/hr	Current	min Obj-1	min Obj-2
t_{PG}	10	47	47
Delay case	P2V5	P1V4	P1V4
PCP intersection timepoint	15.492	12.690	12.690
RTV intersection timepoint	30.257	36.019	36.019
PCP average delay	83.503	51.988	51.988
RTV average delay	43.804	43.454	43.454
Overall average delay	74.519	50.057	50.057
Average delay difference	39.699	8.534	8.534
Reduce PCP delay		-31.515	-31.515
(%)		-37.741%	-37.741%
Reduce RTV delay		-0.350	-0.350
(%)		-0.799%	-0.799%
Reduce overall delay		-24.462	-24.462
(%)		-32.827%	-32.827%

Note:
Obj-1: Minimize the overall (PCP and RTV) average delay.
Obj-2: Minimize the difference in average delay between the two movements.
Negative signs indicate a decrease in delay; positive signs indicate an increase.

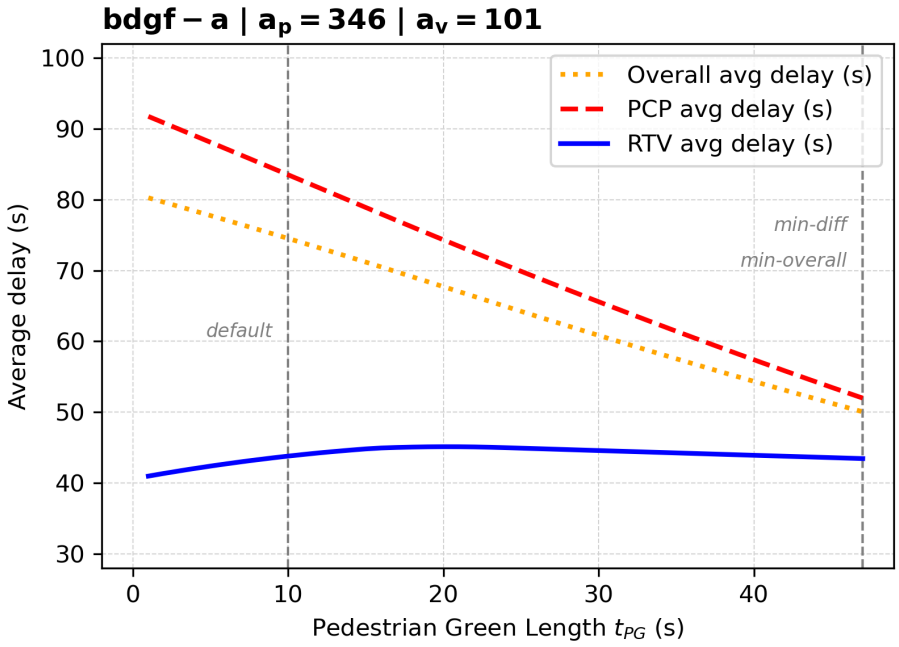

Figure 4.14: Trend of delay values for Bade-Guangfu, Approach A.

doi:10.6342/NTU202503442

Table 4.14: Optimization results for Heping-Xinsheng, Approach A.

a_p = 418 ped/hr a_v = 451 pcu/hr	Current	min Obj-1	min Obj-2
t_{PG}	15	34	24
Delay case	P2V5	P1V6	P1V5
PCP intersection timepoint	16.806	13.706	15.449
RTV intersection timepoint	81.864	96.691	89.165
PCP average delay	70.526	54.300	62.579
RTV average delay	59.343	67.087	63.176
Overall average delay	64.723	60.935	62.889
Average delay difference	11.183	12.787	0.597
Reduce PCP delay		-16.226	-7.947
(%)		-23.007%	-11.268%
Reduce RTV delay		+7.744	+3.833
(%)		+13.050%	+6.459%
Reduce overall delay		-3.788	-1.834
(%)		-5.853%	-2.834%

Note:
Obj-1: Minimize the overall (PCP and RTV) average delay.
Obj-2: Minimize the difference in average delay between the two movements.
Negative signs indicate a decrease in delay; positive signs indicate an increase.

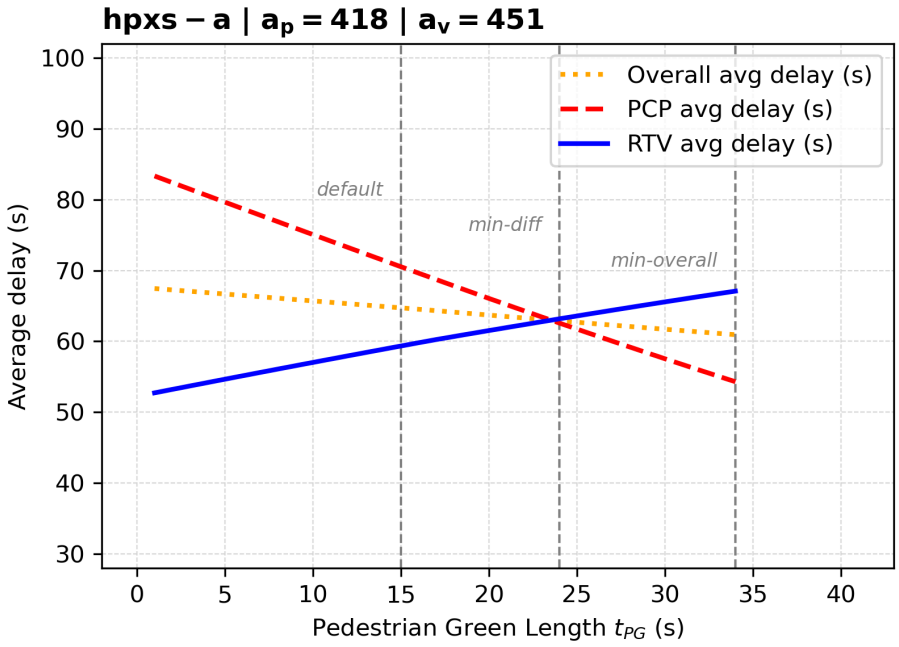

Figure 4.15: Trend of delay values for Heping-Xinsheng, Approach A.

doi:10.6342/NTU202503442

Table 4.15: Optimization results for Heping-Xinsheng, Approach B.

a_p = 428 ped/hr a_v = 82 pcu/hr	Current	min Obj-1	min Obj-2
t_{PG}	21	32	32
Delay Case	P2V5	P1V4	P1V4
PCP intersection timepoint	22.706	20.914	20.914
RTV intersection timepoint	41.241	39.817	39.817
PCP average delay	70.029	60.387	60.387
RTV average delay	48.856	47.791	47.791
Overall average delay	66.628	58.363	58.363
Average delay difference	21.173	12.595	12.595
Reduce PCP delay		-9.642	-9.642
(%)		-13.769%	-13.769%
Reduce RTV delay		-1.065	-1.065
(%)		-2.180%	-2.180%
Reduce overall delay		-8.265	-8.265
(%)		-12.405%	-12.405%

Note:
Obj-1: Minimize the overall (PCP and RTV) average delay.
Obj-2: Minimize the difference in average delay between the two movements.
Negative signs indicate a decrease in delay; positive signs indicate an increase.

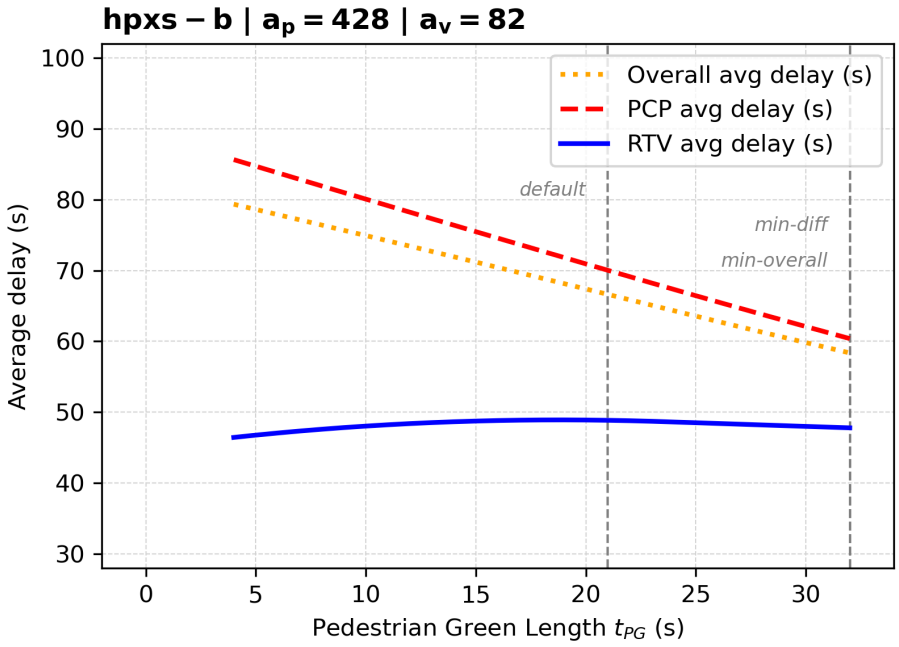

Figure 4.16: Trend of delay values for Heping-Xinsheng, Approach B.

doi:10.6342/NTU202503442

Table 4.16: Optimization results for Songgao-Songren, Approach C.

a_p = 331 ped/hr a_v = 196 pcu/hr	Current	min Obj-1	min Obj-2
t_{PG}	28	68	39
Delay case	P1V5	P1V4	P1V5
PCP intersection timepoint	21.302	14.990	19.566
RTV intersection timepoint	53.893	68.591	60.590
PCP average delay	68.646	37.617	59.190
RTV average delay	57.845	57.395	59.190
Overall average delay	64.635	44.961	59.190
Average delay difference	10.802	19.778	0.000
Reduce PCP delay		-31.029	-9.456
(%)		-45.201%	-13.775%
Reduce RTV delay		-0.450	+1.345
(%)		-0.778%	+2.325%
Reduce overall delay		-19.674	-5.445
(%)		-30.439%	-8.424%

Note:
Obj-1: Minimize the overall (PCP and RTV) average delay.
Obj-2: Minimize the difference in average delay between the two movements.
Negative signs indicate a decrease in delay; positive signs indicate an increase.

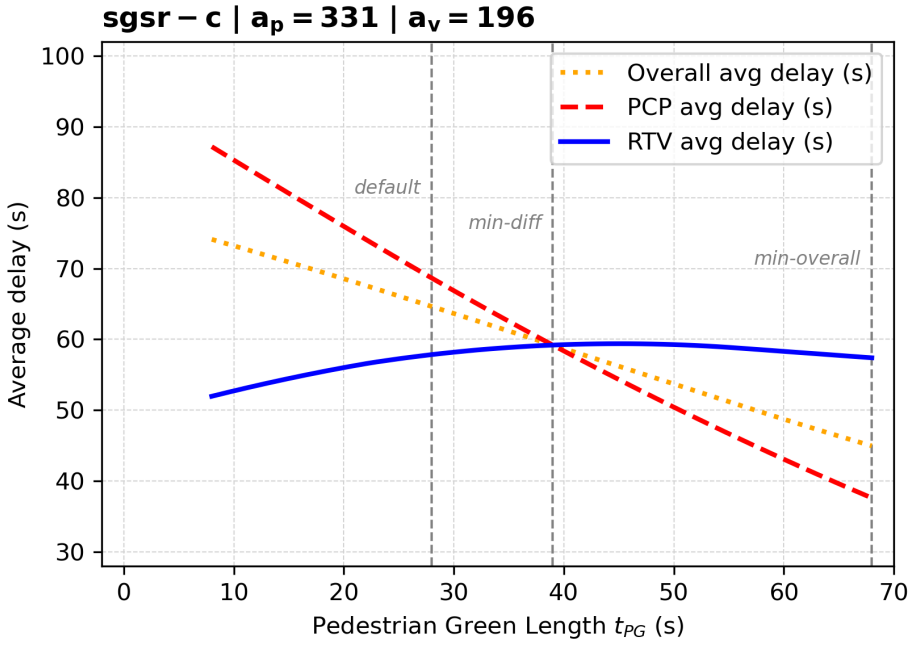

Figure 4.17: Trend of delay values for Songgao-Songren, Approach C.

doi:10.6342/NTU202503442

Table 4.17: Optimization results for Zhongxiao-Guangfu, Approach A.

a_p = 630 ped/hr a_v = 146 pcu/hr	Current	min Obj-1	min Obj-2
t_{PG}	1	10	1
Delay case	P2V5	P2V6	P2V5
PCP intersection timepoint	21.889	21.398	21.889
RTV intersection timepoint	46.598	53.114	46.598
PCP average delay	78.471	70.573	78.471
RTV average delay	83.426	87.935	83.426
Overall average delay	79.403	73.839	79.403
Average delay difference	4.955	17.632	4.955
Reduce PCP delay		-7.898	0
(%)		-10.065%	0%
Reduce RTV delay		+4.509	0
(%)		+5.405%	0%
Reduce overall delay		-5.564	0
(%)		-7.007%	0%

Note:
Obj-1: Minimize the overall (PCP and RTV) average delay.
Obj-2: Minimize the difference in average delay between the two movements.
Negative signs indicate a decrease in delay; positive signs indicate an increase.

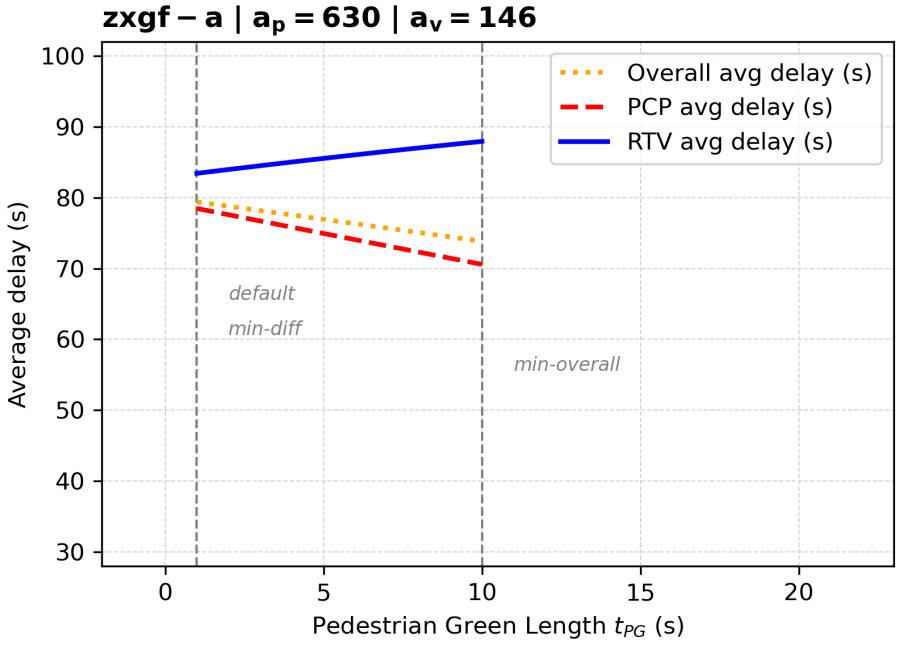

Figure 4.18: Trend of delay values for Zhongxiao-Guangfu, Approach A.

doi:10.6342/NTU202503442

From the optimization results of the six selected intersection approaches, it can be observed that, when pedestrian priority is considered, parallel-crossing pedestrians generally experience shorter average delays with longer pedestrian green durations. However, the delay trend for right-turning vehicles behaves differently.

For intersection approaches with high PCP and RTV demand (Bade-Guangfu-B, Heping-Xinsheng-A, and Zhongxiao-Guangfu-A), those right-turning vehicles tend to experience longer average delays as the pedestrian green duration increases. This can be attributed to the fact that pedestrians are allowed to cross for a longer period, thereby blocking vehicle movements for an extended time. Under such conditions, determining an appropriate pedestrian green duration is essential to balance performance between the two movements. Furthermore, since the PCP arrival rates are observed to be higher than the RTV arrival rates at the aforementioned approaches, if all road users are considered equal, the overall average delay trend typically suggests a longer pedestrian green time (t_{PG}) to minimize total delay. However, this may result in increased delays for RTV movements compared to the current signal timing plan.

For intersection approaches with low RTV demand (Bade-Guangfu-A and Heping-Xinsheng-B), the trend lines of RTV delay appear to be unaffected by PCP movements, regardless of the pedestrian green time (t_{PG}) setting. This may be because the vehicle queues are short enough to clear quickly after the PCP flow has finished discharging.

Zhongxiao-Guangfu-A has the narrowest feasible range for pedestrian green time adjustments. When t_{PG} is less than 1 second (providing only t_{PE} = 5 seconds for PCP movement), the PCP flow becomes oversaturated, as the given time is insufficient for complete discharge. Conversely, when t_{PG} exceeds 10 seconds, the RTV flow becomes oversaturated due to prolonged blockage by PCP movements.

doi:10.6342/NTU202503442

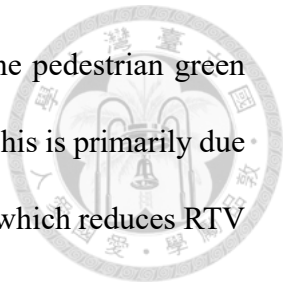

Songgao-Songren-C exhibits an unusual RTV delay trend. As the pedestrian green time t_{PG} increases **from 8 to 45 seconds,** RTV delays also increase. This is primarily due to the extended conflict duration between PCP and RTV movements, which reduces RTV dischargeability.

However, when t_{PG} further increases **from 45 to 68 seconds,** the average RTV delay shows a slight decreasing trend. This is attributed to the corresponding reduction in pedestrian red time, which leads to fewer pedestrians accumulating on both sides of the crosswalk. As a result, pedestrians dissipate more quickly, allowing RTVs to discharge more efficiently despite the longer overall dissipation period.

Figures 4.19 and 4.20 illustrate the multi-movement delay models for Songgao-Songren-C, corresponding to the t_{PG} settings that minimize Obj-1 and Obj-2, respectively, as summarized in Table 4.16. These delay profiles can be compared with the default setting ($t_{PG} = 28$ s) shown in Figure 4.11. These delay trends are further validated through a traffic simulation model, as detailed in Section 4.4.3.

4.4.3 Comparison with Vissim Outputs

Since this research features the variation of saturation flow rates throughout green, yellow, and flashing intervals, it is more appropriate to validate the proposed model using simulation software such as PTV Vissim, rather than relying on traditional delay formulas that assume constant saturation flow rates. PTV Vissim is a widely adopted traffic simulation tool capable of capturing the stochastic nature of traffic flow and simulating second-by-second interactions between pedestrians and vehicles. For this research, a simulation model was developed for Songgao-Songren-C.

doi:10.6342/NTU202503442

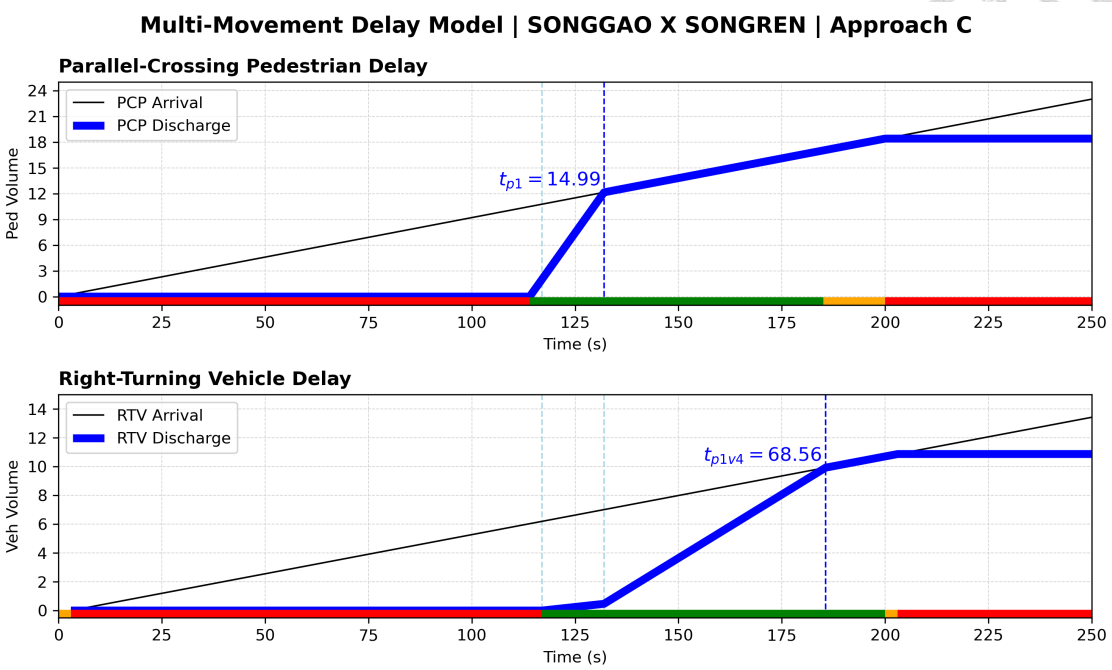

Figure 4.19: Multi-movement delay model for Songgao-Songren, Approach C under a pedestrian green time setting of t_{PG} = 68 seconds, satisfying the minimization of Obj-1.

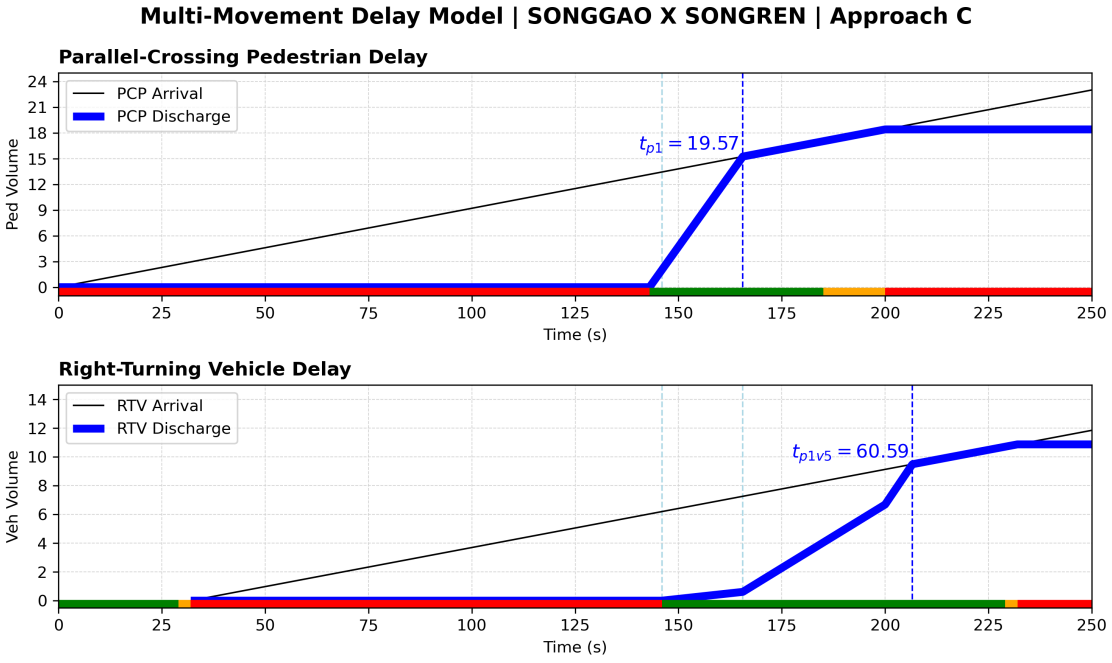

Figure 4.20: Multi-movement delay model for Songgao-Songren, Approach C under a pedestrian green time setting of t_{PG} = 39 seconds, satisfying the minimization of Obj-2.

doi:10.6342/NTU202503442

Simulation Model Development

The road geometry of the Songgao-Songren intersection was reconstructed, and the conflict areas were configured to prioritize pedestrian crossings, as illustrated in Figure 4.21. Detectors were placed upstream and downstream of the outer lane to capture the travel time of right-turning vehicles. Additional detectors were positioned at both ends of the crosswalk to record the travel time of parallel-crossing pedestrians. The signal controller setup is shown in Figure 4.22. In each scenario, the pedestrian green duration on the target intersection approach was adjusted within its allowable range to produce varying average travel times for both PCP and RTV movements.

The warm-up period was set to 600 seconds to allow traffic conditions to stabilize before analysis. Traffic data for each scenario were collected over a 3600-second interval (from 600 to 4200 seconds), and results were averaged by signal cycle. To ensure the stability and reliability of the results, each scenario, with a modified pedestrian green time (t_{PG}), was simulated 30 times using different random seeds.

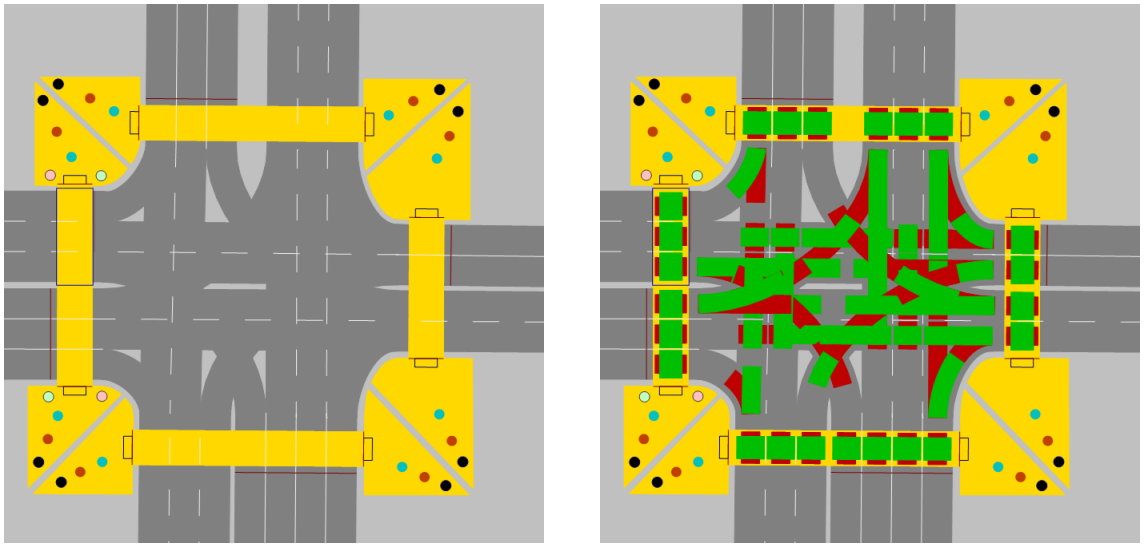

(a) Road geometry setup. (b) Conflict area setup.

Figure 4.21: Vissim simulation model setup (Songgao-Songren, Approach C).

doi:10.6342/NTU202503442

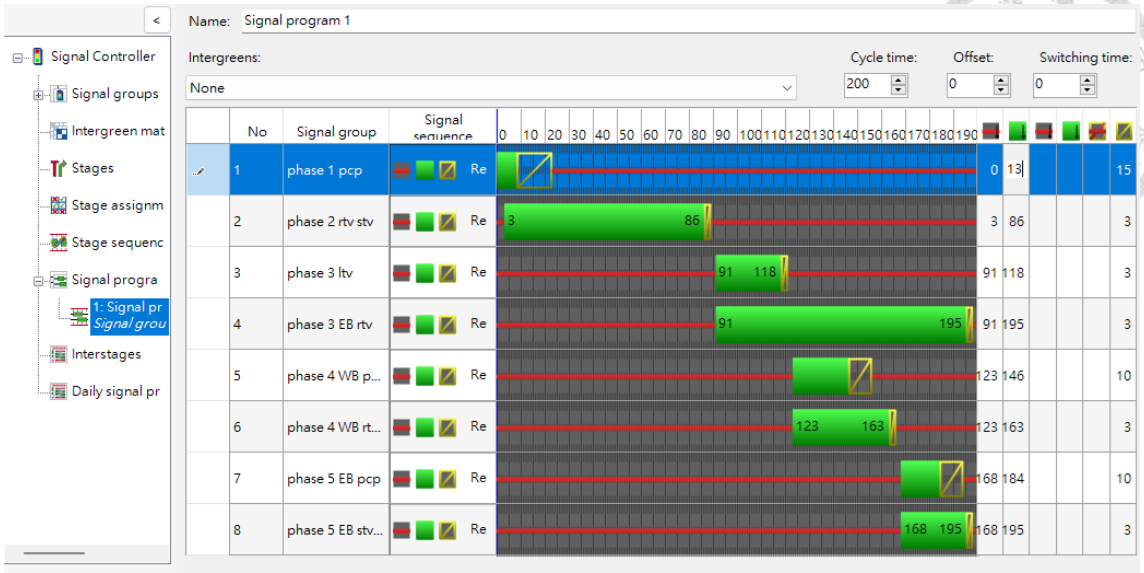

Figure 4.22: Signal controller setup (Songgao-Songren, Approach C).

(a) Ped green phase. (b) Ped flashing phase. (c) Ped red phase.

Figure 4.23: PCP-RTV interactions during pedestrian green, flashing, and red phases.

Figures 4.23a to 4.23c illustrate the interactions between PCP and RTV movements during the concurrent stage. Vehicles fully yield to pedestrians when the PCP flow is high at the beginning of the green phase but may attempt to find acceptable gaps to pass through the conflict area as the PCP flow nears completion. Once the pedestrian phase ends, vehicles can discharge at the free-flow saturation flow rate, that is, their maximum dischargeability.

doi:10.6342/NTU202503442

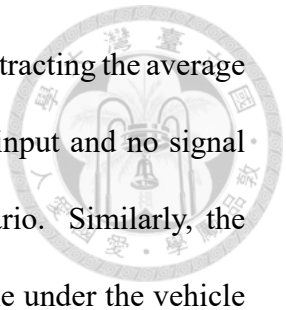

The average PCP delay in the simulation model is calculated by subtracting the average travel time under the pedestrian free-flow scenario (i.e., no vehicle input and no signal control) from the average travel time observed in the current scenario. Similarly, the average RTV delay is estimated by subtracting the average travel time under the vehicle free-flow scenario (i.e., no pedestrian input and no signal control) from that of the current scenario.

Comparison of Average Delay Trends

Figure 4.24a shows the mathematically modeled PCP and RTV delay trends as the pedestrian green duration increases, while Figure 4.24b presents the corresponding trends obtained from the Vissim simulation. Both methods produce a similar trend: PCP average delays decrease as t_{PG} increases. Although RTV average delays also generally increase with longer t_{PG}, the Vissim results show a more gradual rise, whereas the proposed model exhibits a more pronounced concave-downward curve.

At lower t_{PG} settings (from 0 to 7 seconds), the trend lines are interrupted in the model-based plot, indicating that the PCP flow becomes oversaturated, leading to infeasibility when t_{PG} is set within this range. In contrast, the trend lines continue in the Vissim-based plot, showing a very steep decrease. This is because Vissim is still capable of simulating oversaturated conditions; however, some agents may be unable to complete their crossing or pass through the intersection within the 3600-second simulation period and are thus not fully recorded. Those that do complete their movement **contribute disproportionately large delay values to the average delay trend.**

doi:10.6342/NTU202503442

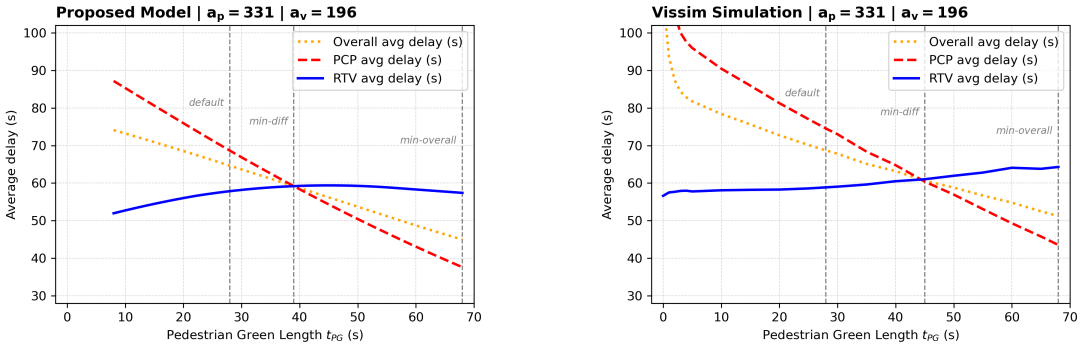

(a) Model-based delay trend.

(b) Vissim-simulated delay trend.

Figure 4.24: Comparison of average delay trends between the proposed model and Vissim simulation (Songgao-Songren, Approach C).

Table 4.18: Comparison of objectives between the proposed model and Vissim simulation (Songgao-Songren, Approach C).

	a_p = 331 ped/hr a_v = 196 pcu/hr	Model-based	Vissim-simulated	Relative difference
Current	t_{PG}	28	28	
	PCP average delay	68.646	74.532	-7.897%
	RTV average delay	57.845	58.859	-1.723%
	Overall average delay	64.635	68.699	-5.916%
	Average delay difference	10.802	15.673	
min Obj-1	t_{PG}	68	68	
	PCP average delay	37.617	43.523	-13.570%
	RTV average delay	57.395	64.298	-10.736%
	Overall average delay	44.961	51.254	-12.278%
	Average delay difference	19.778	20.775	
min Obj-2	t_{PG}	39	45	
	PCP average delay	59.190	60.404	-2.010%
	RTV average delay	59.190	61.022	-3.002%
	Overall average delay	59.190	60.634	-2.382%
	Average delay difference	0.000	0.618	

Note:
Obj-1: Minimize the overall (PCP and RTV) average delay.
Obj-2: Minimize the difference in average delay between the two movements.
The relative difference is calculated based on Vissim results.

doi:10.6342/NTU202503442

Table 4.18 presents a comparison of objective delay values between the model-based and Vissim-based results. It can be observed that the simulated delays are generally higher than those produced by the proposed mathematical model. Under Obj-1, the suggested t_{PG} is the same in both approaches, but a systematic difference in overall average delay can be seen throughout the trend curve. Under Obj-2, the suggested t_{PG} differs by 6 seconds, yet it results in a similar overall average delay.

It should be noted that **the simulation method may contain systematic errors due to slight differences in road geometry settings and road user behavior parameters.** Nevertheless, the overall trends in average delay variations for PCP and RTV remain consistent across both methods.

4.5 Sensitivity Analysis

Different Arrival Rate Combinations

To further evaluate the performance of the proposed model and the simulation process, a sensitivity analysis was conducted using additional scenarios with varying PCP and RTV arrival rates. In general, increased pedestrian and vehicle demand leads to longer discharge times, as queues and crowds accumulate before their respective green phases begin. Some scenarios may indicate that the default signal timing plan requires adjustment to prevent oversaturation.

doi:10.6342/NTU202503442

Songgao-Songren C was again used for sensitivity analysis. Table 4.19 presents the delay case identifications under different combinations of PCP and RTV arrival rates, with the pedestrian green duration t_{PG} fixed at 28 seconds. The tested arrival inputs range from 50 to 400 ped/hr in increments of 50 for PCP, and from 100 to 500 pcu/hr in increments of 100 for RTV. Figure 4.25 illustrates the model-based average delay values within a signal cycle in a three-dimensional plot.

It can be observed that as the pedestrian arrival rate increases, the PCP delay case consistently remains at P1, indicating that pedestrian dischargeability is not significantly affected. In contrast, the RTV delay case shifts from P1V4 to P1V6, suggesting that the intersection point between the AL and DL lines occurs progressively later. When the intersection timepoint t_{PiVj} falls outside the signal cycle, it indicates an oversaturated condition and, therefore, cannot be represented in the delay trend figure.

Figure 4.26 presents the average delay values simulated by Vissim. The trends for both movements generally align with those produced by the proposed model. Although Vissim is capable of outputting average delay values under high PCP and RTV arrival rates, the results exhibit an abnormally steep increase. Since Vissim does not explicitly report oversaturated conditions, such situations can be identified using simulation visuals and derived metrics, such as volume-to-capacity (v/c) ratios calculated from related statistics.

doi:10.6342/NTU202503442

Table 4.19: Delay case identifications under various arrival rate combinations, with the pedestrian green duration fixed at 28 seconds.

Delay case		PCP arrival rate (ped/hr)							
		50	100	150	200	250	300	350	400
RTV arrival rate (pcu/hr)	100	p1v4	p1v4	p1v4	p1v4	p1v4	p1v4	p1v5	p1v5
	200	p1v5	p1v5	p1v5	p1v5	p1v5	p1v5	p1v5	p1v5
	300	p1v5	p1v5	p1v5	p1v5	p1v5	p1v5	p1v5	p1v5
	400	p1v5	p1v5	p1v5	p1v5	p1v5	p1v6	p1v6	overst
	500	overst	overst	overst	overst	overst	overst	overst	overst

Note:
"overst" indicates that the arrival rate combination leads to an oversaturated condition.

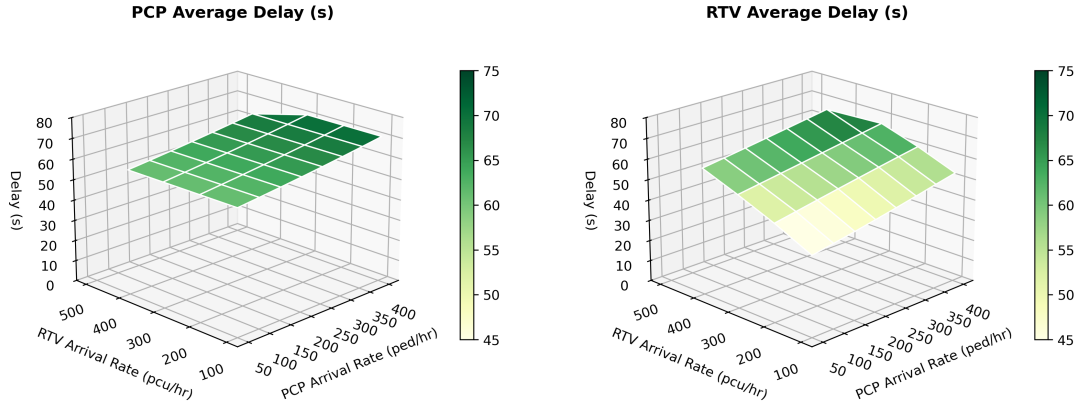

Figure 4.25: Model-based delay trends under different arrival rate combinations.

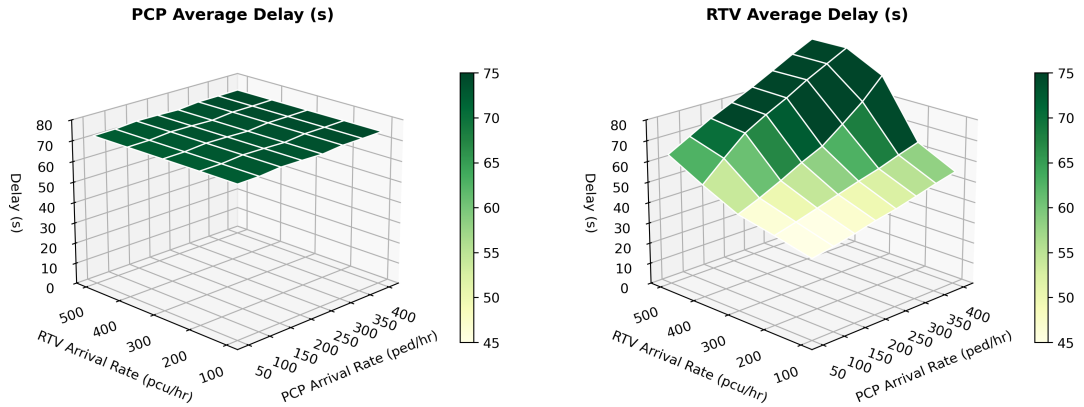

Figure 4.26: Vissim-simulated delay trends under different arrival rate combinations.

doi:10.6342/NTU202503442

Low PCP and Low RTV Arrival Rates

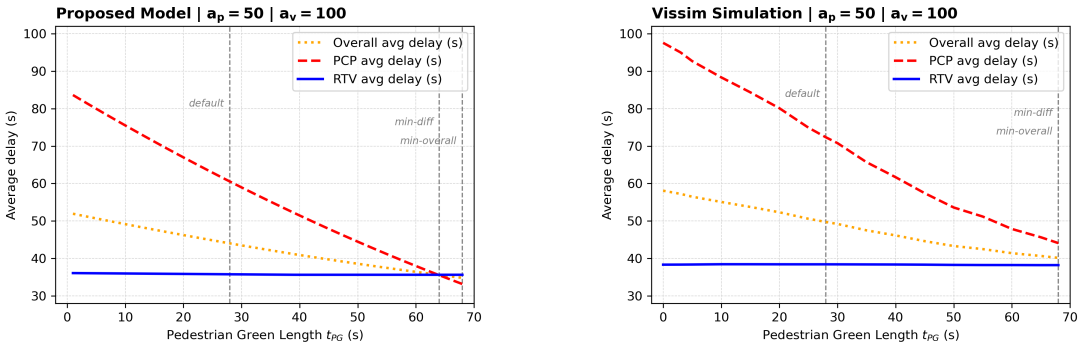

(a) Model-based delay trend. (b) Vissim-simulated delay trend.

Figure 4.27: Comparison of average delay trends (a_p = 50 ped/hr and a_v = 100 pcu/hr).

When both PCP and RTV arrival rates are low, both movements can generally complete discharging within any given t_{PG} duration. Figure 4.27 presents both the model-based and Vissim-simulated delay trends. As expected, pedestrians experience lower delays as the pedestrian green time increases. Meanwhile, the average delay for right-turning vehicles remains approximately constant across different t_{PG} settings, as the influence of pedestrian flow is minimal.

Under such conditions, the optimal t_{PG} tends to be the maximum allowable pedestrian green length ($t_{PG_{\max}}$), at which both the overall average delay and the average delay difference reach their minimum values.

doi:10.6342/NTU202503442

Low PCP and High RTV Arrival Rates

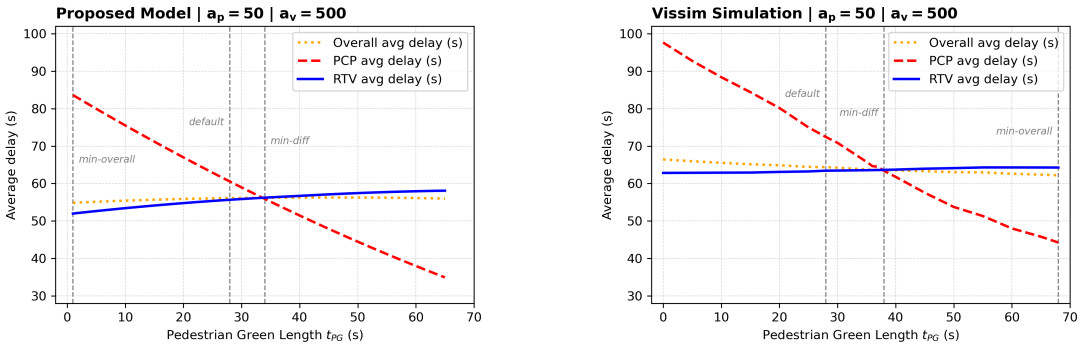

(a) Model-based delay trend. (b) Vissim-simulated delay trend.

Figure 4.28: Comparison of average delay trends (a_p = 50 ped/hr and a_v = 500 pcu/hr).

Figure 4.28 illustrates both the model-based and Vissim-simulated delay trends under low PCP and high RTV arrival rate inputs. Due to the assumption of pedestrian priority, the PCP flow is not affected by RTV movements. Therefore, the pedestrian average delay trend remains similar to the previous scenario, gradually decreasing as t_{PG} increases.

However, RTV movements become more sensitive compared to the previous scenario. As pedestrian green time increases, the resulting blockage causes greater average delays for right-turning vehicles. The model-based results exhibit higher sensitivity than those obtained from the Vissim simulation.

Furthermore, since the delay reduction for pedestrians is more pronounced while the vehicular flow has a higher total volume, the overall average delay trend becomes less stable, showing no well-defined optimal t_{PG} setting. Under this condition, minimizing the delay difference between PCP and RTV movements (Obj-2) becomes a more valuable reference for determining the pedestrian green time, suggesting an appropriate range around 30 to 40 seconds. The RTV movement becomes oversaturated when t_{PG} exceeds 60 seconds.

doi:10.6342/NTU202503442

High PCP and Low RTV Arrival Rates

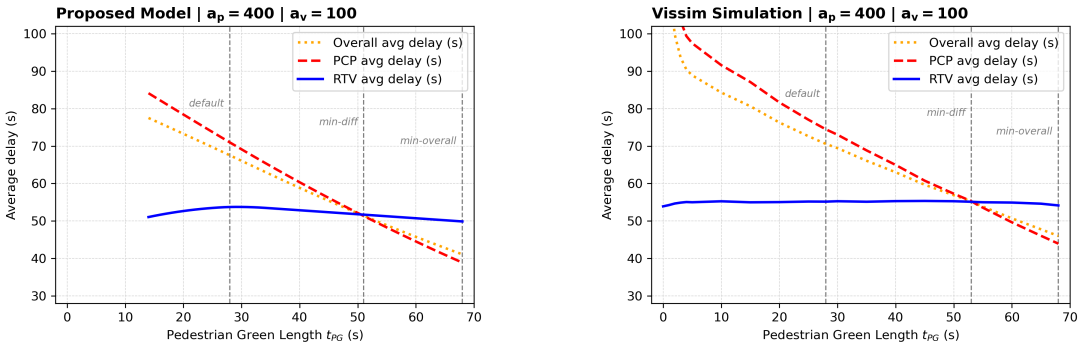

(a) Model-based delay trend. (b) Vissim-simulated delay trend.

Figure 4.29: Comparison of average delay trends (a_p = 400 ped/hr and a_v = 100 pcu/hr).

Figure 4.29 illustrates both the model-based and Vissim-simulated delay trends under high PCP and low RTV arrival rates. As in previous scenarios, the average pedestrian delay gradually decreases as t_{PG} increases. However, when t_{PG} is set too short, pedestrians are unable to complete crossing within a signal cycle, resulting in an oversaturated condition characterized by effectively infinite delay values.

An interesting observation, similar to the default input case (a_p = 331 ped/hr and a_v = 196 pcu/hr) shown in Figure 4.24, is that the average delay for right-turning vehicles increases when t_{PG} is less than 29 seconds and then slightly decreases beyond that point. Based on visual observations from the Vissim simulation, this trend can be interpreted as follows: as the pedestrian green duration (t_{PG}) increases, pedestrian flow increasingly blocks the right-turning vehicles. However, at the same time, the pedestrian red duration (t_{PR}) becomes shorter, resulting in a smaller accumulation of pedestrians at the curb. **This reduced crowd can finish discharging more quickly, which in turn helps to relieve the blockage experienced by right-turning vehicles.** Consequently, a slight reduction in RTV delay is observed beyond a certain t_{PG} value.

doi:10.6342/NTU202503442

High PCP and High RTV Arrival Rates

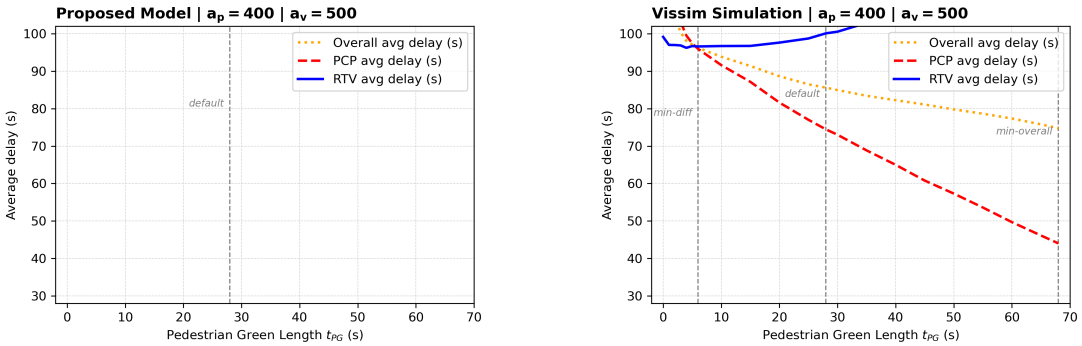

(a) Model-based delay trend. (b) Vissim-simulated delay trend.

Figure 4.30: Comparison of average delay trends (a_p = 400 ped/hr and a_v = 500 pcu/hr).

Figure 4.30 illustrates both the model-based and Vissim-simulated delay trends under high PCP and RTV arrival rates. In fact, such demand levels can cause either pedestrian or vehicular flows to overflow, meaning that no feasible solution can be achieved through pedestrian signal timing adjustments alone. The model-based delay trend plot yields no outputs because the calculated delays are effectively infinite under these conditions.

Although Vissim simulations still produce average delay values, the figure shows that RTV average delays are generally too large for vehicles to discharge within a single signal cycle, often exceeding 100 seconds, because the high pedestrian demand consistently blocks right turning vehicles, regardless of the t_{PG} setting.

In reality, peak hour flow rates typically last for one to two hours. During this period, either PCP or RTV movements at an intersection approach will eventually discharge, albeit over numerous signal cycles. Under such high-demand conditions, strategies such as implementing exclusive pedestrian phases may be considered, as recommended in previous studies.

doi:10.6342/NTU202503442

Chapter 5 Conclusions and Suggestions

5.1 Conclusions

This study aimed to optimize signal timing at intersection approaches based on two primary objectives evaluated within a signal cycle:

- **Obj-1:** Minimize the overall (PCP and RTV) average delay
- **Obj-2:** Minimize the difference in average delay between the two movements

With growing emphasis on the Humanity-Oriented Traffic Environment, extending the pedestrian green duration is recommended to enhance pedestrian right-of-way, particularly when right-turning vehicle drivers demonstrate high compliance (i.e., consistently yield to pedestrians). In such contexts, the minimization of Obj-1 usually supports this outcome.

However, when driver behavior is uncertain or non-compliance is a concern, Obj-2 can serve as a reference for determining the lower bound of the pedestrian green duration. This helps limit pedestrian exposure to potential vehicle conflicts while promoting a more balanced distribution of delays between PCP and RTV movements.

In practice, the concurrent signal stage often includes two PCP-RTV movement pairs from opposite directions (e.g., southbound and northbound), all sharing the same pedestrian green duration. However, when the arrival rate combinations of the two movement pairs differ significantly, minor adjustments to their respective signal timings may be considered to minimize delay for each direction individually.

doi:10.6342/NTU202503442

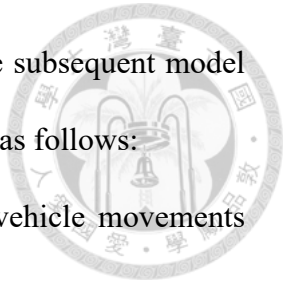

Based on the PCP-RTV discharge rate regression, along with the subsequent model results and sensitivity analysis, the main findings can be summarized as follows:

1. Pedestrian flow influences the performance of right-turning vehicle movements over time when a concurrent signal stage is applied.
2. The average delay for Parallel-Crossing Pedestrians (PCPs) is not significantly affected by changes in their own arrival rate.
3. The average delay for Right-Turning Vehicles (RTVs) is influenced by the arrival rates of both PCPs and RTVs.
4. PCP average delay generally decreases as the pedestrian green phase is extended.
5. RTV average delay exhibits more complex behavior as the pedestrian green phase increases. Continuous pedestrian discharge during the early green contributes to increased RTV delay. However, when pedestrian demand is low and the pedestrian red phase is short, fewer pedestrians accumulate, creating opportunities for quicker RTV discharge and potentially lower delays.

5.2 Limitations and Future Work

Although this study explores the development of a multi-movement delay model by incorporating interactions between PCPs and RTVs, certain aspects were relatively simplified. The following suggestions are proposed for future model development:

1. The model assumes equal pedestrian volumes approaching from both ends of the crosswalk (see Section 3.2.3). In reality, the near-side pedestrian flow affects RTV movements first, followed by the far-side flow. If pedestrian volumes from the two ends differ significantly, the PCP discharge curve may shift, and the resulting impact on RTVs could become asymmetric.

doi:10.6342/NTU202503442

2. The pedestrian discharge rate is assumed to be 1.1 times higher during the flashing phase compared to the green and early phases. Similarly, the vehicle discharge rate is assumed to be 1.1 times higher during the yellow phase compared to the green phase (see Section 4.3). These assumptions are based on the idea that road users tend to speed up when the signal is about to turn red. However, the validity of these multipliers requires further verification. In some countries or regions, pedestrians may behave more cautiously, such as stopping and waiting for the next signal cycle during the flashing phase. In such cases, the multiplier may be less than 1.0.
3. As mentioned in the *Taiwan Highway Capacity Manual* (2022), road geometry is one of the factors influencing flow rates. For example, the right-turn radius can affect the storage capacity of turning lanes. However, this parameter was not considered in our study due to the relocation of vehicle detectors. Therefore, it remains a relevant topic for future investigation.
4. Although a longer pedestrian green duration is generally recommended to reduce overall delay, it may also increase exposure to potential conflicts with turning vehicles. Future development of the optimization model could incorporate safety considerations either as additional performance indicators or as explicit constraints to better balance delay minimization with pedestrian safety.

doi:10.6342/NTU202503442

doi:10.6342/NTU202503442

References

Akçelik, R. (1988). The highway capacity manual delay formula for signalized intersections. *ITE Journal*, *58*(3), 23–27.

Akgüngör, A. P., & Bullen, A. G. R. (1999). Analytical delay models for signalized intersections. *Transportation Frontiers for the Next Millennium: 69th Annual Meeting of the Institute of Transportation Engineers*.

Allsop, R. E. (1981). *Computer program sigset for calculating delay-minimising traffic signal timings: Description and manual for users* (Technical Report). Transport and Road Research Laboratory. Crowthorne, Berkshire, UK.

Braun, R. R., & Roddin, M. F. (1978). *Quantifying the benefits of separating pedestrians and vehicles* (National Cooperative Highway Research Program Report No. 189). Transportation Research Board. Washington, D.C.

Chen, P., Qi, H., & Sun, J. (2014). Investigation of saturation flow on shared right-turn lane at signalized intersections. *Transportation Research Record*, *2461*(1), 66–75. https://doi.org/10.3141/2461-09

Heydecker, B. G. (1992). Sequencing of traffic signals. *Mathematics in Transport Planning and Control*, (38).

Ma, W., Liu, Y., & Head, L. (2014). Optimization of pedestrian phase patterns at signalized intersections: A multi-objective approach. *Journal of Advanced Transportation*, *48*(8), 1138–1152. https://doi.org/10.1002/atr.1256

doi:10.6342/NTU202503442

Milazzo, J. S., Rouphail, N. M., Hummer, J. E., & Allen, D. P. (1998). Effect of pedestrians on capacity of signalized intersections. *Transportation Research Record*, *1646*(1), 37–46. https://doi.org/10.3141/1646-05

PTV Group. (2025). *Ptv vissim 2025 user manual*. PTV Planung Transport Verkehr GmbH. Karlsruhe, Germany.

Roshani, M., & Bargegol, I. (2017). Effect of pedestrians on the saturation flow rate of right turn movements at signalized intersection - case study from rasht city. *IOP Conference Series: Materials Science and Engineering*, *245*(4), 042032. https://doi.org/10.1088/1757-899X/245/4/042032

Rouphail, N. M., & Eads, B. S. (1997). Pedestrian impedance of turning-movement saturation flow rates: Comparison of simulation, analytical, and field observations. *Transportation Research Record*, *1578*(1), 56–63. https://doi.org/10.3141/1578-08

Silcock, J. P. (1997). Designing signal-controlled junctions for group-based operation. *Transportation Research Part A: Policy and Practice*, *31*(2), 157–173. https://doi.org/10.1016/S0965-8564(96)00008-0

Transportation Research Board. (2000). *Highway capacity manual*.

Transportation Research Board. (2010). *Highway capacity manual* (5th ed.).

Virkler, M. R. (1998). Pedestrian compliance effects on signal delay. *Transportation Research Record*, *1636*(1), 88–91. https://doi.org/10.3141/1636-14

Webster, F. V. (1958). *Traffic signal settings* (Road Research Technical Paper No. 39). Road Research Laboratory. London.

doi:10.6342/NTU202503442

Wong, C. K., & Wong, S. C. (2003). Lane-based optimization of signal timings for isolated junctions. *Transportation Research Part B: Methodological*, *37*(1), 63–84. https://doi.org/10.1016/S0191-2615(01)00045-5

Yu, C., Ma, W., Han, K., & Yang, X. (2017). Optimization of vehicle and pedestrian signals at isolated intersections. *Transportation Research Part B: Methodological*, *98*, 135–153. https://doi.org/10.1016/j.trb.2016.12.015

Yu, C., Ma, W., & Yang, X. (2020). A time-slot based signal scheme model for fixed-time control at isolated intersections. *Transportation Research Part B: Methodological*, *140*, 176–192. https://doi.org/10.1016/j.trb.2020.08.004

交通部運輸研究所. (2022). 臺灣公路容量手冊.

內政部營建署. (2001). 市區道路工程規劃及設計規範之研究. https://myway.nlma.gov.tw/

吳崇歆. (2015). 號誌化路口行人一段式及兩段式穿越比較研究 [碩士論文]. 國立臺灣大學土木工程學研究所.

扈菀庭. (2024). 考量行人優先條件下之號誌設計準則探討. *113* 年道路交通安全與執法研討會.

易緯工程顧問股份有限公司. (2022). 110 年度臺北市交通流量及特性調查委託專業服務案 (111 年度後續擴充一般路口、圓環、路段交通量調查) [臺北市交通管制工程處委託]. https://data.taipei/dataset/detail?id=367128a7-24d6-4aae-aef5-2549232b8d10

符人懿. (2011). 號誌化路口行人早開時相與控制策略之研究 [碩士論文]. 淡江大學運輸管理學系.

臺北市政府交通局. (2022). 臺北市路口號誌時制計畫. https://data.taipei/dataset/detail?id=0d639f73-cbcc-42c3-aa53-20efac199701

doi:10.6342/NTU202503442

賴朝睿. (2018). 右轉車輛與行人同一時相對混合直右車道飽和流率之影響分析與改善策略評估 [碩士論文]. 國立臺灣大學土木工程學研究所.

道路交通標誌標線號誌設置規則 [2024 年 10 月 22 日修正]. (2024). https://law.moj.gov.tw/LawClass/LawAll.aspx?pcode=K0040014

道路交通管理處罰條例 [2024 年 5 月 29 日修正]. (2024). https://law.moj.gov.tw/ENG/LawClass/LawAll.aspx?pcode=K0040012

黃厚淳. (2004). 設置行人專用時相對車輛與行人延滯影響之研究 [碩士論文]. 國立交通大學交通運輸研究所.

doi:10.6342/NTU202503442

Appendix A Full Data Collection

A.1 Procedure for Collecting Discharge Rate Pairs

Figure A.1 illustrates the process of selecting (s_p, s_v) discharge rate pairs from each observed intersection approach. These valid rate pairs serve as input for generating a regression curve that represents the discharge rate relationship between PCP and RTV movements. The following procedures were conducted for each intersection approach:

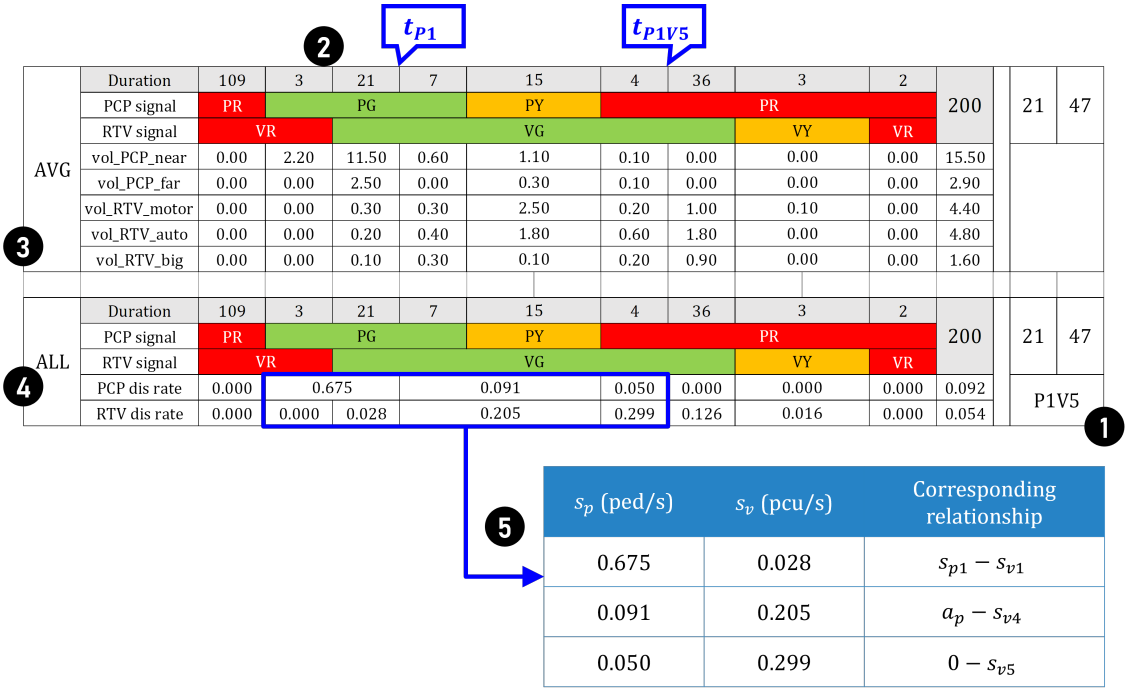

Figure A.1: Process of obtaining effective discharge rate pairs.

1. Observe the PCP and RTV dissipation starting from the onset of the concurrent green phase. Average the dissipation timepoints for both movements to determine the initial t_{Pi} and t_{PiVj} values and identify the corresponding delay case.

doi:10.6342/NTU202503442

2. Insert the determined t_{Pi} and t_{PiVj} values into the timeline as the boundaries of time intervals. This step is essential because the discharge rates may differ significantly before and after the dissipation timepoints, according to their definitions.
3. For each signal cycle, calculate the passing volumes of PCP and RTV within each time interval. Pedestrians are observed approaching from both sides of the crosswalk, while all vehicles originate from the designated right-turn lane. Average the observed volumes across cycles. Sum "vol_PCP_near" and "vol_PCP_far" to obtain the total pedestrian volume. For vehicles, combine "vol_RTV_motor," "vol_RTV_auto," and "vol_RTV_big" using the PCE conversion factors.
4. Discharge rates are obtained by dividing the averaged volumes by their respective time intervals, while arrival rates are calculated using the total volume divided by the cycle length.
5. Collect discharge rate pairs reflecting the PCP-RTV interaction. Specifically, from the start of the concurrent green phase until the RTV movement completes its dissipation, the RTV discharge rate is primarily influenced by changes in the PCP discharge rate.

doi:10.6342/NTU202503442

A.2 Surveyed Traffic Flow Data

Bade-Guangfu, Approach B

Table A.1: Traffic flow survey at Bade-Guangfu B.

Date	2025/4/1	Cycle length	200
Time	18:00 - 18:20	Motorcycle ratio	0.26
Weather	Cloudy	Extra PCE	0.10

Intersection	Bade-Guangfu
PCP crosswalk	B
RTV movement	C →B
RT lane type	Mixed
Flow data No.	SI006
Signal data No.	SKWPX10

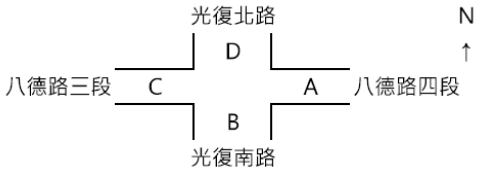

Cycle	Item	other	pcp_lpi	pcp_g_f	pcp_g_b	pcp_y_f	pcp_y_b	rtv_g_f	rtv_g_b	rtv_y_f	rtv_y_b	clear	total	tPi	tPiVj
1	Duration	130	0	4		24	1	23	12	3		3	200	29	53
	PCP signal	PR		PE + PG		PY		PR							
	RTV signal	VR		VG						VY		VR			
	vol_PCP_near	0	0	6		1	0	0	0	0		0	7		
	vol_PCP_far	0	0	0		15	2	0	0	0		2	19		
	vol_RTV_motor	0	0	0		0	0	3	0	0		0	3		
	vol_RTV_auto	0	0	0		0	0	6	1	1		0	8		
	vol_RTV_big	0	0	0		0	0	0	0	0		0	0		
2	Duration	130	0	4		24	1	23	12	3		3	200	29	62
	PCP signal	PR		PE + PG		PY		PR							
	RTV signal	VR		VG						VY		VR			
	vol_PCP_near	0	0	4		1	0	1	1	0		0	7		
	vol_PCP_far	0	0	0		15	3	0	0	0		0	18		
	vol_RTV_motor	0	0	0		0	0	1	0	0		0	1		
	vol_RTV_auto	0	0	0		0	0	5	4	0		0	9		
	vol_RTV_big	0	0	0		0	0	0	0	0		0	0		
3	Duration	130	0	4		24	1	23	12	3		3	200	29	59
	PCP signal	PR		PE + PG		PY		PR							
	RTV signal	VR		VG						VY		VR			
	vol_PCP_near	0	0	4		13	1	0	0	0		0	18		
	vol_PCP_far	0	0	0		13	0	0	0	0		0	13		
	vol_RTV_motor	0	0	0		0	0	3	0	0		0	3		
	vol_RTV_auto	0	0	0		0	0	6	3	2		0	11		
	vol_RTV_big	0	0	0		0	0	0	0	0		0	0		

doi:10.6342/NTU202503442

Cycle	Item	other	pcp_lpi	pcp_g_f	pcp_g_b	pcp_y_f	pcp_y_b	rtv_g_f	rtv_g_b	rtv_y_f	rtv_y_b	clear	total	tPi	tPiVj
4	Duration	130	0	4		24	1	23	12	3		3	200	26	49
	PCP signal	PR		PE + PG		PY		PR							
	RTV signal	VR		VG						VY		VR			
	vol_PCP_near	0	0	4		10	0	0	0	0		0	14		
	vol_PCP_far	0	0	0		10	0	0	0	0		0	10		
	vol_RTV_motor	0	0	0		0	0	3	2	0		0	5		
	vol_RTV_auto	0	0	0		0	0	6	3	3		0	12		
	vol_RTV_big	0	0	0		0	0	0	1	0		0	1		
5	Duration	130	0	4		24	1	23	12	3		3	200	29	44
	PCP signal	PR		PE + PG		PY		PR							
	RTV signal	VR		VG						VY		VR			
	vol_PCP_near	0	0	2		3	2	0	0	0		0	7		
	vol_PCP_far	0	0	0		20	0	0	0	0		0	20		
	vol_RTV_motor	0	0	0		0	0	5	0	0		0	5		
	vol_RTV_auto	0	0	0		0	0	6	4	1		0	11		
	vol_RTV_big	0	0	0		0	0	0	0	0		0	0		
6	Duration	130	0	4		24	1	23	12	3		3	200	26	47
	PCP signal	PR		PE + PG		PY		PR							
	RTV signal	VR		VG						VY		VR			
	vol_PCP_near	0	0	4		6	0	0	0	0		0	10		
	vol_PCP_far	0	0	3		5	0	0	0	0		0	8		
	vol_RTV_motor	0	0	0		1	1	1	0	1		0	4		
	vol_RTV_auto	0	0	0		0	1	5	2	1		0	9		
	vol_RTV_big	0	0	0		0	0	0	0	0		0	0		
AVG	Duration	130	0	4		24	1	23	12	3		3	200	28	52
	PCP signal	PR		PE + PG		PY		PR							
	RTV signal	VR		VG						VY		VR			
	vol_PCP_near	0.00	0.00	4.00		5.67	0.50	0.17	0.17	0.00		0.00	10.50		
	vol_PCP_far	0.00	0.00	0.50		13.00	0.83	0.00	0.00	0.00		0.33	14.67		
	vol_RTV_motor	0.00	0.00	0.00		0.17	0.17	2.67	0.33	0.17		0.00	3.50		
	vol_RTV_auto	0.00	0.00	0.00		0.00	0.17	5.67	2.83	1.33		0.00	10.00		
	vol_RTV_big	0.00	0.00	0.00		0.00	0.00	0.00	0.17	0.00		0.00	0.17		
ALL	Duration	130	0	4		24	1	23	12	3		3	200	28	52
	PCP signal	PR		PE + PG		PY		PR							
	RTV signal	VR		VG						VY		VR			
	PCP dis rate	0.000	N/A	1.125		0.778	1.333	0.007	0.014	0.000		0.111	0.126	P2V5	
	RTV dis rate	0.000	N/A	0.000		0.004	0.253	0.307	0.285	0.473		0.000	0.061		

doi:10.6342/NTU202503442

Bade-Guangfu, Approach A

Table A.2: Traffic flow survey at Bade-Guangfu A.

Date	2025/4/1	Cycle length	200
Time	18:20 - 18:40	Motorcycle ratio	0.57
Weather	Cloudy	Extra PCE	0.00

Intersection	Bade-Guangfu
PCP crosswalk	A
RTV movement	B →A
RT lane type	Mixed
Flow data No.	SI006
Signal data No.	SKWPX10

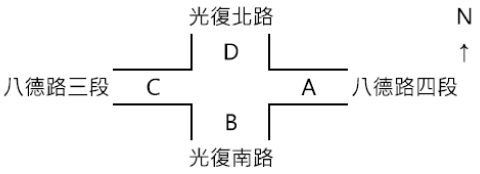

Cycle	Item	other	pcp_lpi	pcp_g_f	pcp_g_b	pcp_y_f	pcp_y_b	rtv_g_f	rtv_g_b	rtv_y_f	rtv_y_b	clear	total		tPi	tPiVj
1	Duration	105	0	10		12	3	10	54	3		3				
	PCP signal	PR		PE + PG		PY		PR					200		22	35
	RTV signal	VR		VG						VY		VR				
	vol_PCP_near	0	0	12		0	0	0	0	0		0	12			
	vol_PCP_far	0	0	4		10	0	0	0	0		0	14			
	vol_RTV_motor	0	0	0		0	2	0	4	0		0	6			
	vol_RTV_auto	0	0	0		0	0	3	1	1		0	5			
	vol_RTV_big	0	0	0		0	0	0	0	0		0	0			
2	Duration	105	0	10		12	3	10	54	3		3				
	PCP signal	PR		PE + PG		PY		PR					200		22	38
	RTV signal	VR		VG						VY		VR				
	vol_PCP_near	0	0	11		0	0	0	0	0		0	11			
	vol_PCP_far	0	0	2		6	0	0	0	0		0	8			
	vol_RTV_motor	0	0	0		0	1	0	2	0		0	3			
	vol_RTV_auto	0	0	0		0	0	3	3	1		0	7			
	vol_RTV_big	0	0	0		0	0	0	0	0		0	0			
3	Duration	105	0	10		12	3	10	54	3		3				
	PCP signal	PR		PE + PG		PY		PR					200		21	35
	RTV signal	VR		VG						VY		VR				
	vol_PCP_near	0	0	6		2	0	0	0	0		0	8			
	vol_PCP_far	0	0	3		7	1	0	0	0		0	11			
	vol_RTV_motor	0	0	0		0	0	1	2	0		0	3			
	vol_RTV_auto	0	0	0		0	0	2	0	0		0	2			
	vol_RTV_big	0	0	0		0	0	0	0	0		0	0			
4	Duration	105	0	10		12	3	10	54	3		3				
	PCP signal	PR		PE + PG		PY		PR					200		21	23
	RTV signal	VR		VG						VY		VR				
	vol_PCP_near	0	0	13		1	0	0	0	0		0	14			
	vol_PCP_far	0	0	1		4	0	0	0	0		0	5			
	vol_RTV_motor	0	0	0		2	0	0	4	1		0	7			
	vol_RTV_auto	0	0	0		0	0	0	0	0		0	0			
	vol_RTV_big	0	0	0		0	0	0	0	0		0	0			

doi:10.6342/NTU202503442

Cycle	Item	other	pcp_lpi	pcp_g_f	pcp_g_b	pcp_y_f	pcp_y_b	rtv_g_f	rtv_g_b	rtv_y_f	rtv_y_b	clear	total		tPi	tPiVj
5	Duration	105	0	10		12	3	10	54	3		3	200		22	42
	PCP signal	PR	PE + PG			PY		PR								
	RTV signal	VR		VG						VY		VR				
	vol_PCP_near	0	0	3		0	0	1	0	0		0	4			
	vol_PCP_far	0	0	2		4	1	0	2	0		0	9			
	vol_RTV_motor	0	0	0		0	1	3	1	0		0	5			
	vol_RTV_auto	0	0	0		0	0	1	2	1		0	4			
	vol_RTV_big	0	0	0		0	0	0	0	0		0	0			
AVG	Duration	105	0	10		12	3	10	54	3		3	200		22	35
	PCP signal	PR	PE + PG			PY		PR								
	RTV signal	VR		VG						VY		VR				
	vol_PCP_near	0.00	0.00	9.00		0.60	0.00	0.20	0.00	0.00		0.00	9.80			
	vol_PCP_far	0.00	0.00	2.40		6.20	0.40	0.00	0.40	0.00		0.00	9.40			
	vol_RTV_motor	0.00	0.00	0.00		0.40	0.80	0.80	2.60	0.20		0.00	4.80			
	vol_RTV_auto	0.00	0.00	0.00		0.00	0.00	1.80	1.20	0.60		0.00	3.60			
	vol_RTV_big	0.00	0.00	0.00		0.00	0.00	0.00	0.00	0.00		0.00	0.00			
ALL	Duration	105	0	10		12	3	10	54	3		3	200		22	35
	PCP signal	PR	PE + PG			PY		PR								
	RTV signal	VR		VG						VY		VR				
	PCP dis rate	0.000	N/A	1.140		0.567	0.133	0.020	0.007	0.000		0.000	0.096		P2V5	
	RTV dis rate	0.000	N/A	0.000		0.014	0.112	0.214	0.042	0.228		0.000	0.028			

doi:10.6342/NTU202503442

Heping-Xinsheng, Approach A

Table A.3: Traffic flow survey at Heping-Xinsheng A.

Date	2025/4/7	Cycle length	200
Time	07:30 - 08:00	Motorcycle ratio	0.61
Weather	Sunny	Extra PCE	0.00

Intersection	Heping-Xinsheng
PCP crosswalk	A
RTV movement	B →A
RT lane type	Exclusive
Flow data No.	EI053
Signal data No.	SFYKD10

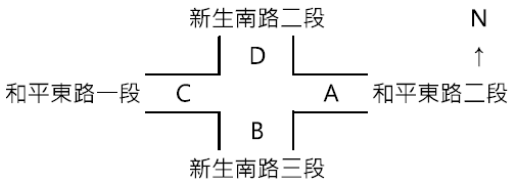

Cycle	Item	other	pcp_lpi	pcp_g_f	pcp_g_b	pcp_y_f	pcp_y_b	rtv_g_f	rtv_g_b	rtv_y_f	rtv_y_b	clear	total	tPi	tPiVj
1	Duration	91	10	15		5	15	24	34	3		3	200	20	63
	PCP signal	PR	PE + PG			PY		PR							
	RTV signal	VR		VG						VY		VR			
	vol_PCP_near	0	8	3		0	0	0	0	0		0	11		
	vol_PCP_far	0	1	6		1	0	0	0	0		0	8		
	vol_RTV_motor	0	0	2		0	1	10	14	2		0	29		
	vol_RTV_auto	0	0	0		0	4	5	7	0		0	16		
	vol_RTV_big	0	0	0		0	0	1	0	0		0	1		
2	Duration	91	10	15		5	15	24	34	3		3	200	15	41
	PCP signal	PR	PE + PG			PY		PR							
	RTV signal	VR		VG						VY		VR			
	vol_PCP_near	0	9	3		0	1	0	0	0		0	13		
	vol_PCP_far	0	0	4		0	1	0	0	0		0	5		
	vol_RTV_motor	0	0	0		2	0	6	11	1		0	20		
	vol_RTV_auto	0	0	0		2	0	6	3	1		0	12		
	vol_RTV_big	0	0	0		0	1	0	0	0		0	1		
3	Duration	91	10	15		5	15	24	34	3		3	200	17	39
	PCP signal	PR	PE + PG			PY		PR							
	RTV signal	VR		VG						VY		VR			
	vol_PCP_near	0	7	1		2	0	0	0	0		0	10		
	vol_PCP_far	0	1	10		1	0	0	0	0		0	12		
	vol_RTV_motor	0	0	0		0	2	12	10	1		0	25		
	vol_RTV_auto	0	0	0		1	5	2	3	0		0	11		
	vol_RTV_big	0	0	0		0	0	0	0	0		0	0		
4	Duration	91	10	15		5	15	24	34	3		3	200	17	87
	PCP signal	PR	PE + PG			PY		PR							
	RTV signal	VR		VG						VY		VR			
	vol_PCP_near	0	9	2		0	0	0	0	0		0	11		
	vol_PCP_far	0	1	6		0	2	0	0	0		0	9		
	vol_RTV_motor	0	0	0		2	1	3	5	3		0	14		
	vol_RTV_auto	0	0	0		1	2	7	8	3		0	21		
	vol_RTV_big	0	0	0		0	0	1	1	0		0	2		

doi:10.6342/NTU202503442

Cycle	Item	other	pcp_lpi	pcp_g_f	pcp_g_b	pcp_y_f	pcp_y_b	rtv_g_f	rtv_g_b	rtv_y_f	rtv_y_b	clear	total	tPi	tPiVj
5	Duration	91	10	15		5	15	24	34	3		3	200	30	56
	PCP signal	PR	PE + PG			PY		PR							
	RTV signal	VR		VG						VY		VR			
	vol_PCP_near	0	9	2		0	0	0	0	0		0	11		
	vol_PCP_far	0	1	11		1	1	0	0	0		0	14		
	vol_RTV_motor	0	0	0		0	3	3	5	5		0	16		
	vol_RTV_auto	0	0	0		0	2	4	3	1		0	10		
	vol_RTV_big	0	0	0		0	0	2	0	0		0	2		
6	Duration	91	10	15		5	15	24	34	3		3	200	23	55
	PCP signal	PR	PE + PG			PY		PR							
	RTV signal	VR		VG						VY		VR			
	vol_PCP_near	0	6	4		1	2	0	0	0		0	13		
	vol_PCP_far	0	4	6		0	0	0	0	0		0	10		
	vol_RTV_motor	0	0	0		0	6	7	10	3		0	26		
	vol_RTV_auto	0	0	0		0	1	7	5	1		0	14		
	vol_RTV_big	0	0	0		0	0	0	0	0		0	0		
7	Duration	91	10	15		5	15	24	34	3		3	200	24	55
	PCP signal	PR	PE + PG			PY		PR							
	RTV signal	VR		VG						VY		VR			
	vol_PCP_near	0	7	2		0	1	0	0	0		0	10		
	vol_PCP_far	0	2	15		3	2	0	0	0		0	22		
	vol_RTV_motor	0	0	0		0	4	4	9	1		0	18		
	vol_RTV_auto	0	0	0		0	2	7	4	0		0	13		
	vol_RTV_big	0	0	0		0	0	0	0	0		0	0		
8	Duration	91	10	15		5	15	24	34	3		3	200	18	52
	PCP signal	PR	PE + PG			PY		PR							
	RTV signal	VR		VG						VY		VR			
	vol_PCP_near	0	8	3		1	3	0	0	0		0	15		
	vol_PCP_far	0	10	4		0	4	0	0	0		0	18		
	vol_RTV_motor	0	0	0		2	0	10	9	0		0	21		
	vol_RTV_auto	0	0	0		0	0	6	5	2		0	13		
	vol_RTV_big	0	0	0		0	0	0	0	0		0	0		
9	Duration	91	10	15		5	15	24	34	3		3	200	17	83
	PCP signal	PR	PE + PG			PY		PR							
	RTV signal	VR		VG						VY		VR			
	vol_PCP_near	0	3	0		0	1	0	0	0		0	4		
	vol_PCP_far	0	2	6		1	3	1	0	0		0	13		
	vol_RTV_motor	0	0	0		0	1	4	21	6		0	32		
	vol_RTV_auto	0	0	0		0	0	6	2	3		0	11		
	vol_RTV_big	0	0	0		0	0	0	2	0		0	2		
AVG	Duration	91	10	15		5	15	24	34	3		3	200	20	59
	PCP signal	PR	PE + PG			PY		PR							
	RTV signal	VR		VG						VY		VR			
	vol_PCP_near	0.00	7.33	2.22		0.44	0.89	0.00	0.00	0.00		0.00	10.89		
	vol_PCP_far	0.00	2.44	7.56		0.78	1.44	0.11	0.00	0.00		0.00	12.33		
	vol_RTV_motor	0.00	0.00	0.22		0.67	2.00	6.56	10.44	2.44		0.00	22.33		
	vol_RTV_auto	0.00	0.00	0.00		0.44	1.78	5.56	4.44	1.22		0.00	13.44		
	vol_RTV_big	0.00	0.00	0.00		0.00	0.11	0.44	0.33	0.00		0.00	0.89		
ALL	Duration	91	10	15		5	15	24	34	3		3	200	20	59
	PCP signal	PR	PE + PG			PY		PR							
	RTV signal	VR		VG						VY		VR			
	PCP dis rate	0.000	0.782			0.244	0.156	0.005	0.000	0.000		0.000	0.116	P2V5	
	RTV dis rate	0.000	0.000	0.006		0.145	0.193	0.393	0.284	0.750		0.000	0.125		

doi:10.6342/NTU202503442

Heping-Xinsheng, Approach B

Table A.4: Traffic flow survey at Heping-Xinsheng B.

Date	2025/4/7	Cycle length	200
Time	08:00 - 08:30	Motorcycle ratio	0.61
Weather	Sunny	Extra PCE	0.00

Intersection	Heping-Xinsheng
PCP crosswalk	B
RTV movement	C →B
RT lane type	Exclusive
Flow data No.	EI053
Signal data No.	SFYKD10

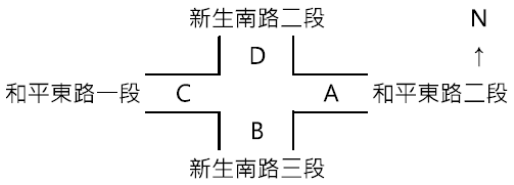

Cycle	Item	other	pcp_lpi	pcp_g_f	pcp_g_b	pcp_y_f	pcp_y_b	rtv_g_f	rtv_g_b	rtv_y_f	rtv_y_b	clear	total	tPi	tPiVj
1	Duration	104	5	21		8	12	44		3		3	200	27	31
	PCP signal	PR	PE + PG			PY		PR							
	RTV signal	VR		VG						VY		VR			
	vol_PCP_near	0	3	4		1	0	0		0		0	8		
	vol_PCP_far	0	0	10		0	3	2		0		0	15		
	vol_RTV_motor	0	0	0		4	0	1		0		0	5		
	vol_RTV_auto	0	0	0		0	0	1		0		0	1		
	vol_RTV_big	0	0	0		0	0	0		0		0	0		
2	Duration	104	5	21		8	12	44		3		3	200	29	35
	PCP signal	PR	PE + PG			PY		PR							
	RTV signal	VR		VG						VY		VR			
	vol_PCP_near	0	4	5		1	1	0		0		0	11		
	vol_PCP_far	0	0	7		0	2	0		0		0	9		
	vol_RTV_motor	0	0	0		0	2	1		0		0	3		
	vol_RTV_auto	0	0	0		0	0	1		0		0	1		
	vol_RTV_big	0	0	0		0	0	0		0		0	0		
3	Duration	104	5	21		8	12	44		3		3	200	21	26
	PCP signal	PR	PE + PG			PY		PR							
	RTV signal	VR		VG						VY		VR			
	vol_PCP_near	0	4	9		0	0	0		0		0	13		
	vol_PCP_far	0	0	7		0	3	0		0		0	10		
	vol_RTV_motor	0	0	0		3	0	0		0		0	3		
	vol_RTV_auto	0	0	0		0	0	2		0		0	2		
	vol_RTV_big	0	0	0		0	0	0		0		0	0		
4	Duration	104	5	21		8	12	44		3		3	200	23	29
	PCP signal	PR	PE + PG			PY		PR							
	RTV signal	VR		VG						VY		VR			
	vol_PCP_near	0	5	9		1	0	0		0		0	15		
	vol_PCP_far	0	0	6		0	0	0		0		0	6		
	vol_RTV_motor	0	0	0		3	0	0		0		0	3		
	vol_RTV_auto	0	0	0		0	2	1		0		0	3		
	vol_RTV_big	0	0	0		0	0	0		0		0	0		

doi:10.6342/NTU202503442

Cycle	Item	other	pcp_lpi	pcp_g_f	pcp_g_b	pcp_y_f	pcp_y_b	rtv_g_f	rtv_g_b	rtv_y_f	rtv_y_b	clear	total	tPi	tPiVj
5	Duration	104	5	21		8	12	44		3		3	200	23	34
	PCP signal	PR	PE + PG			PY		PR							
	RTV signal	VR		VG						VY		VR			
	vol_PCP_near	0	5	3		1	0	1		0		0	10		
	vol_PCP_far	0	0	10		0	0	0		0		0	10		
	vol_RTV_motor	0	0	0		0	2	2		0		0	4		
	vol_RTV_auto	0	0	0		0	2	2		0		0	4		
	vol_RTV_big	0	0	0		0	0	0		0		0	0		
6	Duration	104	5	21		8	12	44		3		3	200	24	35
	PCP signal	PR	PE + PG			PY		PR							
	RTV signal	VR		VG						VY		VR			
	vol_PCP_near	0	4	12		2	0	0		0		0	18		
	vol_PCP_far	0	0	7		0	0	0		0		0	7		
	vol_RTV_motor	0	0	0		1	1	2		0		0	4		
	vol_RTV_auto	0	0	0		0	2	2		0		0	4		
	vol_RTV_big	0	0	0		0	0	1		0		0	1		
7	Duration	104	5	21		8	12	44		3		3	200	28	34
	PCP signal	PR	PE + PG			PY		PR							
	RTV signal	VR		VG						VY		VR			
	vol_PCP_near	0	6	9		1	0	0		0		0	16		
	vol_PCP_far	0	0	10		1	2	0		0		0	13		
	vol_RTV_motor	0	0	0		0	3	3		0		0	6		
	vol_RTV_auto	0	0	0		0	2	1		0		0	3		
	vol_RTV_big	0	0	0		0	0	0		0		0	0		
8	Duration	104	5	21		8	12	44		3		3	200	29	44
	PCP signal	PR	PE + PG			PY		PR							
	RTV signal	VR		VG						VY		VR			
	vol_PCP_near	0	4	8		1	2	0		0		0	15		
	vol_PCP_far	0	0	10		3	1	0		0		0	14		
	vol_RTV_motor	0	0	0		2	2	1		0		0	5		
	vol_RTV_auto	0	0	0		0	1	1		0		0	2		
	vol_RTV_big	0	0	0		0	0	0		0		0	0		
AVG	Duration	104	5	21		8	12	44		3		3	200	26	34
	PCP signal	PR	PE + PG			PY		PR							
	RTV signal	VR		VG						VY		VR			
	vol_PCP_near	0.00	4.38	7.38		1.00	0.38	0.13		0.00		0.00	13.25		
	vol_PCP_far	0.00	0.00	8.38		0.50	1.38	0.25		0.00		0.00	10.50		
	vol_RTV_motor	0.00	0.00	0.00		1.63	1.25	1.25		0.00		0.00	4.13		
	vol_RTV_auto	0.00	0.00	0.00		0.00	1.13	1.38		0.00		0.00	2.50		
	vol_RTV_big	0.00	0.00	0.00		0.00	0.00	0.13		0.00		0.00	0.13		
ALL	Duration	104	5	21		8	12	44		3		3	200	26	34
	PCP signal	PR	PE + PG			PY		PR							
	RTV signal	VR		VG						VY		VR			
	PCP dis rate	0.000	0.774			0.188	0.146	0.009		0.000		0.000	0.119	P1V4	
	RTV dis rate	0.000	0.000	0.000		0.085	0.138	0.050		0.000		0.000	0.023		

doi:10.6342/NTU202503442

Songgao-Songren, Approach C

Table A.5: Traffic flow survey at Songgao-Songren C.

Date	2025/4/8	Cycle length	200
Time	08:00 - 08:30	Motorcycle ratio	0.41
Weather	Sunny	Extra PCE	0.05

Intersection	Songgao-Songren
PCP crosswalk	C
RTV movement	D →C
RT lane type	Mixed
Flow data No.	SI048
Signal data No.	SIVS610

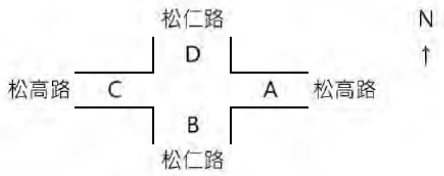

Cycle	Item	other	pcp_lpi	pcp_g_f	pcp_g_b	pcp_y_f	pcp_y_b	rtv_g_f	rtv_g_b	rtv_y_f	rtv_y_b	clear	total	tPi	tPiVj
1	Duration	109	3	21	7	15		4	36	3		2	200	15	42
	PCP signal	PR	PE + PG			PY		PR							
	RTV signal	VR		VG						VY		VR			
	vol_PCP_near	0	2	10	1	1		0	0	0		0	14		
	vol_PCP_far	0	0	1	0	0		0	0	0		0	1		
	vol_RTV_motor	0	0	0	1	0		0	1	0		0	2		
	vol_RTV_auto	0	0	1	0	2		0	0	0		0	3		
	vol_RTV_big	0	0	0	0	0		0	2	0		0	2		
2	Duration	109	3	21	7	15		4	36	3		2	200	23	36
	PCP signal	PR	PG			PY		PR							
	RTV signal	VR		VG						VY		VR			
	vol_PCP_near	0	2	8	0	0		0	0	0		0	10		
	vol_PCP_far	0	0	5	0	1		0	0	0		0	6		
	vol_RTV_motor	0	0	0	1	0		0	1	0		0	2		
	vol_RTV_auto	0	0	0	2	3		0	0	0		0	5		
	vol_RTV_big	0	0	0	0	0		0	0	0		0	0		
3	Duration	109	3	21	7	15		4	36	3		2	200	23	58
	PCP signal	PR	PE + PG			PY		PR							
	RTV signal	VR		VG						VY		VR			
	vol_PCP_near	0	2	9	0	1		0	0	0		0	12		
	vol_PCP_far	0	0	2	0	0		0	0	0		0	2		
	vol_RTV_motor	0	0	0	0	3		0	1	1		0	5		
	vol_RTV_auto	0	0	0	0	3		2	3	0		0	8		
	vol_RTV_big	0	0	0	1	0		0	0	0		0	1		
4	Duration	109	3	21	7	15		4	36	3		2	200	30	33
	PCP signal	PR	PE + PG			PY		PR							
	RTV signal	VR		VG						VY		VR			
	vol_PCP_near	0	3	7	2	0		0	0	0		0	12		
	vol_PCP_far	0	0	4	0	0		0	0	0		0	4		
	vol_RTV_motor	0	0	1	0	2		0	1	0		0	4		
	vol_RTV_auto	0	0	0	1	1		0	5	0		0	7		
	vol_RTV_big	0	0	0	0	0		0	2	0		0	2		

doi:10.6342/NTU202503442

Cycle	Item	other	pcp_lpi	pcp_g_f	pcp_g_b	pcp_y_f	pcp_y_b	rtv_g_f	rtv_g_b	rtv_y_f	rtv_y_b	clear	total	tPi	tPiVj
5	Duration	109	3	21	7	15		4	36	3		2	200	23	39
	PCP signal	PR	PE + PG			PY		PR							
	RTV signal	VR		VG						VY		VR			
	vol_PCP_near	0	0	19	0	1		1	0	0		0	21		
	vol_PCP_far	0	0	2	0	0		0	0	0		0	2		
	vol_RTV_motor	0	0	0	0	4		0	0	0		0	4		
	vol_RTV_auto	0	0	0	0	3		0	0	0		0	3		
	vol_RTV_big	0	0	0	1	0		0	0	0		0	1		
6	Duration	109	3	21	7	15		4	36	3		2	200	17	53
	PCP signal	PR	PE + PG			PY		PR							
	RTV signal	VR		VG						VY		VR			
	vol_PCP_near	0	2	6	0	0		0	0	0		0	8		
	vol_PCP_far	0	0	4	0	0		0	0	0		0	4		
	vol_RTV_motor	0	0	1	0	4		2	0	0		0	7		
	vol_RTV_auto	0	0	0	0	3		2	3	0		0	8		
	vol_RTV_big	0	0	0	0	1		0	0	0		0	1		
7	Duration	109	3	21	7	15		4	36	3		2	200	15	68
	PCP signal	PR	PE + PG			PY		PR							
	RTV signal	VR		VG						VY		VR			
	vol_PCP_near	0	2	14	2	5		0	0	0		0	23		
	vol_PCP_far	0	0	3	0	2		1	0	0		0	6		
	vol_RTV_motor	0	0	0	0	0		0	2	0		0	2		
	vol_RTV_auto	0	0	0	0	0		0	5	0		0	5		
	vol_RTV_big	0	0	0	0	0		0	3	0		0	3		
8	Duration	109	3	21	7	15		4	36	3		2	200	15	58
	PCP signal	PR	PE + PG			PY		PR							
	RTV signal	VR		VG						VY		VR			
	vol_PCP_near	0	3	11	0	2		0	0	0		0	16		
	vol_PCP_far	0	0	0	0	0		0	0	0		0	0		
	vol_RTV_motor	0	0	0	0	2		0	1	0		0	3		
	vol_RTV_auto	0	0	1	0	0		0	2	0		0	3		
	vol_RTV_big	0	0	1	0	0		1	1	0		0	3		
9	Duration	109	3	21	7	15		4	36	3		2	200	23	46
	PCP signal	PR	PE + PG			PY		PR							
	RTV signal	VR		VG						VY		VR			
	vol_PCP_near	0	3	12	1	1		0	0	0		0	17		
	vol_PCP_far	0	0	3	0	0		0	0	0		0	3		
	vol_RTV_motor	0	0	1	1	5		0	3	0		0	10		
	vol_RTV_auto	0	0	0	0	2		1	0	0		0	3		
	vol_RTV_big	0	0	0	0	0		0	1	0		0	1		
10	Duration	109	3	21	7	15		4	36	3		2	200	21	38
	PCP signal	PR	PE + PG			PY		PR							
	RTV signal	VR		VG						VY		VR			
	vol_PCP_near	0	3	19	0	0		0	0	0		0	22		
	vol_PCP_far	0	0	1	0	0		0	0	0		0	1		
	vol_RTV_motor	0	0	0	0	5		0	0	0		0	5		
	vol_RTV_auto	0	0	0	1	1		1	0	0		0	3		
	vol_RTV_big	0	0	0	1	0		1	0	0		0	2		
AVG	Duration	109	3	21	7	15		4	36	3		2	200	21	47
	PCP signal	PR	PE + PG			PY		PR							
	RTV signal	VR		VG						VY		VR			
	vol_PCP_near	0.00	2.20	11.50	0.60	1.10		0.10	0.00	0.00		0.00	15.50		
	vol_PCP_far	0.00	0.00	2.50	0.00	0.30		0.10	0.00	0.00		0.00	2.90		
	vol_RTV_motor	0.00	0.00	0.30	0.30	2.50		0.20	1.00	0.10		0.00	4.40		
	vol_RTV_auto	0.00	0.00	0.20	0.40	1.80		0.60	1.80	0.00		0.00	4.80		
	vol_RTV_big	0.00	0.00	0.10	0.30	0.10		0.20	0.90	0.00		0.00	1.60		
ALL	Duration	109	3	21	7	15		4	36	3		2	200	21	47
	PCP signal	PR	PE + PG			PY		PR							
	RTV signal	VR		VG						VY		VR			
	PCP dis rate	0.000	0.675			0.091		0.050	0.000	0.000		0.000	0.092	P1V5	
	RTV dis rate	0.000	0.000	0.028		0.205		0.299	0.126	0.016		0.000	0.054		

doi:10.6342/NTU202503442

Zhongxiao-Guangfu, Approach A

Table A.6: Traffic flow survey at Zhongxiao-Guangfu A.

Date	2025/4/11	Cycle length	200
Time	18:00 - 18:50	Motorcycle ratio	0.45
Weather	Sunny	Extra PCE	0.05

Intersection	Zhongxiao-Guangfu
PCP crosswalk	A
RTV movement	B →A
RT lane type	Mixed
Flow data No.	EI035
Signal data No.	SJFPW10

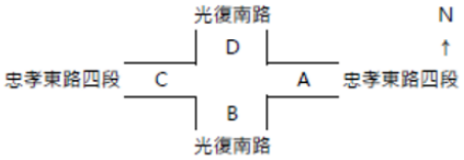

Cycle	Item	other	pcp_lpi	pcp_g_f	pcp_g_b	pcp_y_f	pcp_y_b	rtv_g_f	rtv_g_b	rtv_y_f	rtv_y_b	clear	total	tPi	tPiVj
1	Duration	138	5	1		23	7	6	14	3		3	200	26	35
	PCP signal	PR	PE + PG			PY		PR							
	RTV signal	VR		VG						VY		VR			
	vol_PCP_near	0	8	0		8	0	0	0	0		0	16		
	vol_PCP_far	0	0	0		9	0	0	0	0		0	9		
	vol_RTV_motor	0	0	0		0	6	0	1	2		0	9		
	vol_RTV_auto	0	0	0		0	2	2	3	1		0	8		
	vol_RTV_big	0	0	0		0	0	0	0	0		0	0		
2	Duration	138	5	1		23	7	6	14	3		3	200	30	45
	PCP signal	PR	PE + PG			PY		PR							
	RTV signal	VR		VG						VY		VR			
	vol_PCP_near	0	7	0		17	0	0	0	0		0	24		
	vol_PCP_far	0	0	0		5	3	0	0	0		0	8		
	vol_RTV_motor	0	0	0		0	0	1	0	0		0	1		
	vol_RTV_auto	0	0	0		0	0	1	3	0		0	4		
	vol_RTV_big	0	0	0		0	0	0	0	0		0	0		
3	Duration	138	5	1		23	7	6	14	3		3	200	25	40
	PCP signal	PR	PE + PG			PY		PR							
	RTV signal	VR		VG						VY		VR			
	vol_PCP_near	0	9	0		17	0	0	0	0		0	26		
	vol_PCP_far	0	0	0		12	2	0	0	0		0	14		
	vol_RTV_motor	0	0	0		0	0	7	0	0		0	7		
	vol_RTV_auto	0	0	0		0	0	0	4	0		0	4		
	vol_RTV_big	0	0	0		0	0	0	0	0		0	0		
4	Duration	138	5	1		23	7	6	14	3		3	200	30	53
	PCP signal	PR	PE + PG			PY		PR							
	RTV signal	VR		VG						VY		VR			
	vol_PCP_near	0	7	0		18	0	0	0	0		0	25		
	vol_PCP_far	0	0	0		14	5	1	0	0		0	20		
	vol_RTV_motor	0	0	0		0	0	0	2	0		0	2		
	vol_RTV_auto	0	0	0		0	0	0	4	3		0	7		
	vol_RTV_big	0	0	0		0	0	0	0	0		0	0		

doi:10.6342/NTU202503442

Cycle	Item	other	pcp_lpi	pcp_g_f	pcp_g_b	pcp_y_f	pcp_y_b	rtv_g_f	rtv_g_b	rtv_y_f	rtv_y_b	clear	total	tPi	tPiVj
5	Duration	138	5	1		23	7	6	14	3		3	200	30	40
	PCP signal	PR		PE + PG		PY		PR							
	RTV signal	VR		VG						VY		VR			
	vol_PCP_near	0	10	0		23	0	0	0	0		0	33		
	vol_PCP_far	0	0	0		6	2	0	0	0		0	8		
	vol_RTV_motor	0	0	0		0	0	2	1	1		0	4		
	vol_RTV_auto	0	0	0		0	0	2	1	1		0	4		
	vol_RTV_big	0	0	0		0	0	0	0	0		0	0		
6	Duration	138	5	1		23	7	6	14	3		3	200	30	45
	PCP signal	PR		PE + PG		PY		PR							
	RTV signal	VR		VG						VY		VR			
	vol_PCP_near	0	6	0		30	0	0	0	0		0	36		
	vol_PCP_far	0	0	0		8	1	0	0	0		0	9		
	vol_RTV_motor	0	0	0		0	0	6	2	0		0	8		
	vol_RTV_auto	0	0	0		0	0	1	4	0		0	5		
	vol_RTV_big	0	0	0		0	0	0	0	0		0	0		
7	Duration	138	5	1		23	7	6	14	3		3	200	30	42
	PCP signal	PR		PE + PG		PY		PR							
	RTV signal	VR		VG						VY		VR			
	vol_PCP_near	0	7	0		34	0	0	0	0		0	41		
	vol_PCP_far	0	0	0		10	0	0	0	0		0	10		
	vol_RTV_motor	0	0	0		0	0	1	1	2		0	4		
	vol_RTV_auto	0	0	0		0	0	2	3	0		0	5		
	vol_RTV_big	0	0	0		0	0	0	0	0		0	0		
8	Duration	138	5	1		23	7	6	14	3		3	200	30	50
	PCP signal	PR		PE + PG		PY		PR							
	RTV signal	VR		VG						VY		VR			
	vol_PCP_near	0	6	0		12	0	0	0	0		0	18		
	vol_PCP_far	0	0	0		4	4	0	0	0		0	8		
	vol_RTV_motor	0	0	0		2	0	0	2	2		0	6		
	vol_RTV_auto	0	0	0		0	0	0	5	2		0	7		
	vol_RTV_big	0	0	0		0	0	0	0	0		0	0		
9	Duration	138	5	1		23	7	6	14	3		3	200	28	33
	PCP signal	PR		PE + PG		PY		PR							
	RTV signal	VR		VG						VY		VR			
	vol_PCP_near	0	7	0		19	0	0	0	0		0	26		
	vol_PCP_far	0	0	0		11	0	0	0	0		0	11		
	vol_RTV_motor	0	0	0		0	0	3	0	2		0	5		
	vol_RTV_auto	0	0	0		0	0	1	4	1		0	6		
	vol_RTV_big	0	0	0		0	0	0	0	1		0	1		
10	Duration	138	5	1		23	7	6	14	3		3	200	25	36
	PCP signal	PR		PE + PG		PY		PR							
	RTV signal	VR		VG						VY		VR			
	vol_PCP_near	0	5	0		5	0	0	0	0		0	10		
	vol_PCP_far	0	0	0		8	0	0	0	0		0	8		
	vol_RTV_motor	0	0	0		1	0	0	2	0		0	3		
	vol_RTV_auto	0	0	0		0	2	1	2	0		0	5		
	vol_RTV_big	0	0	0		0	0	1	0	0		0	1		
11	Duration	138	5	1		23	7	6	14	3		3	200	30	40
	PCP signal	PR		PE + PG		PY		PR							
	RTV signal	VR		VG						VY		VR			
	vol_PCP_near	0	4	0		5	0	0	0	0		0	9		
	vol_PCP_far	0	0	0		12	1	0	0	0		0	13		
	vol_RTV_motor	0	0	0		0	0	1	1	0		0	2		
	vol_RTV_auto	0	0	0		0	0	4	2	0		0	6		
	vol_RTV_big	0	0	0		0	0	0	0	0		0	0		
12	Duration	138	5	1		23	7	6	14	3		3	200	28	41
	PCP signal	PR		PE + PG		PY		PR							
	RTV signal	VR		VG						VY		VR			
	vol_PCP_near	0	7	0		18	0	0	0	0		0	25		
	vol_PCP_far	0	0	0		11	2	0	0	0		0	13		
	vol_RTV_motor	0	0	0		1	0	1	2	1		0	5		
	vol_RTV_auto	0	0	0		0	1	1	3	0		0	5		
	vol_RTV_big	0	0	0		0	0	0	0	0		0	0		

doi:10.6342/NTU202503442

Cycle	Item	other	pcp_lpi	pcp_g_f	pcp_g_b	pcp_y_f	pcp_y_b	rtv_g_f	rtv_g_b	rtv_y_f	rtv_y_b	clear	total		tPi	tPiVj
AVG	Duration	138	5	1		23	7	6	14	3		3	200		29	42
	PCP signal	PR	PE + PG			PY		PR								
	RTV signal	VR		VG						VY		VR				
	vol_PCP_near	0.00	6.92	0.00		17.17	0.00	0.00	0.00	0.00		0.00	24.08			
	vol_PCP_far	0.00	0.00	0.00		9.17	1.67	0.08	0.00	0.00		0.00	10.92			
	vol_RTV_motor	0.00	0.00	0.00		0.33	0.50	1.83	1.17	0.83		0.00	4.67			
	vol_RTV_auto	0.00	0.00	0.00		0.00	0.42	1.25	3.17	0.67		0.00	5.50			
	vol_RTV_big	0.00	0.00	0.00		0.00	0.00	0.08	0.00	0.08		0.00	0.17			
ALL	Duration	138	5	1		23	7	6	14	3		3	200		29	42
	PCP signal	PR	PE + PG			PY		PR								
	RTV signal	VR		VG						VY		VR				
	PCP dis rate	0.000	1.153			1.145	0.238	0.014	0.000	0.000		0.000	0.175		P2V5	
	RTV dis rate	0.000	0.000	0.000		0.007	0.093	0.387	0.265	0.422		0.000	0.041			

doi:10.6342/NTU202503442

doi:10.6342/NTU202503442